

Work Package 4
CO2 storage assessment – numerical simulation of the India case study



Organisation(s)	Indian Institute of Technology, Bombay
Author(s)	Dr D N Singh, Dr Ajendra Singh
Reviewer	Anne-Kari Furre, Philip Ringrose, Lars Grande
Type of deliverable	Report
Dissemination level	
WP	4
Issue date	
Document version	

Keywords:

CCS, Numerical Simulation, Pore Pressure

Summary:

A study of possible CCS application at the onshore field Baghewala, Bikaner Nagaur Basin India is discussed. The primary analysis includes identification of key reservoir and caprock units for storage and monitoring. Furthermore, a simple 3D homogeneous model based upon petrophysical properties from well data is generated and simulated under different injection rates of CO₂ to identify the associated changes in pore pressure. Based upon the learnings from this model, a field scale model is generated to present a more realistic study for CO₂ saturation and pore pressure changes in identified reservoir units. The Geomechanical properties such as Young Modulus, Shear Modulus, Bulk Modulus and Poisson ratio is obtained from compressional and shear velocity measurement from the downhole wireline log. This gives a description of geomechanical parameters in the reservoir and caprock zones.

Table of Content

1. Introduction.....	3
2. Geological Background.....	4
3. Data Repository.....	9
4. Acoustic Measurements.....	13
5. XRD Analysis.....	14
6. Modeling Methodology.....	15
7. Numerical Simulation.....	16
8. Geomechanical Assessment.....	28
9. Conclusion.....	31
10. Disclaimer.....	32
11. References.....	33
12. Appendix.....	34

1. Introduction

Capturing and storing CO₂ in geological formations is a significant potential technique for reducing world emissions. The United Nations Intergovernmental Panel on Climate Change (IPCC) states in its Special Report on Carbon Dioxide Capture and Storage (2005) that CO₂ capture and storage may account for up to half of all emission reductions this century. However, significant challenges should be addressed to reach this goal. The technical potential for storing CO₂ in geological formations across the planet is substantially demonstrated by considerable subsurface storage potential in abandoned oil and gas fields and other formations such as saline aquifers. These subsurface formations provide a viable geological option since these porous zones have been holding fluid either oil and gas or water for millions of years.

In CCS (Carbon Capture and Storage) application, Carbon dioxide (CO₂) will preferably be injected and stored in the formation as a supercritical fluid. Subsequently, it traverses the linked voids inside the rock, akin to other fluid substances such as water, oil, and gas. For saline formations to be acceptable for CO₂ storage, they must possess adequate porosity and permeability to accommodate the injection of vast quantities of CO₂ in a supercritical state at a pace that matches the supply. Additionally, an impermeable caprock must be in place on top of the storage unit, serving as a seal, to prevent the migration of CO₂ into adjacent formations or the ocean.

Carbon dioxide (CO₂) is retained inside a subsurface reservoir by utilizing one or more of five fundamental trapping mechanisms: stratigraphic, structural, residual, solubility, and mineral trapping. Typically, the primary methods of trapping oil and gas are either through the geological arrangement of rock layers (stratigraphic trapping), tectonic events such as folding and faulting of rock units (structural trapping), or a mixture of both. Residual trapping occurs when CO₂ becomes confined inside the pores of rocks due to the capillary pressure. After the injection ceases, water from the adjacent rocks encroaches on the pore spaces holding CO₂. During this process, the CO₂ is rendered immobile due to the increased pressure exerted by the water. A significant portion of the CO₂ that is injected will eventually dissolve in the saline water or the residual oil in the rock. This method of trapping CO₂ by dissolving it in brine present in pore spaces is known as solubility trapping. Solubility trapping results in the creation of a more dense fluid that has the potential to sink to the lowermost part of the storage formation.

The dissolved CO₂ may undergo chemical reactions with the surrounding rocks, producing stable minerals, depending on the rock formation. Mineral trapping, sometimes referred to as the most reliable method of storage for CO₂, is a gradual process that can span thousands of years.

The storage potential of the reservoir is primarily linked to its porosity and permeability. Porosity is a quantitative assessment of the voids or empty spaces inside a rock that have the capacity to hold and contain fluids. Permeability is a quantitative assessment of a rock's capacity to facilitate the movement of fluids. The permeability of a rock is significantly influenced by its pore spaces' morphology, dimensions, and interconnection. Hence, a quantitative estimate of these critical parameters will help in evaluating the CO₂ injection rate scheme and in understanding the time scale of the project.

Oil and gas reservoirs are a subset of saline formations, and they generally have similar properties. They are permeable rock formations acting as a reservoir with an impermeable cap rock acting as a seal. In contrast, the seals that cover the storage formation often exhibit low porosity and permeability, which allows them to capture the CO₂ effectively. Injectivity is a crucial characteristic of the storage site, referring to the rate at which CO₂ may be injected without initiating fracturing and fault reactivation of a nearby fault due to the poroelastic response of the rock.

The work described in this report documents highlights of the workflow and methodology for the feasibility study of CO₂ injection in Baghewala Field, Bikaner Nagaur Basin, India. The prospective storage zones are envisaged in Jodhpur Formation while overlying Bilara, Hanseran and Nagaur formation will act as a caprock limiting the buoyancy driven upward movement of the CO₂ plume.

2. Geological Background

The Bikaner-Nagaur basin, classified as a peri cratonic basin according to Ram (2015), spans approximately 77,500 square kilometres and is situated in the northwestern region of the Indian subcontinent (Figure 1). The basin is filled with sediments from the Upper Proterozoic-Lower Palaeozoic Marwar Supergroup, which have a maximum thickness of 1500 m according to Kumar and Chandra (2005). The basin is also covered by a thin layer of Mesozoic and Tertiary sediments. The basin is surrounded by the Delhi Sargodha basement high in the northern and northeastern directions, the Aravalli fold belt in the eastern direction, and the

Pokhran high in the southwestern direction. It also expands westward into the Punjab platform of the Middle Indus basin in Pakistan.

The Bikaner-Nagaur basin was created by stretching along the Najd fault system of the Arabian plate during the late Proterozoic to early Cambrian period. This stretching was connected to the final stage of the Pan-African orogeny (Al-Husseini 2000). The Najd fault system, which extends for approximately 1000 km in a northwest-southeast direction, is visible on the Arabian shield. This fault system was active throughout the Late Neoproterozoic and early Cambrian periods (Luning et al., 2009). The migration towards east along the Najd faults resulted in the creation of a sequence of rift-grabens, including the Punjab rift and Bikaner-Nagaur basin, in the eastern region of Gondwanaland during the late Neoproterozoic era (Al-Husseini 2000).

Till recently, exploration efforts have been limited to the western edge of the basin, where the potential for hydrocarbon extraction from the Proterozoic Jodhpur and Cambrian Bilara formations has already been confirmed. The Bhagewala field was explored in the same region along with Punam and Nanuwala field in its vicinity. The Pericratonic Bikaner-Nagaur basin contains a sedimentary sequence that ranges in age from the Neoproterozoic to the early Cambrian. This sequence, known as the Marwar supergroup, is composed of three main groups: the Jodhpur group, the Bilara and Hanseran Evaporite Group (HEG), and the Nagaur group. These groups are arranged in chronological order and are covered by a thin layer of Mesozoic and Tertiary sediments (Figure 2) (Prasad et al., 2010).

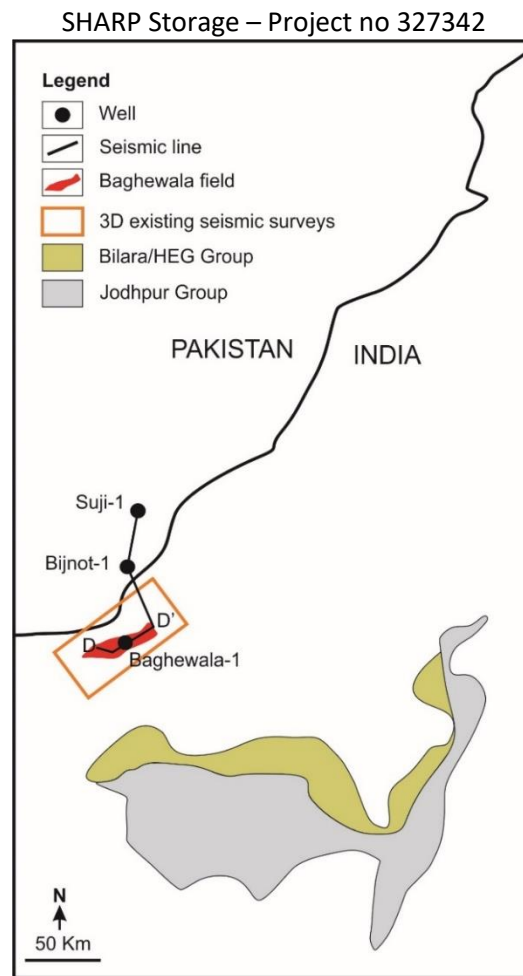


Figure 1. Basemap describes the location of the Baghewala field in the Rajasthan Basin, Western India.

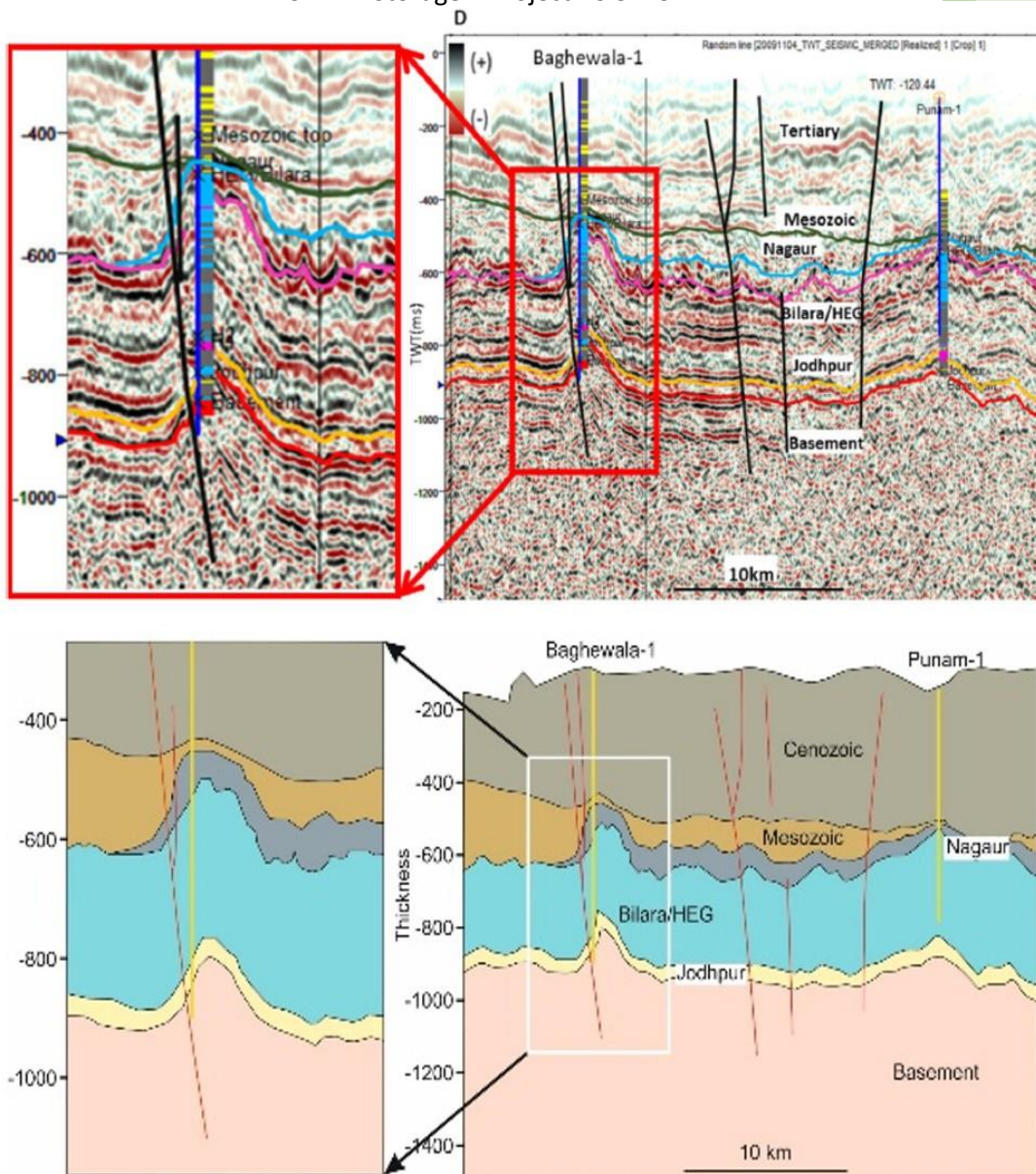


Figure 2 A 2D seismic cross-section marked by DD' in Figure 1. The seismic profile has all the key stratigraphy boundary marked as different horizons and Baghwala -1 marked. The equivalent interpretation of the 2D seismic profile is given below with an enlarged view highlighting the Baghwala Field present on the fault-bounded anticline structure.

Age	Lithostratigraphy				Thickness	Lithology	Plays
	Group/Formation						
	Central and northern parts of the basin	South Western parts of the basin	Southern parts of the basin				
Cambrian	Nagaur Group		Tunkian Fm.	Tunidian Fm.	75-500 m		Monitoring area
			Nagaur Fm.	Nagaur Fm.			
Neo-proterozoic	Bilara Group	Birmania Fm.	Pondlo Fm.	Hanseran Evaporite Group (HEG)	100-656 m		Monitoring & storage complex
			Gotan Fm.				
			Dhanapa Fm.				
Neo-proterozoic	Jodhpur Group		Girbhakar Fm.		125-423 m		Storage site
		Radha Fm.	Sonia Fm.				
Meso-proterozoic	BASEMENT ROCKS: Malani Igneous Suite of rocks and/or Delhi metamorphites						

Meta sediments/volcanics

Evaporite/Limestone/Dolostone

Sandstone

Shale

Figure 3. Stratigraphy map describing all the formation from Neoproterozoic to Quaternary in the Bikaner Nagaur Basin. The possible zones of source, reservoir and trap are also marked in the right column (after Kumar et al, 2005)

The Jodhpur group is a sedimentary deposit formed in a syn-rift environment, characterized by the presence of fluvial-deltaic sediments. This is followed by a transgression deposit consisting of carbonate and halite, known as the Bilara-HEG group. Mazumdar and Strauss (2006) established the age equivalency of Bilara carbonate and HEG halite by analysing the isotopic composition of sulphur and strontium (Mazumdar and Strauss, 2006). The transition between the two rock formations, known as the gradational contact, indicates the beginning of the process of sedimentary deposition. This process involves the accumulation of thick layers of shale and sandstone, which were formed by the deposition of sediment in river and lake environments. The Marwar Supergroup in the Bikaner-Nagaur basin of India is geographically connected with the Salt Range Formation in Pakistan. However, the Marwar Supergroup in India is comparatively thin and less deformed compared to its counterpart in Pakistan (Cozzi et al., 2012; Chauhan et al., 1991, 2004).

3. Data Repository

Datasets from two wells, WELL 1 and WELL 2(Figure 4), in the Baghewala field were made available on 15.12.2023 by Oil India Limited (OIL), the details of which are mentioned below.

Well	Wireline log						Processed logs	Well Completion Report
	GR	SP	NPHI	RHOB	Resistivity (Deep, Medium, Shallow)	Image Log		
WELL 1	<input checked="" type="checkbox"/>	<input checked="" type="checkbox"/>	<input checked="" type="checkbox"/>	<input checked="" type="checkbox"/>	<input checked="" type="checkbox"/>	<input checked="" type="checkbox"/>	<input checked="" type="checkbox"/>	<input checked="" type="checkbox"/>
WELL 2	<input checked="" type="checkbox"/>	<input checked="" type="checkbox"/>	<input checked="" type="checkbox"/>	<input checked="" type="checkbox"/>	<input checked="" type="checkbox"/>	X	<input checked="" type="checkbox"/>	<input checked="" type="checkbox"/>

Table. 1 A brief description of the dataset provided by OIL for the Baghewala Field, Bikaner Nagaur Basin, India.

Along with the above-mentioned wireline log data, OIL provided nine rock cores (diameter 36 mm) from WELL 1 from Jodhpur Formation and five cores (diameter 37.5 mm) from WELL 2 from Upper Carbonate Formation of Baghewala Fields and their details are given below in the tables:

Sr. no	Name of the sample	True vertical depth (m)	Length (mm)
1	3H	XX61.59	82
2	4H	XX61.81	85
3	5V	XX62.05	83
4	41H	XX70.90	77
5	43H	XX71.34	76
6	46H	XX72.26	80
7	69H	XX77.61	71
8	71H	XX78.10	76
9	72V	XX78.27	70

Table 2: Details of Samples from WELL 1 of Baghewala field.

Sl. no	Name of the sample	True vertical depth (m)	Length (mm)
--------	--------------------	-------------------------	-------------

1	1-3H	X71.12	82
2	2-46H	X04.74	85
3	5-87H	X32.37	83
4	7-118H	X49.03	77
5	8-136H	X59.54	76

Table 3: Details of Samples from WELL 2 of Baghwala field.

3.1 WELL 1

The well WELL 1 was spudded on 18.1.2018 till a target depth of 1050 m. The different formation encountered in the well along with their lithology and description is mentioned in (Figure 5)..The depth structure map for the Jodhpur formation is presented in (Figure 5.) The well was drilled for the appraisal of Jodhpur formation.

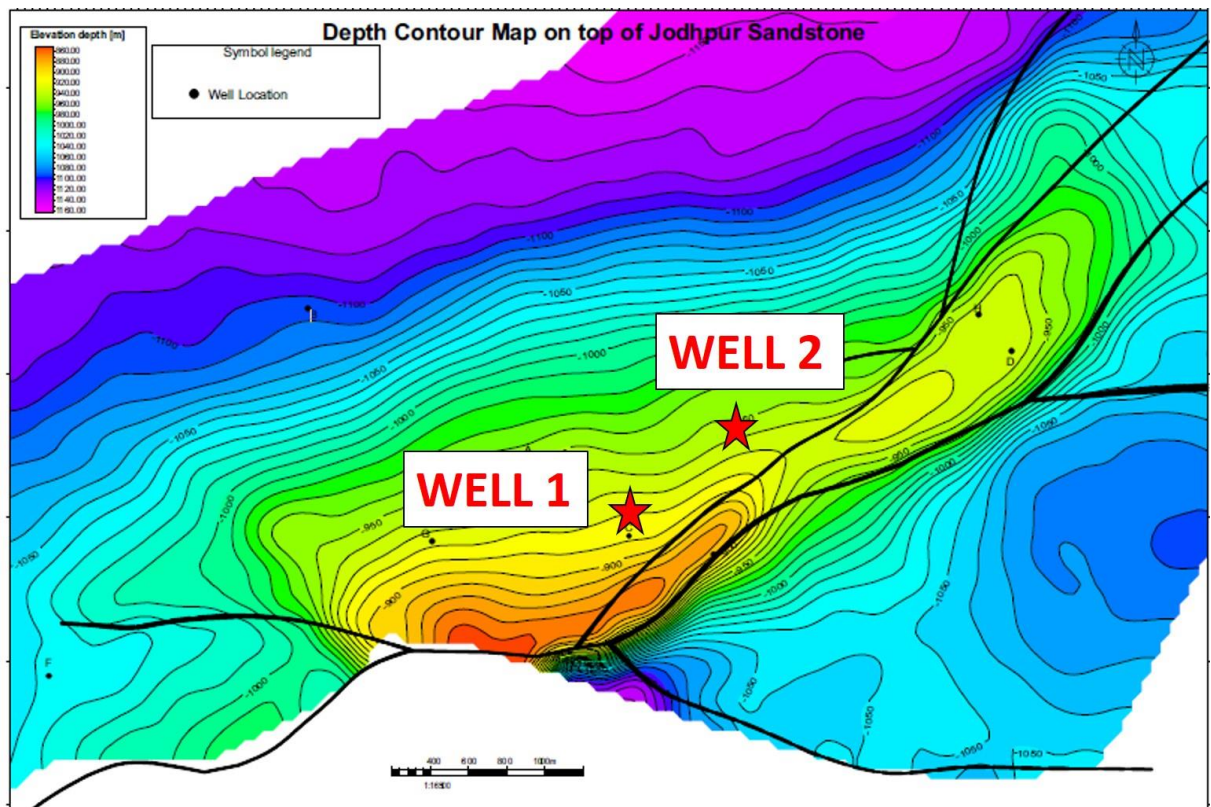


Figure 4 A depth structure map for Jodhpur formation top highlighting the two well (under red color) under study namely WELL 1 and WELL 2

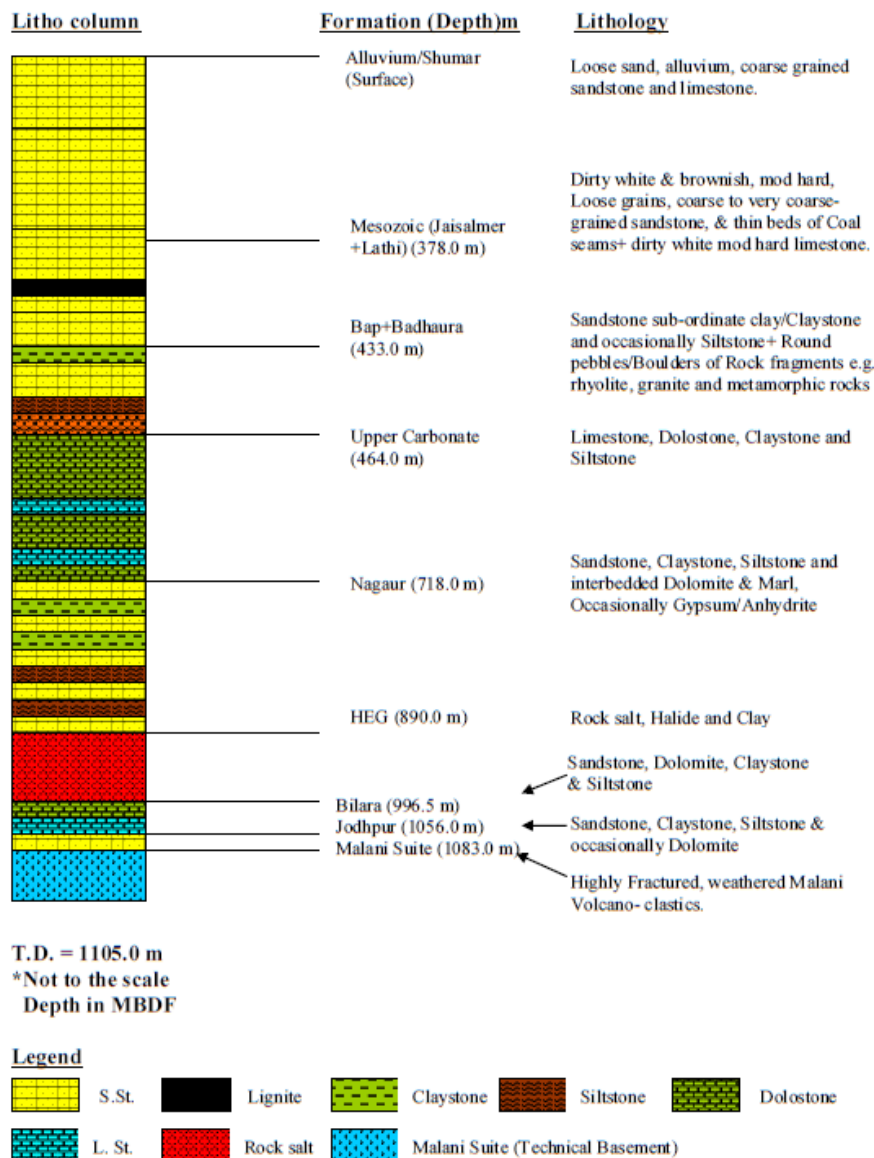
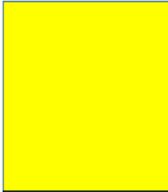












Figure 5 Lithological description from the well completion report WELL 1

3.2 WELL 2

The well WELL 2 was spudded on 15.8.2019 till a target depth of 734 m was reached. The litho-column of the well indicates different lithology and their description is mentioned in (Figure 6). The well penetrated the Upper Carbonate formation and was terminated there at 734 m only. The depth structure map of the Upper Carbonate formation is shown in (Figure 7). The core sample are provided from Upper Carbonate formation and are marked with depth in (Figure 8)

Lithology	Formation	Description
	Alluvium	Loose sand, alluvium, coarse grained sandstone and limestone
  	Jaisalmer + Lathi	Dirty white and brownish, moderately hard. Loose grain, coarse to very coarse grained sandstone. Thin bed of Coal seams with dirty white and moderately hard limestone.
   	Bap+Badhaura	Sandstone subordinate Clay/Claystone and occasionally Siltstone round pebbles boulders of rock fragments, rhyolite, granite and metamorphic rock
  	Upper Carbonate	Limestone, Dolostone, Claystone and Siltstone

Legend



Figure 6 Lithological description from the well completion report WELL 2

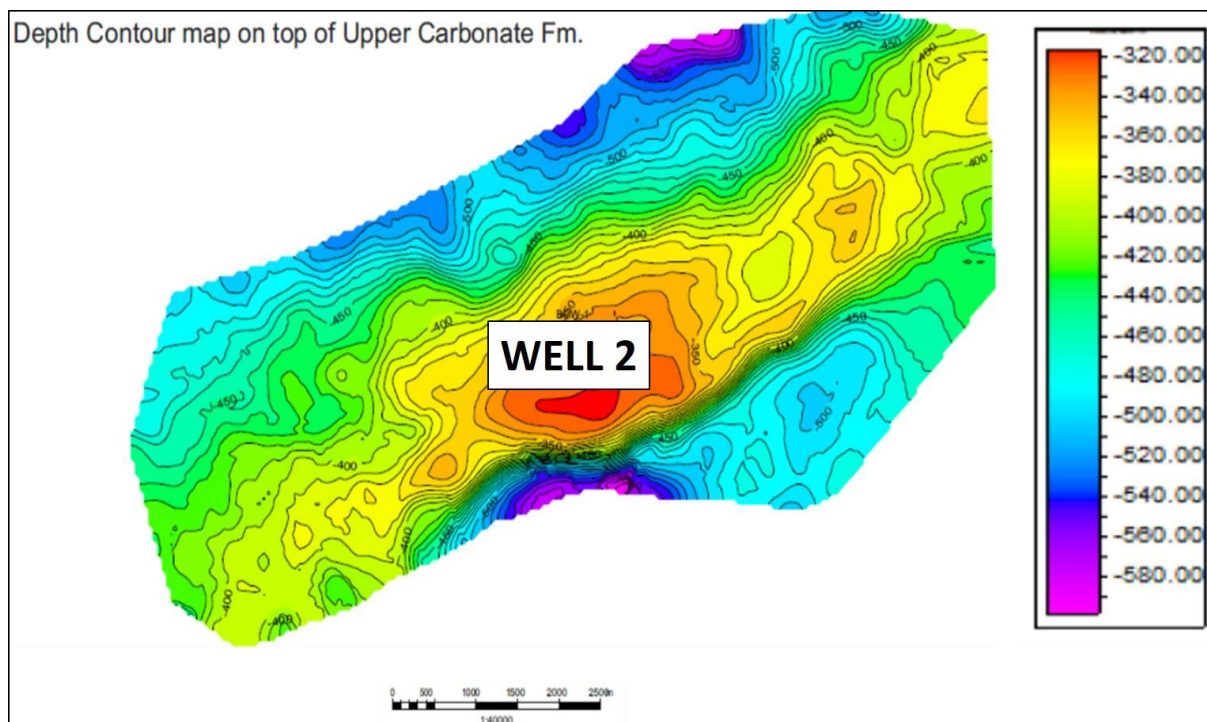


Figure 7 Depth structure for Upper Carbonate formation top with different wells annotated on it. The WELL 2 is marked at the centre.

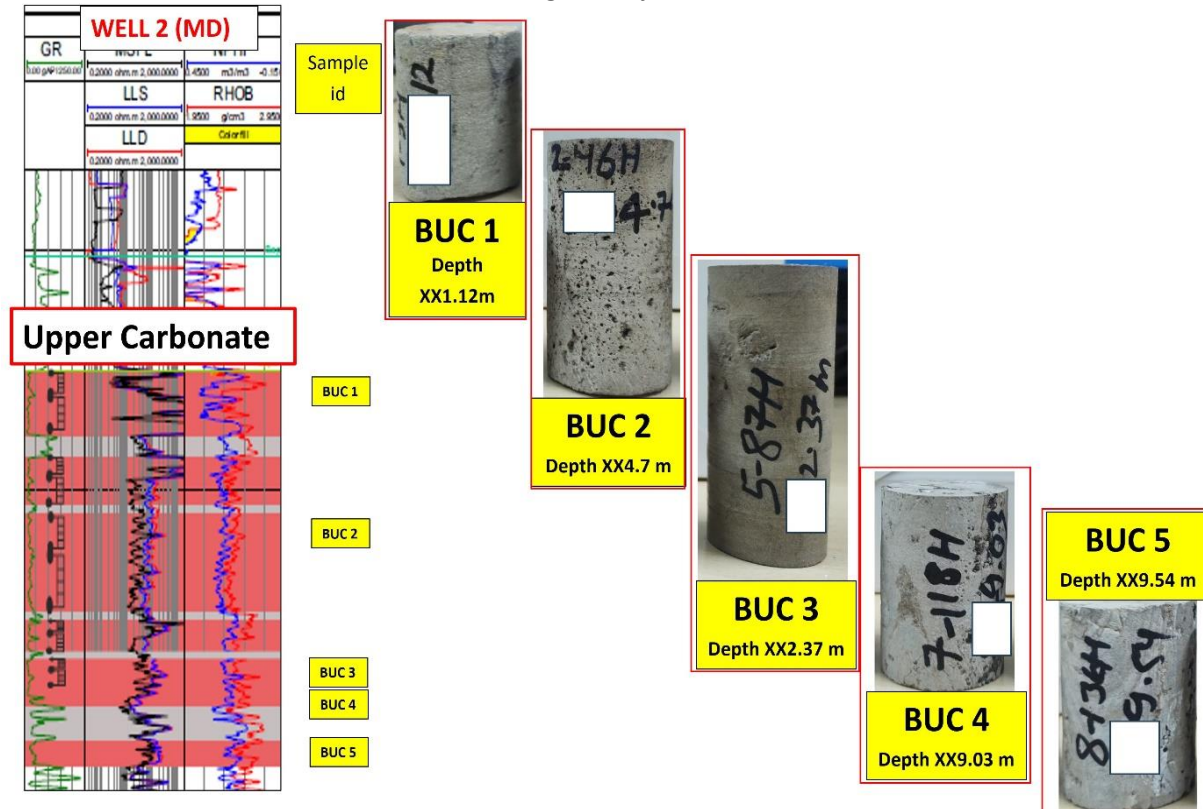


Figure 8. A brief layout of the core samples obtained along the WELL 2 well. The samples are marked from top to bottom and annotated in their respective image on the right.

4. Acoustic Measurements

The provided rock cores which were saturated with oil i.e no cleaning was done and core are in native state and have been tested for the p-wave (V_p) and s-wave (V_s) velocity under unconfined conditions for preliminary characterization. The results have been plotted with the depth of the samples which have been depicted in Figure 9

Measuring the shear wave velocity (V_s) and compressional wave velocity (V_p) of a rock core is a crucial aspect of rock mechanics and geophysics studies. This process involves subjecting the rock core to controlled stress conditions while recording the time it takes for both shear and compressional waves to travel through the material. V_s represents the speed of shear waves, which propagate perpendicular to the direction of the applied force, providing insights into the rock's resistance to deformation. On the other hand, V_p , the speed of compressional waves, indicates the rock's ability to transmit compressive forces. By carefully measuring V_s and V_p , various information viz. mechanical properties and structural characteristics of the rock core, behaviour under various conditions such as pressure and stress can be understood.

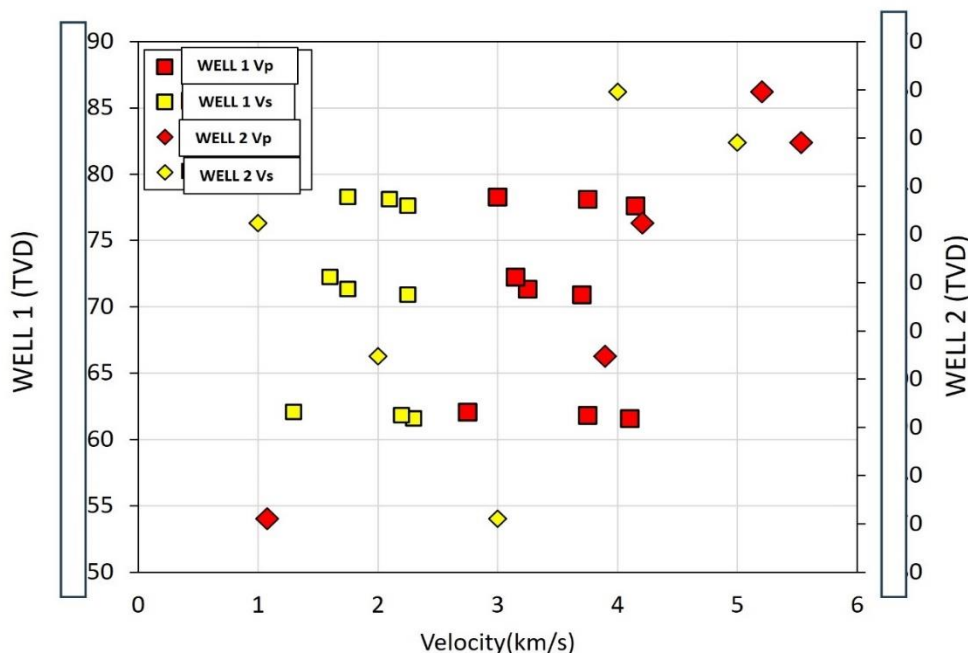


Figure 9 V_p and V_s variation for samples from WELL 1 and WELL 2 with reference depth

5. XRD analysis

For understanding the mineralogy of the core sample, XRD analysis was performed. The analysis was done using X' pert high score plus software.

S.No.	Compound name	Chemical Formula	Percentage (%)
1.	Silica	SiO_2	86%
2.	Orthoclase	KAlSi_3O_8	9%
3.	Others	-	5%

Table 4 Quantitative assessment of minerals present in sample BUC 1

S.No.	Compound name	Chemical Formula	Score	Percentage (%)
4.	Dolomite	CaCO_3	89	94
5.	Ankerite	$\text{Ca}(\text{Fe}^{++}, \text{Mg}, \text{Mn})(\text{CO}_3)_2$	25	4
6.	Otavite	CdCO_3	28	3

Table 5 Quantitative assessment of minerals present in sample BUC 2

S.No.	Compound name	Chemical Formula	Score	Percentage (%)
1.	Dolomite	CaMgCO_3	92	89
2.	Otavite	CdCO_3	32	6
3.	Ankerite	$\text{Ca}(\text{Fe}^{++}, \text{Mg}, \text{Mn})(\text{CO}_3)_2$	15	5

Table 6 Quantitative assessment of minerals present in sample BUC3

S.No.	Compound name	Chemical Formula	Score	Percentage (%)
-------	---------------	------------------	-------	----------------

1.	Dolomite	CaMgCO ₃	44	62
2.	Periclase	MgO	59	22
3.	Rhodochrosite		17	5

Table 7 Quantitative assessment of minerals present in sample BUC 4

S.No.	Compound name	Chemical Formula	Score	Percentage (%)
1.	Dolomite	CaMgCO ₃	44	81.2
2.	Magnesite	MgO	59	6.9%
3.	Others	-	17	11.9

Table 8 Quantitative assessment of minerals present in sample BUC 5

6. Modeling Methodology

The proposed methodology encapsulates a systematic process of quantifying the risk associated with CO₂ injection in Jodhpur and Upper Carbonate Formation in Baghewala Field, Bikaner Nagaur Basin, India (Figure 9). Initially, the structural geometry of each of the formations will be developed from the depth structure map available in the shared well reports of WELL 1 and WELL 2. This would serve as a 3D reservoir model for populating petrophysical properties and geochemistry studies. Further, the model will be developed for Geomechanical studies by incorporating mechanical properties such as (Youngs Modulus, Friction angle, Cohesion etc.) of the reservoir derived from the wireline logs, XLOTs, and Laboratory-based study from the core sample collected earlier. The mechanical properties of the overburden and under burden rocks would have an impact on the mechanical properties in the reservoir, which will have spatial and temporal variation inherent in them. We will use the Thermo-Hydro-Mechanical-Chemical (THMC) simulation available in the CMG GEM (Computer Modeling Group, Calgary, Canada) simulator for the numerical simulation. This simulator works on Finite element-based numerical simulation with two-way coupling to model changes in porosity and permeability with the variation in *in situ* stress due to CO₂ saturation and pore pressure changes in the reservoir. The boundary condition for the Geomechanical study would be constrained by overburden and underburden rocks. Further, the simulation results would be calibrated based on the existing stress regime; the unpragmatic results would indicate a modification in modeled mechanical property variation. Once a validation is established for the simulation study, a sensitivity analysis will be performed to indicate key parameters impacting the output. Accordingly, further prediction based on a suitable model validation would be proposed (Figure 10).

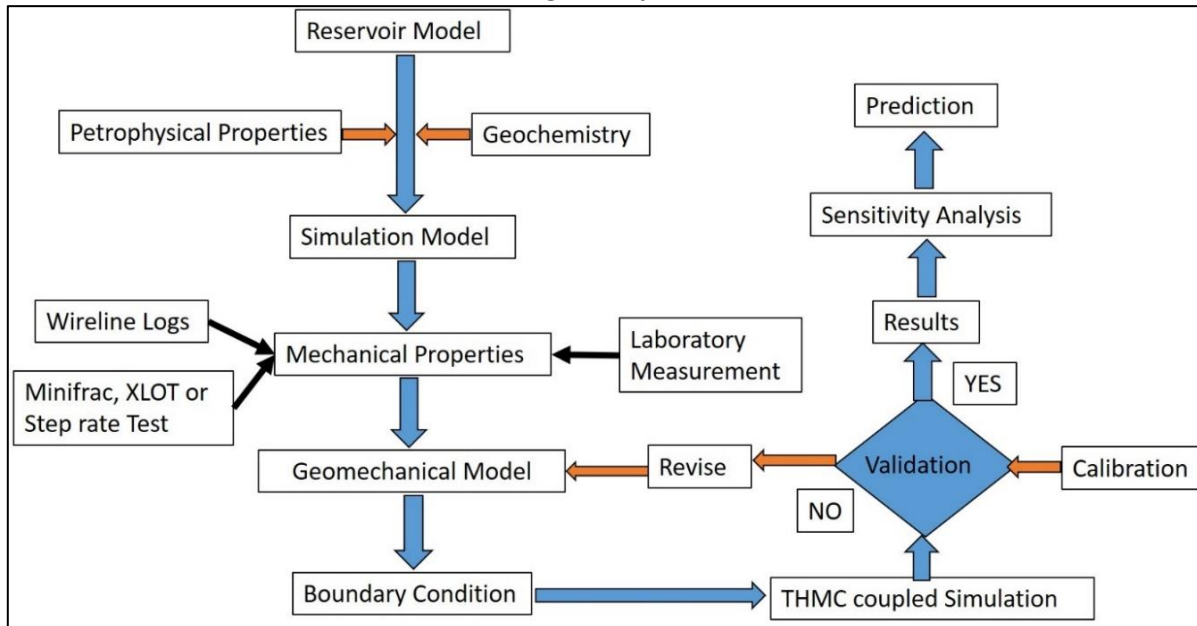


Figure 10 The workflow illustrating different components of a two-way coupled Geomechanical study to model risk associated with CO₂ injection in Baghewala Field, Bikaner Nagaur Basin, India.

7. Numerical Simulation

7.1 Homogenous Model

In the present work, the model thickness is based on the interpretation of the wireline log data provided by Oil India Limited. The GR log, along with the Mud logging data, clearly indicates the lithology which delineates the porous and impervious zone. Therefore, the thickness of the different formations initiating from Upper Carbonate at 464 m (tvd) till Malani suite at 1083 m (tvd) is ascertained (Figure 11). This enabled the determination of the thickness of different formations in the model to be studied. The lateral extent of the layer is, however, more significant than the vertical separation. Therefore, a limited lateral extent of 1km by 1km was selected to study the model behaviour.

The 3D reservoir model is discretized into 5000 (25 x 25 x 8) grid cells (lateral grid cells of 124 x 124 ft dimensions) with one injection well WELL 1 at its centre (Figure 12) operating at a bottom hole gas rate of 1000 ft³/day for an injection period of 15 years. The lateral boundary of the model is closed, representing a no-flow boundary condition. This allows reservoir pore pressure to reach a higher value in a shorter duration of time, as will be the case if a sealing fault or no flow boundary exists in the vicinity of the injection well. The injection pressure is chosen in such a way that no zone reaches the lithostatic gradient of 1psi/ft.

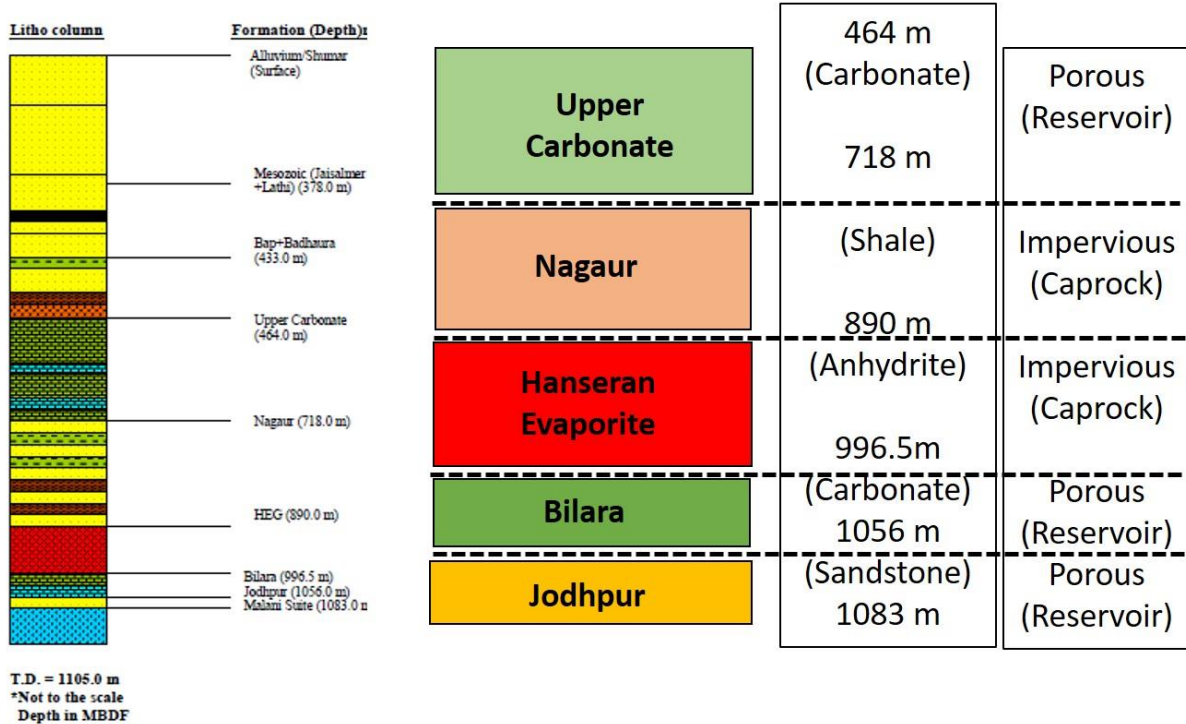


Figure 11 The model formulation for identifying the thickness of different formations along with storage type.

The fluid model was selected as compositional simulation model in CMG-GEM as the concentration of CO₂ may vary in gas and liquid phase. The Peng Robinson Equation of State is used to quantify the fluid properties of supercritical CO₂ at the reservoir condition. The rock fluid properties, such as the relative permeability curve are adopted from (Zheng et al., 2023), where the Jodhpur and Bilara formation is treated as reservoir rock type and the above formations Hanseran evaporite and Nagaur formation as Caprock, and their relative permeability data are selected from shale rock type (Zheng et al.,2023). The initial pressure condition in the model is set as 1600 psi for 3000 ft in accordance to pore pressure gradient of (0.43 psi/ft). For the injection schedule, only the Jodhpur formation is selected as the zone of injection as we wish to study the CO₂ migration in both the Bilara and Jodhpur formations, and the buoyancy effect of supercritical CO₂ would cause the spreading of the CO₂ zone in an upward direction and spatially spreading with the passage of time. In total three difference cases are studied, in accordance to the different grid refinement in Jodhpur and Bilara formation grid blocks. In total, 3 cases are modeled and studied; the details of the model are mentioned below.

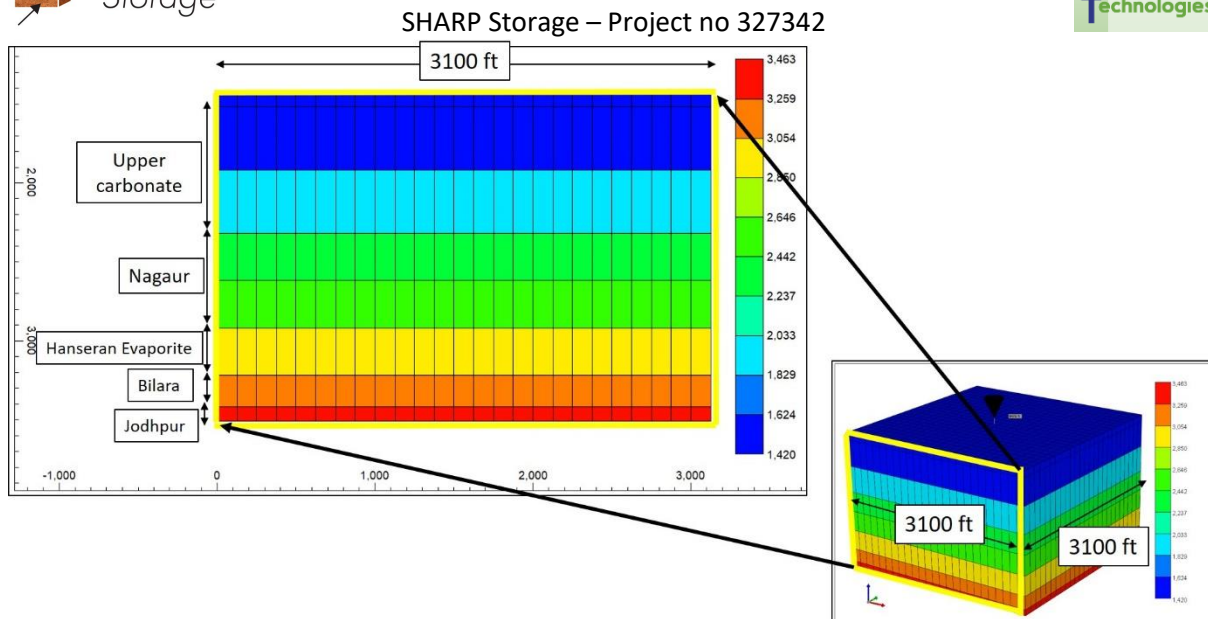


Figure 12 The schematic diagram describing the different formations thickness and their discretization in the cross sectional view.

In case A, 25 x 25 grid matrix with injection well WELL 1 at centre are refined, the Bilara and Jodhpur formation grid blocks are split into 2 each in i, j and k direction, resulting in dimensions of 62.5 x 62.5 x 100 ft (I x j x k) in Bilara formation, and 62.5 x 62.5 x 45 ft(I x j x k) in Jodhpur formation respectively.(Figure 13)

Similarly, in Case B, grid refinement is done in Jodhpur formation layers, the 3 x 3 grid matrix in Jodhpur formation and the 11 x 11 grid matrix with injection well WELL 1 at the center are refined in Bilara formation is refined, the dimensions of grid blocks in Bilara formation is 62,5 x 62.5 x 50 ft (i x j x k) and in Jodhpur formation is 62.5 x 62.5 x 45 ft (i x j x k) (Figure 14).

In case C, 3 x 3 grid matrix in Jodhpur formation and 19 x 19 grid matrix with injection well WELL 1 at the center are refined in Bilara formation, the dimensions of grid blocks in Bilara formation is 62,5 x 62.5 x 66.6 ft (i x j x k) and in Jodhpur formation is 62.5 x 62.5 x 45 ft (I x j x k). .(Figure 15)

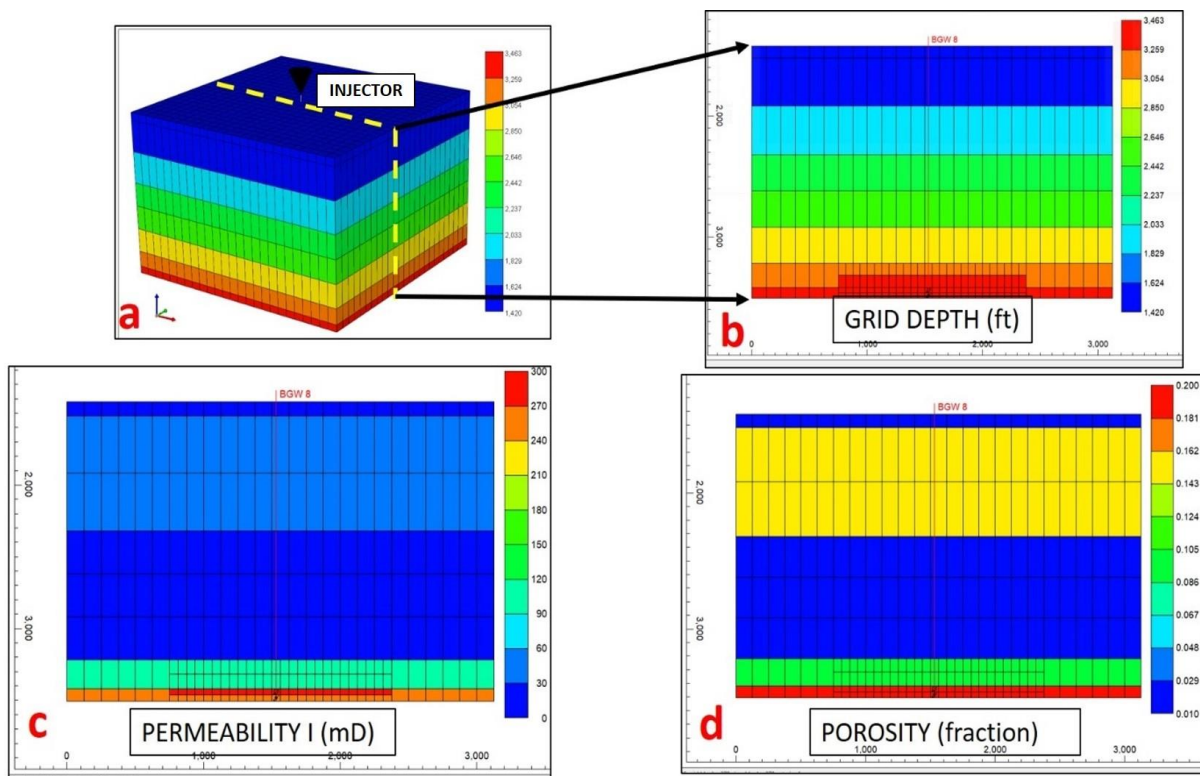


Figure 13 The schematic description of the grid block modification for Case A. The corresponding distribution in a) 3d reservoir grid properties such as b) Grid Depth (ft), c) Permeability (mD) and d) Porosity (Fraction).

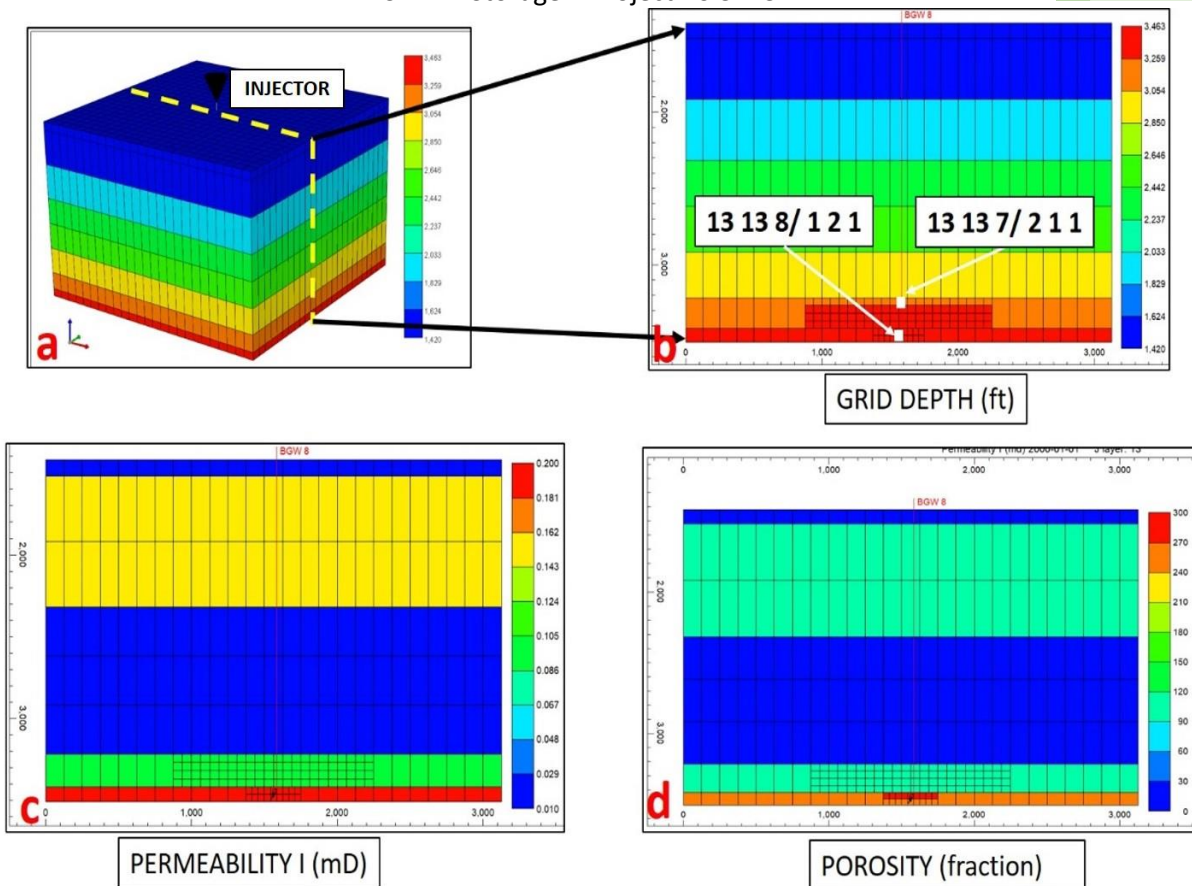


Figure 14 The schematic description of the grid block modification for Case B. The corresponding distribution in a) 3d reservoir grid properties such as b) Grid Depth (ft), c) Permeability (mD) and d) Porosity (Fraction). The two grid blocks selected for exhibiting the variation in these properties is also displayed.

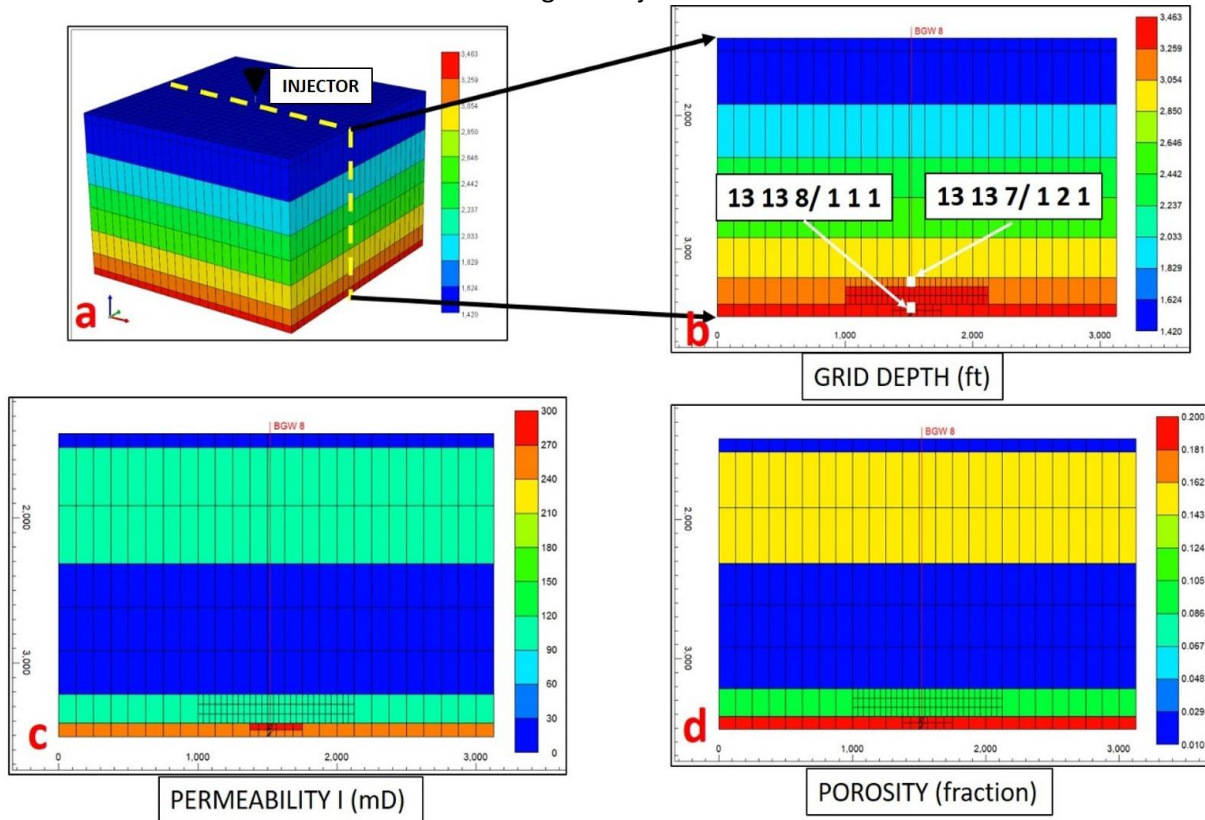


Figure 15 The schematic description of the grid block modification for Case C. The corresponding distribution in a) 3D reservoir grid properties such as b) Grid Depth (ft), c) Permeability (mD) and d) Porosity (Fraction). The two grid blocks selected for exhibiting the variation in these properties is also displayed.

7.2. Results

The simulation of the CO₂ injection in the three different cases is performed to model the spatial variation of Gas saturation and Pressure change in the closed boundary model condition. The CO₂ gas injection in the brine-saturated Bilara and Jodhpur formation leads to upward migration due to density difference in gas and brine. This behaviour of buoyancy driven movement of CO₂ is modelled for bottom-hole injection rate of 1000 ft³ /day , 750 ft³/day and 500 ft³/day respectively. The injection of CO₂ is initiated at the Jodhpur formation and the relative spread of CO₂ plume was visualized in the Bilara and Jodhpur formation. The upward movement of CO₂ is restricted due to presence of impervious Hanseran evaporite and Nagaur formation. This is collectively modelled as thick caprock of 912 ft evaluated from the wireline analysis of INJECTOR well marked by white dotted line in simulation schematic results for all the cases.

7.2.1 CASE A

For the Case A, Figure 16 displays the variation in gas saturation in the grid block (13 13 7/ 111) located in Bilara Formation just below Hanseran Evaporite and grid block (13 13 8/ 121). The gas saturation increased in the grid block (13 13 8/ 121) during the injection period of 15 years to 0.8 for all the injection rates and then it decreased as the injection well is shut in for the remaining 35 years of the observation period. However, grid block (13 13 7/ 111) didn't observe any gas saturation change till late 2003 for all the injection rates which then increased to 0.4 at the end of 50 years of simulation period (Appendix A.1.1 to A.1.9). The pressure response for the grid block(13 13 7/ 111) is shown in (Figure 16). as it is most critical being below caprock and vertically above the injection point. The pressure at the end of 15 years of injection is observed to be highest for the rate of 1000 ft³/day being 3218 psi followed by 2865 psi for 750 ft³/day and lowest at 2552 psi for 500 ft³ /day.(Figure 17). The highest pressure value in all the simulated injection rates is well below the assumed fracture gradient of 1 psi/ft.

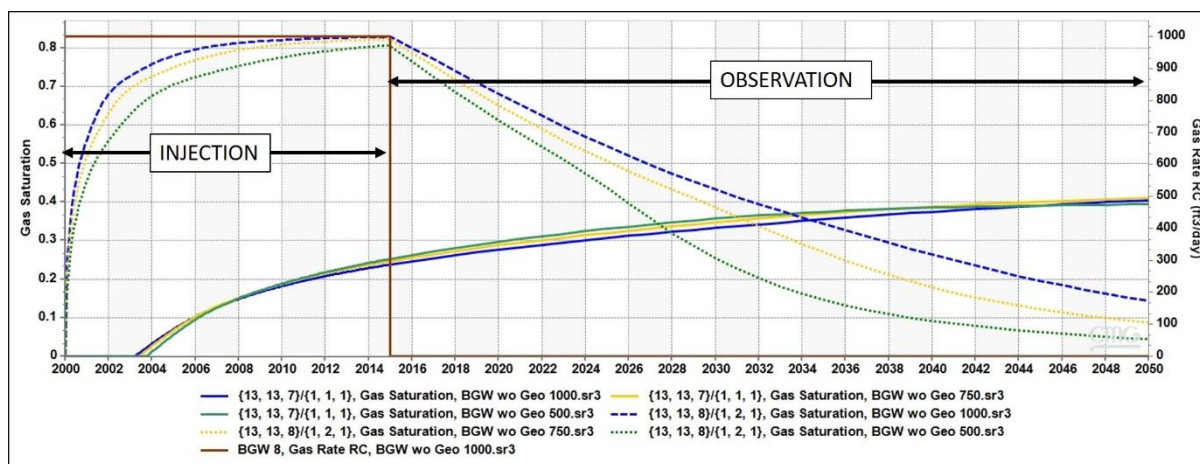


Figure 16 The plot between Gas saturation as a function of time for Case A. The plot include variation in gas saturation for two grid blocks (13 13 7/ 111) located in Bilara Formation just below Hanseran Evaporite and grid block (13 13 8/ 121) located in Jodhpur Formation one of the injection points for CO₂. The blue curve (Solid and Dotted) represents response from 1000 ft³/day, yellow curve (Solid and Dotted) from 750 ft³/day, and the Green curve (Solid and Dotted) from 500 ft³/day injection rates in the studied model.

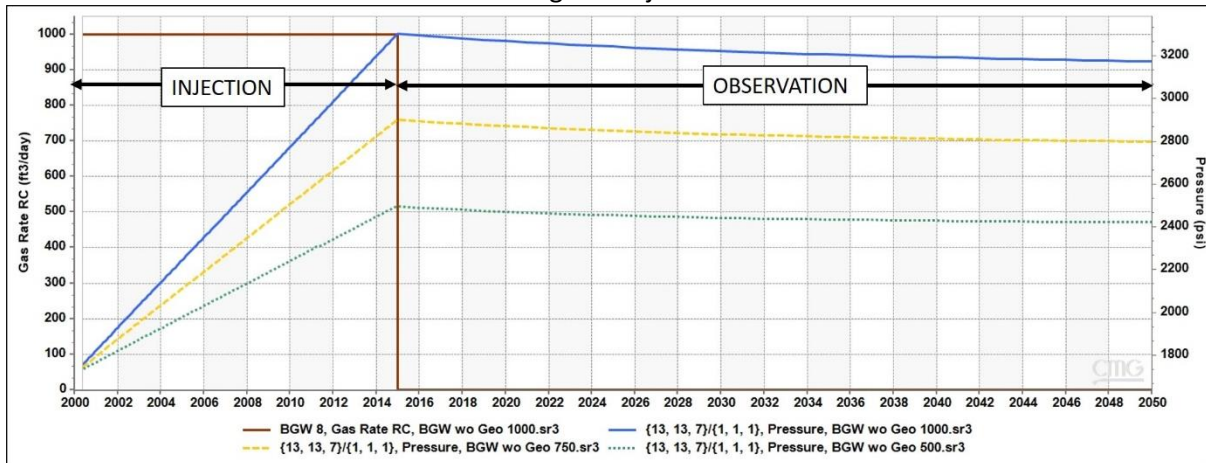


Figure 17 The plot between Pressure as a function of time for Case A. The plot includes variation in gas saturation of grid block (13 13 7/ 111) for different CO₂ injection rates. The blue curve (Solid) represents the response from 1000 ft³/day, the yellow curve (Dotted) from 750 ft³/day, and the Green curve (Dotted) from 500 ft³/day injection rates in the studied model.

7.2.2 CASE B

For the Case B, the Figure 18 displays the variation in gas saturation in the grid block (13 13 7/ 211) located in Bilara Formation just below Hanseran Evaporite and grid block (13 13 8/ 221). The gas saturation increased in the grid block (13 13 8/ 121) during the injection period of 15 years as in Case A to 0.8 for all the injection rates. After the injection ceased the gas saturation decreased to comparably similar values to Case A but the trend in decline is different to Case A where a constant decline is observed. In this Case, a stabilize decrease followed by sharper decrease then again a stable rate of decrement in observed. The grid block (13 13 7/ 211) as in Case A didn't observed any change in initial stage of injection, in this case gas saturation increased after 2008 (nearly after 8 years of injection) .(Figure A.2.1 to A.2.9). The final gas saturation for all the injection rates is similar to the value of 0.4 as in Case A. The pressure response in the grid block (13 13 7/ 211) at the end of 15 years of injection is observed to be highest for the rate of 1000 ft³/day being 3135 psi followed by 2829 psi for 750 ft³/day and lowest at 2452 psi for 500 ft³ /day(Figure 19). The highest pressure value in all the simulated injection rates is below the assumed fracture gradient of 1 psi/ft.(Figure 23 to 31).

SHARP Storage – Project no 327342

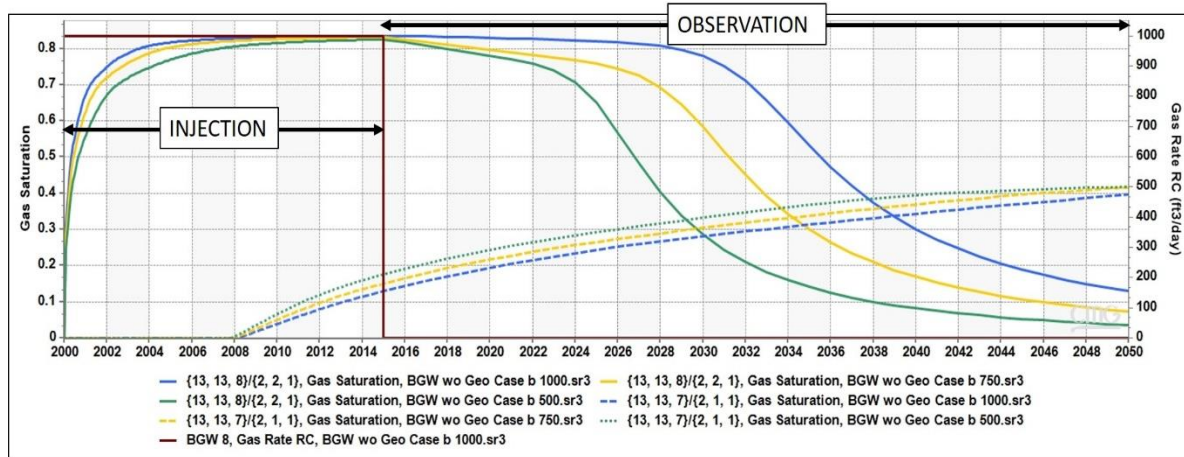


Figure 18 The plot between Gas saturation as a function of time for Case B. The plot includes variation in gas saturation for two grid blocks (13 13 8/ 221) and grid block (13 13 7/ 211) for three different CO₂ injection rates. The blue curve (Solid and Dotted) represents response from 1000 ft³/day, yellow curve (Solid and Dotted) from 750 ft³/day and the Green curve (Solid and Dotted) from 500 ft³/day injection rates in the studied model.

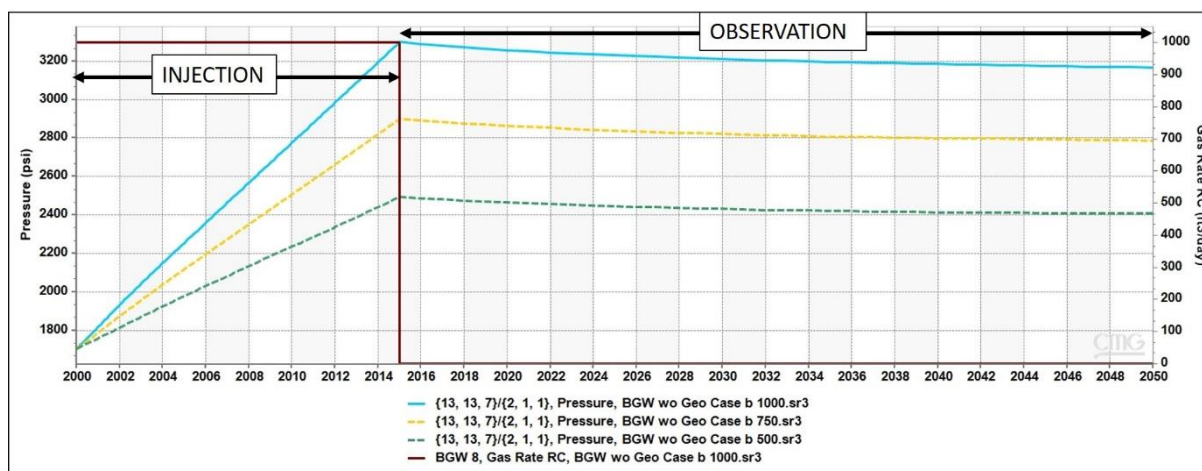


Figure 19 The plot between Pressure as a function of time for Case B. The plot includes variation in gas saturation of grid block (13 13 7/ 111) for three different CO₂ injection rates. The blue curve (Solid) represents the response from 1000 ft³/day, the yellow curve (Dotted) from 750 ft³/day, and the Green curve (Dotted) from 500 ft³/day injection rates in the studied model.

7.2.3 CASE C

In the Case C, the plot between gas saturation and time is shown in (Figure 20). The plot displays gas saturation in the grid block (13 13 7/ 121) located in Bilara Formation and grid block (13 13 8/ 111). Similar to Case A and B, the gas saturation increase during the CO₂ injection phase but the rate of increase is proportional to injection rates and only scenario of 1000ft³/day yield a gas saturation of 0.8, while 750 ft³/day and 500 ft³/day results in the value

of 0.7 and 0.62 respectively. After the injection period, the similar trend of gas saturation decrease is also observed here and a relatively lower gas saturation (<0.1) is reached for all the injection rates. The grid block (13 13 7/ 121) has a dissimilar increase in relation to Case A and B, where injection rate 1000 ft³/day and 500 ft³/day observes the gas saturation change in 2005 while 750 ft³/day scenario display saturation later in 2008 (Figure A.3.1 to A.3.9). The saturation at the end of the observation period is 0.4 which resembles the scenario in Case A and B too. The pressure in grid block grid block (13 13 7/ 121) is highest at the end of injection period of 15 years, the value of pressure response is 3367 psi for the injection rate of 1000ft³/day , 2953 psi for 750ft³/day and 2581 psi in 500 ft³/day(Figure 21). The pressure corresponding to 1000ft³/day is above the 1 psi/ft fracture gradient hence it may cause failure in the injection zone therefore a lower injection rate in this scenario will yield a sustainable result. (A).

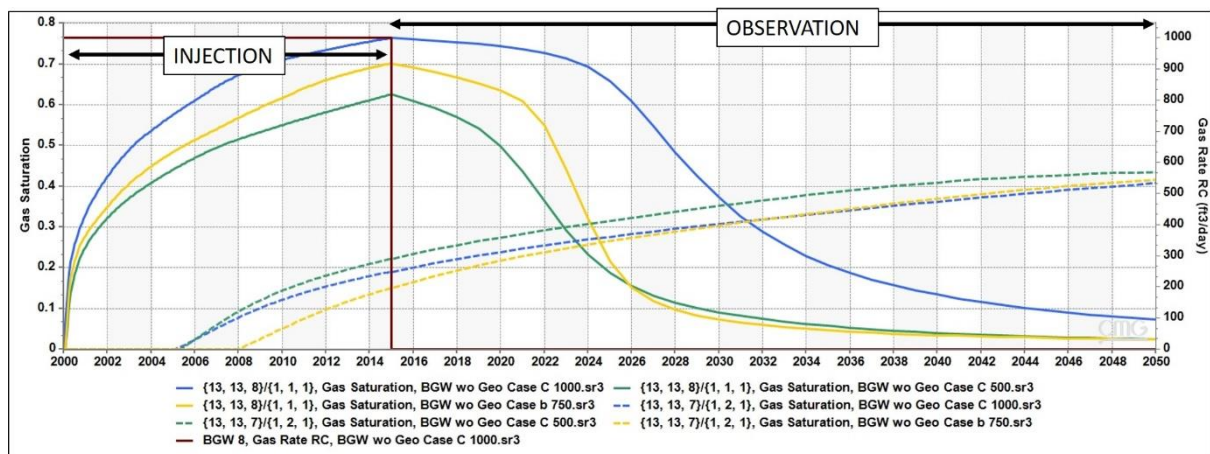


Figure 20 The plot between Gas saturation as a function of time for Case C. The plot include variation in gas saturation for two grid blocks (13 13 8/ 111) and grid block (13 13 7/ 121) for three different CO₂ injection rates. The blue curve (Solid and Dotted) represents response from 1000 ft³/day, yellow curve (Solid and Dotted) from 750 ft³/day and the Green curve (Solid and Dotted) from 500 ft³/day injection rates in the studied model.

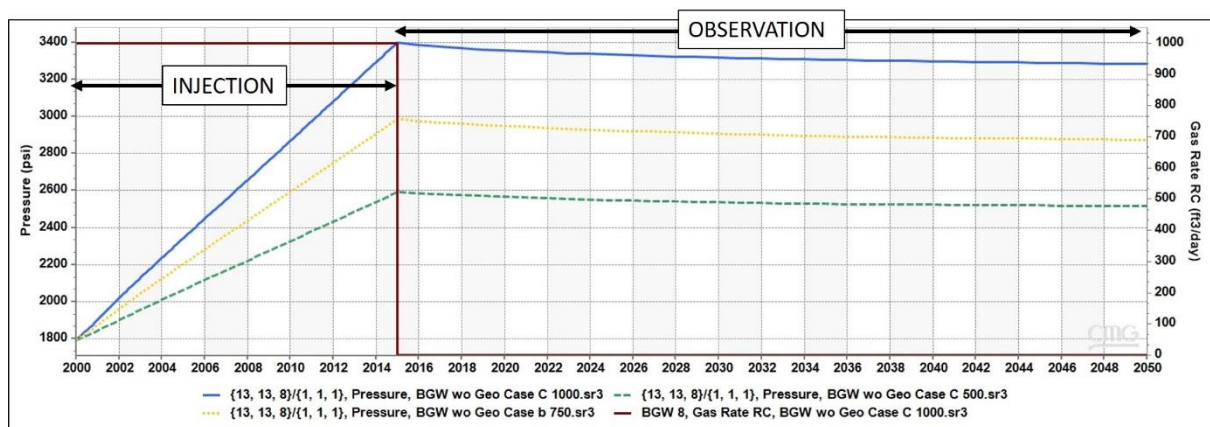


Figure 21 The plot between Pressure as a function of time for Case C. The plot includes variation in gas saturation of grid block (13 13 7/ 111) for three different CO₂ injection rates. The blue curve (Solid) represents the response from 1000 ft³/day, the yellow curve (Dotted) from 750 ft³/day, and the Green curve (Dotted) from 500 ft³/day injection rates in the studied model.

7.3 Field Case

The Field Case model is formulated based on the Depth Structure map for the Jodhpur Formation provided in the well completion report for WELL 1 well. The equivalent 3D model is generated in the CMG software to have a representative simulation model(Figure 22). The model parameters and corresponding statistics are provided below

Sr no	Property	Value
1	Grid Dimension (ni*nj*nk)	162*63*12
2	Grid Thickness(m)	4 to 5
3	Porosity	(0.01 to 0.24)
4	Permeability	(0.01 mD to 350 mD)
5	Water Saturation	100%
6	Initial Pressure	11000 kPa at 1000m
7	Injection Rate	500 m ³ /day for 15 Years

Table 9. The basic parameter related to the Field Case model generated in the CMG software.

The petrophysical input is obtained from the well reports and wireline log data.

SHARP Storage – Project no 327342

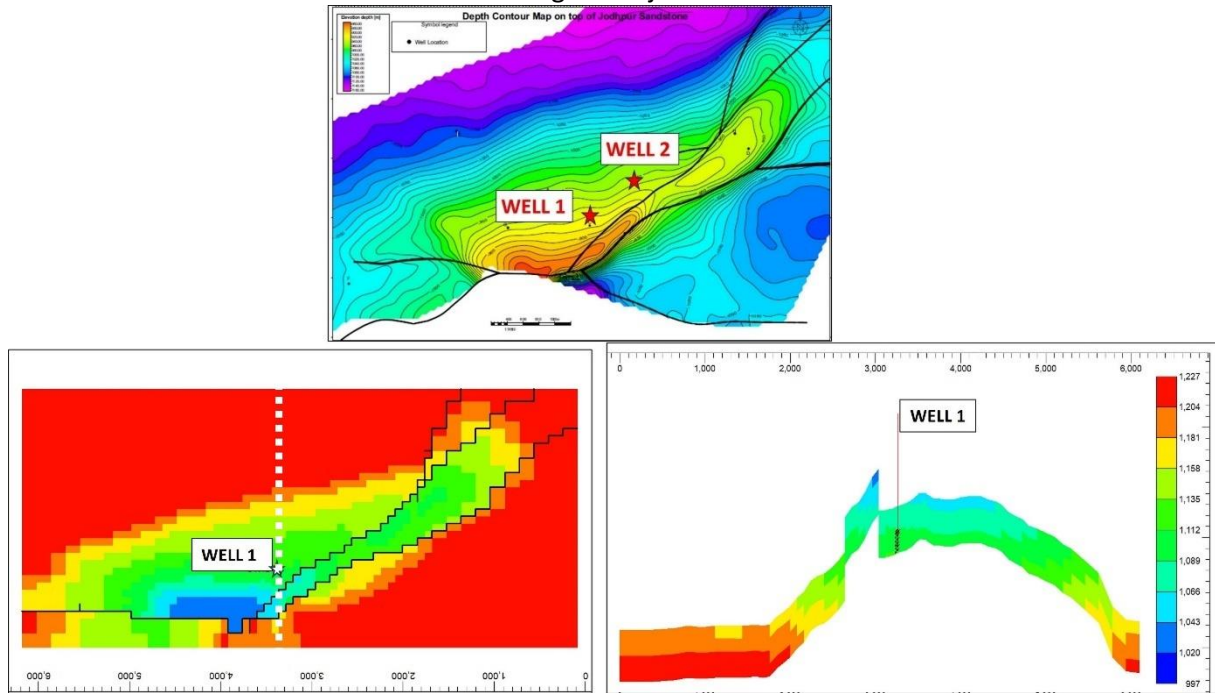


Figure 22 A base map illustrating the depth variation on Jodhpur formation top, below are the equivalent field scale numerical model discretized in rectangular grid system viewed in aerial and cross sectional view.

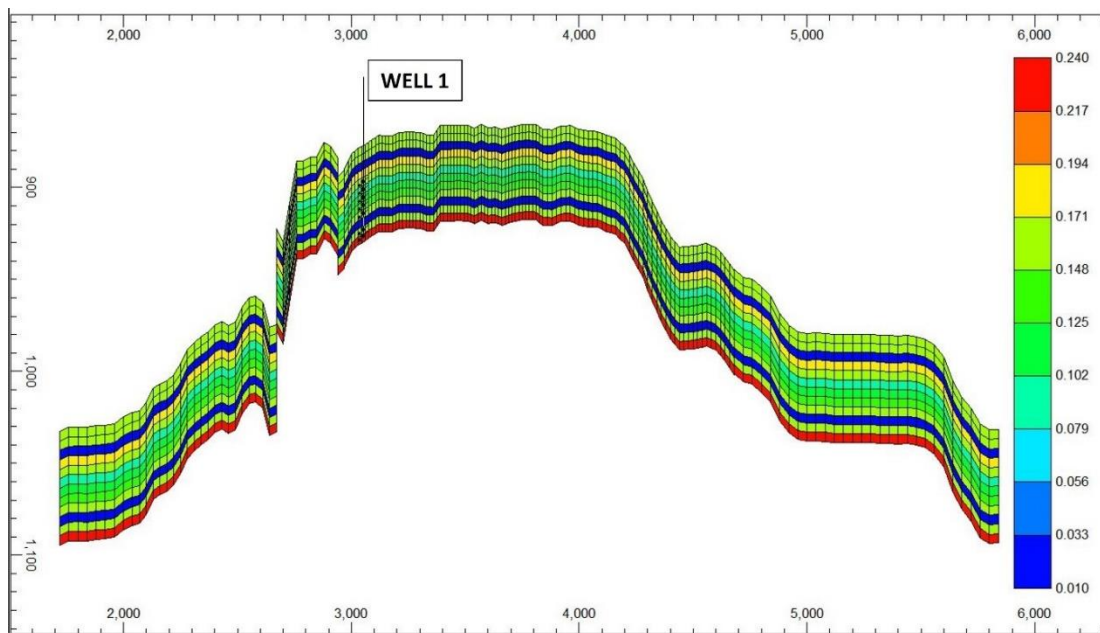


Figure 23 A cross sectional profile for the field scale model at slice J=53, where the injector well WELL 1 is located. The colour indicates the porosity range from 0.01 to 0.24

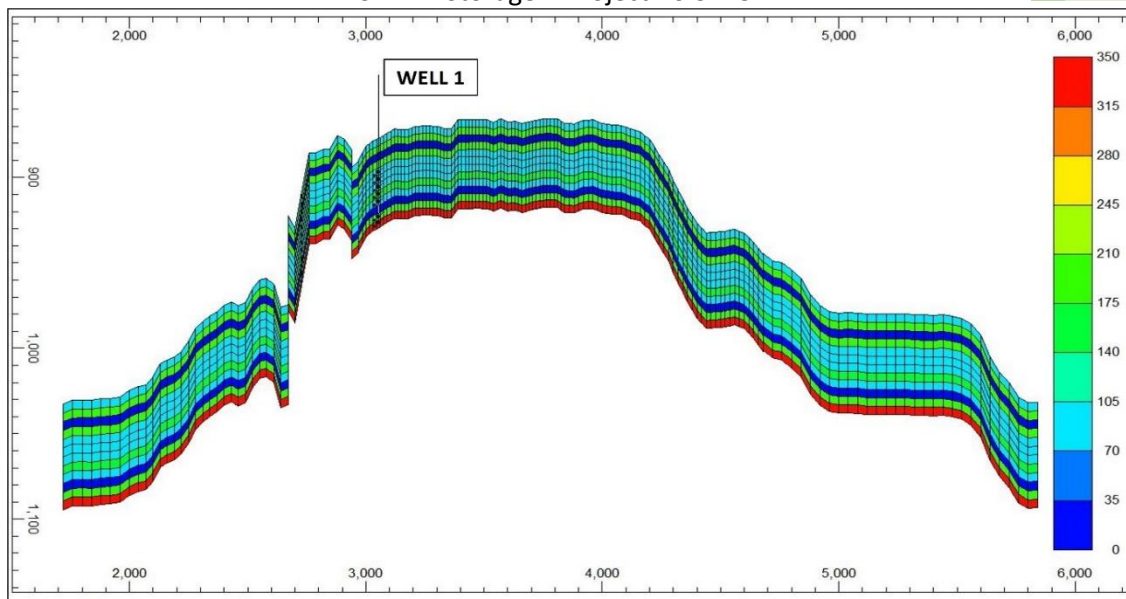


Figure 24 A cross-sectional profile for the field scale model at slice J=53, where the injector well WELL 1 is located. The colour indicates the permeability value range from 0.01mD to 350mD.

The petrophysical properties such as porosity and permeability are based on the information obtained from the wireline logging data and well information from reports. Due to the unavailability of details of other well existing in the field, the proposed model is a layer cake type where the properties remain uniform through the stratigraphy layers (Figure23 and 24).

7.3.1 Result

The simulation run for spatial evolution of the CO₂ saturation is performed in two phase, initial phase being injection for a duration of 15 years, the second phase where the up dip CO₂ saturation movement is visualized for remaining 35 years . In order to track the hydrodynamic trapping comprising of structural, residual and dissolution trapping due to CO₂ injection in the fluid saturated media, three case were simulated considering hysteresis and solubility during CO₂ injection. A time-apse spatial evolution of CO₂ saturation and pore pressure is shown in Figure B.1 to B.12

The Figure 25 shows the CO₂ saturation portioned under supercritical, residual and dissolution phase for the three different case earlier discussed. The hysteresis and solubility phenomenon are determining factor after structural trapping. The comparative analysis for either cases is presented in (Figure X). The dissolution has a lower cumulative supercritical CO₂ molar

volume than hysteresis while only dissolved CO₂ molar volume is observed in this case. Also the trapping due to residual CO₂ saturation is relatively more in the hysteresis case.

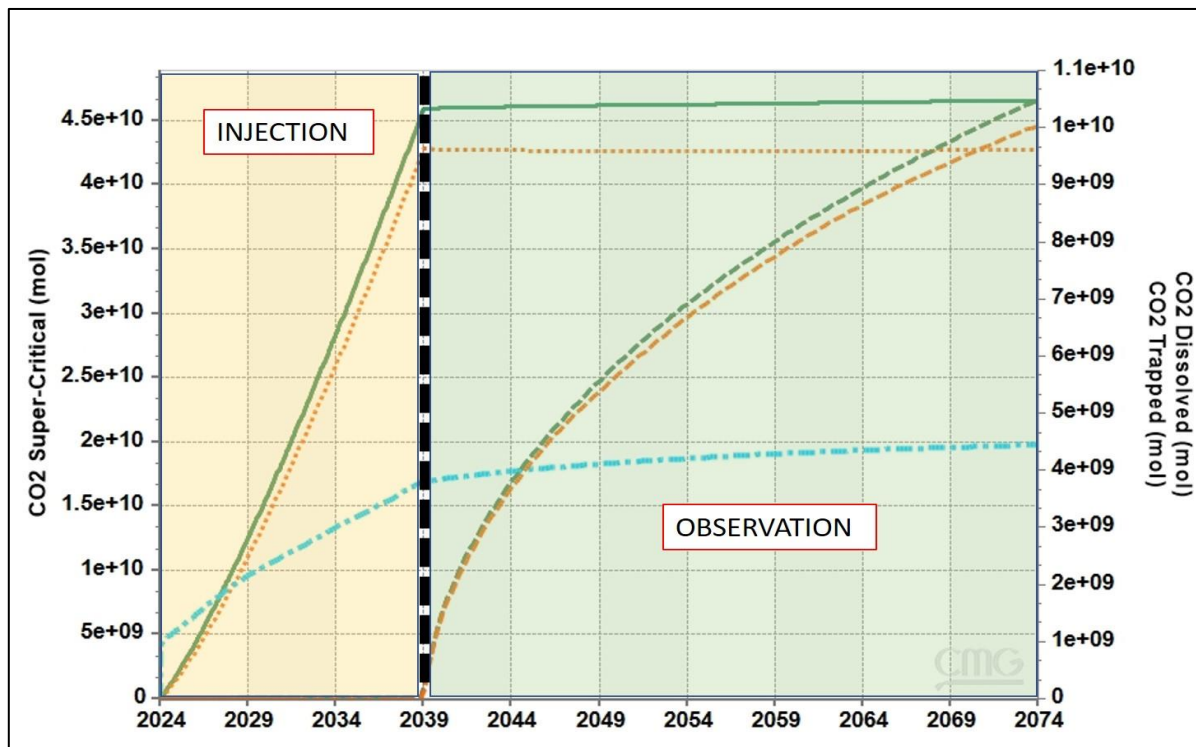


Figure 25 A plot describing the molar volume of CO₂ in supercritical, dissolved, and trapped volume for two different case of hysteresis and hysteresis and solubility. The green curve indicates the with hysteresis study while the orange curve with hysteresis and solubility. The blue stippled curve describes the dissolved Co₂ in with hysteresis and solubility case. The trapped CO₂ volume is observed after end of injection period at 15 years and marked by dotted curve after year 2039

8 Geomechanical Assessment

The Geomechanical characteristic is obtained from Sonic log (Compressional and Shear wave) in the wireline log suite. The elastic properties of the rocks can be correlated with the speed with which sound propagates in them. Using this various correlations are proposed by reseachers (Zoback,2007).The mechanical properties evaluated are Youngs Modulus, Bulk Modulus, Shear Modulus,Poisson Ratio (Figure 26 and 27) and their empirical relation are mentioned below

$$E = \frac{\rho V_s^2 (3V_p^2 - 3V_s^2)}{(V_p^2 - V_s^2)}$$

$$G = \rho V_s^2$$

$$K = \rho \left(V_p^2 - \frac{4}{3} V_s^2 \right)$$

$$v = \frac{(V_p^2 - 2V_s^2)}{2(V_p^2 - V_s^2)}$$

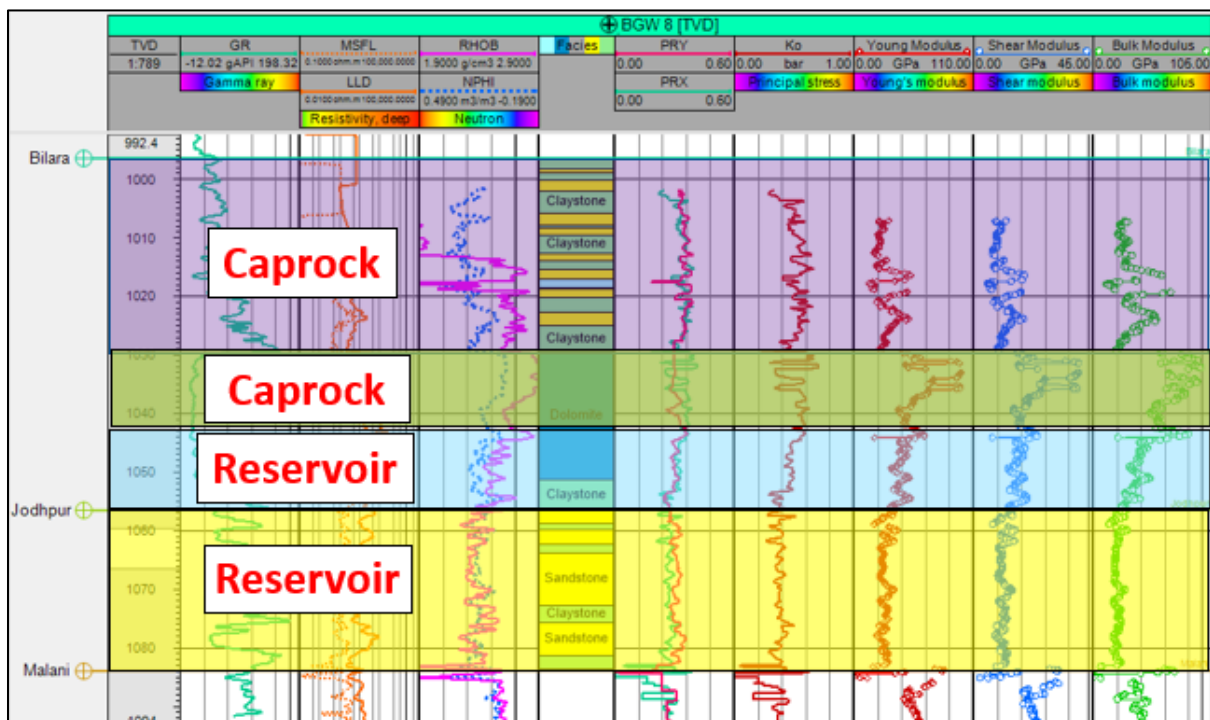


Figure 26 A 1D geomechanical model generated for WELL 1, the evaluated Young Modulus, Poisson Ratio, Shear Modulus, Bulk Modulus. The different zones in the Bilara and Jodhpur formation are classified under Caprock and Reservoir based upon the storage potential linked to the facies present. The geomechanical properties are in agreement where the caprock zones demonstrate a higher strength modulus than reservoir.

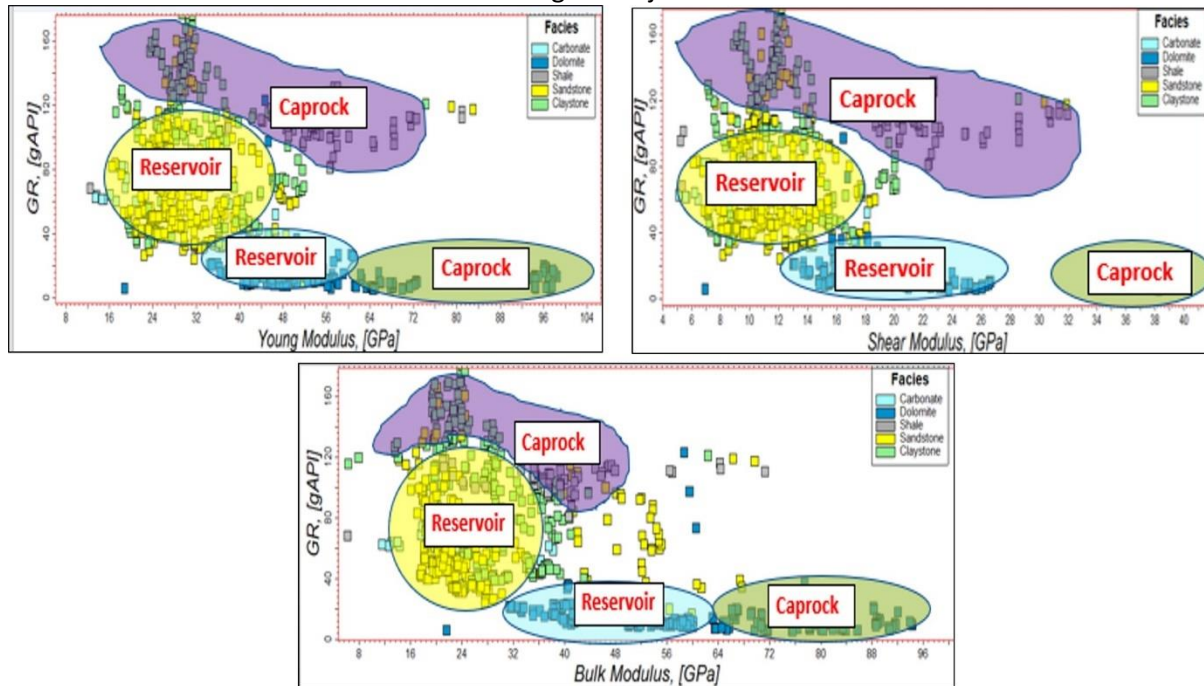


Figure 27 A cross plot between wireline log GR and evaluated geomechanical property Young Modulus, Bulk Modulus, Shear Modulus with Facies property colour coding the data points. The different region of Caprock and Reservoir zones are marked on the crossplot demarcating property in the respective region

Geomechanical Parameters		Site Characterization Data
Caprock 1(Nagaur and HEG)	E=NA G=NA K=NA μ =NA	No data
Caprock 2 (Bilara Claystone)	E= 24GPa G= 9GPa K=21GPa μ =0.34	Borehole Wireline Data

Caprock 3 (Bilara Dolomite)	E= 90GPa G= 40GPa K=73GPa $\mu=0.36$	Borehole Wireline Data
Reservoir(Bilara Dolomite)	E=44GPa G=16GPa K=43GPa $\mu=.3$	Borehole Wireline Data
Reservoir (Jodhpur)	E=28GPa G=10GPa K=21GPa $\mu=0.28$	Borehole Wireline Data

Table 10 A Geomechanical assessment for identifying the Storage Readiness Level based on the information from WELL 1

9. Conclusion

Based on the progress till now, following inferences can be deduced

- The Jodhpur formation may act as a storage unit for prospective CO₂ injection. This is primarily due to good storage and flow potential and is overlain by a thick (180 ft) deposit of carbonates of Bilara formation. Further to restrict the upward migration of CO₂ a substantially thick (900 ft) impermeable salt and shale of the Hanseran and Nagaur formations exist.
- The CO₂ injection response obtained from field scale simulation indicates larger trapped CO₂ saturation in structurally high faulted region. This may suggest effective containment of CO₂
- The simulation study provides encouraging results that proposes further study to understand geomechanical challenges with CO₂ injection. Geomechanical Modeling based stress behavior would give more pragmatic outcome.

The study provides insight in the identification of probable storage complex and geomechanical assessment for CCS application in Baghewala Field, Bikaner Nagaur Basin, India. The storage and monitoring zones needs to further studied for containment and integrity for CO₂ storage. The numerical simulation for CO₂ injection in the studied field provides key information regarding the spatio-temporal evolution of CO₂ plume and the corresponding change in pore pressure. In context to geomechanical characterization, the wireline-based mechanical properties estimation would be helpful in delineating zones of probable failure and understanding the stress behavior changes due to CO₂ injection. Though the due to limited availability of the field data set a calibration and validation of the mechanical properties was not performed. However, this work would serve as a good indicator for preliminary study for understanding the feasibility of CO₂ injection in the Baghewala Field, Bikaner Nagaur Basin, India.

Disclaimer

The discussed work has been done to have a preliminary understanding of CO₂ sequestration in Baghewala Field, Bikaner Nagaur Basin with certain necessary assumptions. The key points of which are discussed below:-

1. The Model parameter such as permeability assumed in the numerical simulation study are pragmatic estimates but doesn't represent the property distribution in field as whole
2. The Geochemistry study was not conducted hence no Mineralogy effect is included in CO₂ saturation simulation.
3. The fault modelled in the field scale model is mere representation of Depth structure map and no fault leakage or stability analysis is conducted to study the effect of fault on CO₂ flow migration.
4. No sensitivity study has been conducted to study the interdependency of model parameters.

References

Al-Husseini M.I.,(2000), Origin of the Arabian plate structures: Amar collision and Najd Rift. *Geo Arabia* 5:527–542

Cozzi A, Rea G, Craig JJ, (2012), From Global Geology to Hydrocarbon Exploration: Ediacaran – Early Cambrian Petroleum Plays of India, Pakistan and Oman. *Geological Society, London* 366: 131-162.

Chauhan DC, Ram B (1999), Ripple marks and synthesis of beach sequences: A study of early Paleozoic sandstone of Jodhpur Group, Western Rajasthan. Paliwal BS (ed) Geological Evolution of Western India, Scientific Publishers, Jodhpur,67-78.

Chowdhary, L. (2023), Discussion “Structural analysis and seismic stratigraphy for delineation of Neoproterozoic–Cambrian petroleum system in the central and eastern part of Bikaner–Nagaur basin, India” by A. Mandal, D. Saha and A. Kumar, Journal of Petroleum Exploration and Production Technology, 2021, 1–17.

Kumar V, Chandra R (2005),Geology and Evolution of Nagaur-Ganganagar basin with special reference to Salt and Potash mineralization. GSI spl. pub. 62:151pp.

Prasad B, Asher R, Borgohai B (2010), Late Proterozoic (Ediacaran) – Early Paleozoic (Cambrian) Acritarchs from the Marwar Supergroup, Bikaner-Nagaur Basin, Rajasthan. Journal of GSI 75: 415-431.

Mazumdar A, Strauss H (2006), Sulfur and Strontium Isotopic Composition of Carbonate and Evaporate Rocks from Late Neoproterozoic-Early Cambrian Bilara Group (Nagaur-Ganganagar Basin, India): Constraints on Intrabasinal Correlation and Global Sulfur cycle. In: Bhat GM et al. (eds) Geology and Hydrocarbon Potential of Neoproterozoic-Cambrian Basins in Asia, Geological Society Special Publication 366.

Ram J., (2012), Neoproterozoic Succession in Peninsular India. In: Bhat GM (eds) Geology and Hydrocarbon Potential of Neoproterozoic-Cambrian Basins in Asia. Geological Society spl. pub., 366, 59-73

Luning S., Kolonic S., Geiger M., Thusu B., Bell J.S., Craig J., (2009), Infracambrian hydrocarbon source rock potential and petroleum prospectivity of NW Africa. Geol Soc 326:161. <https://doi.org/10.1144/SP326.8>

Zheng, D.X, Espinoza, N.Vandamme, M.Pereira, J M.(2022.), CO₂ plume and pressure monitoring through pressure sensors above the caprock, International Journal of Greenhouse Gas Control,117.<https://doi.org/10.1016/j.ijggc.2022.103660>

Zoback, M.D., (2007).,Reservoir Geomechanics. Cambridge University Press. <https://doi.org/10.1017/CBO9780511586477>.

Appendix

A. Homogeneous Model

A.1 Case A

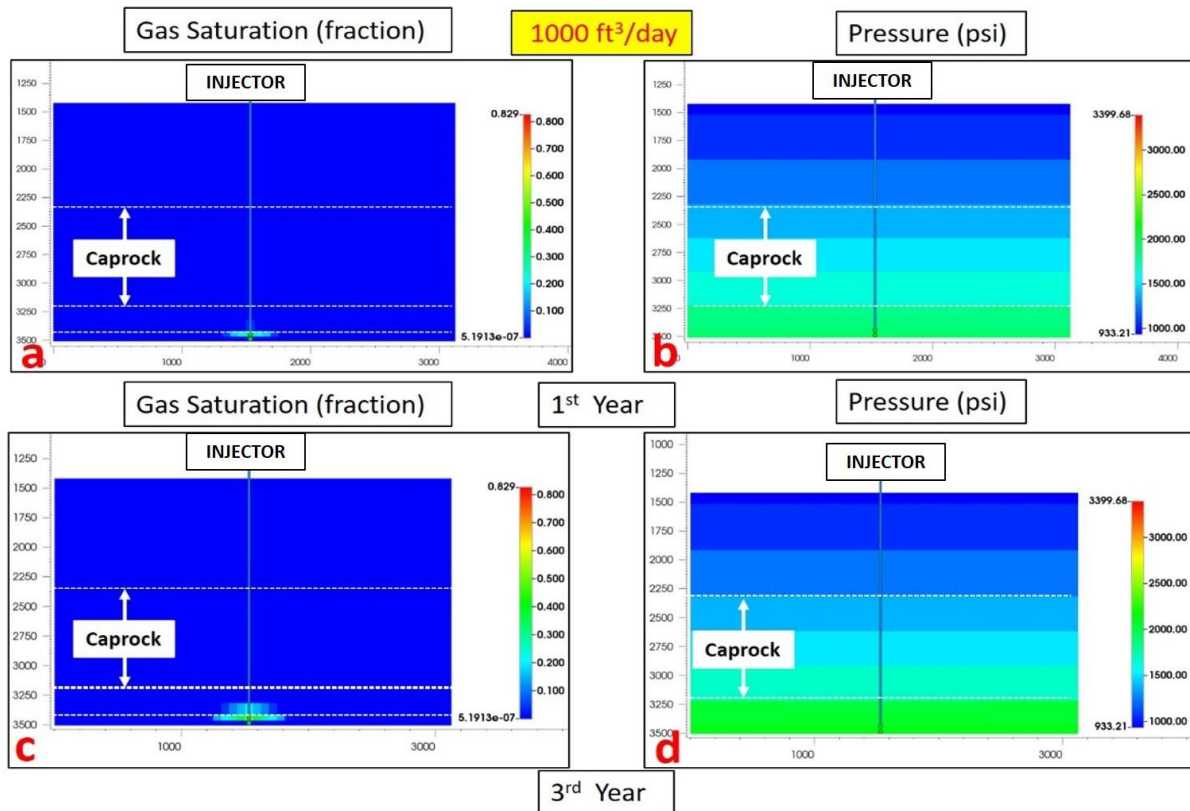


Figure A.1.1 The schematic description for properties at cross-sectional slice J=13 for Case A indicating distribution of Gas Saturation and Pressure(psi) at the end of 1st year a) and b) and 3rd year c) and d) respectively.

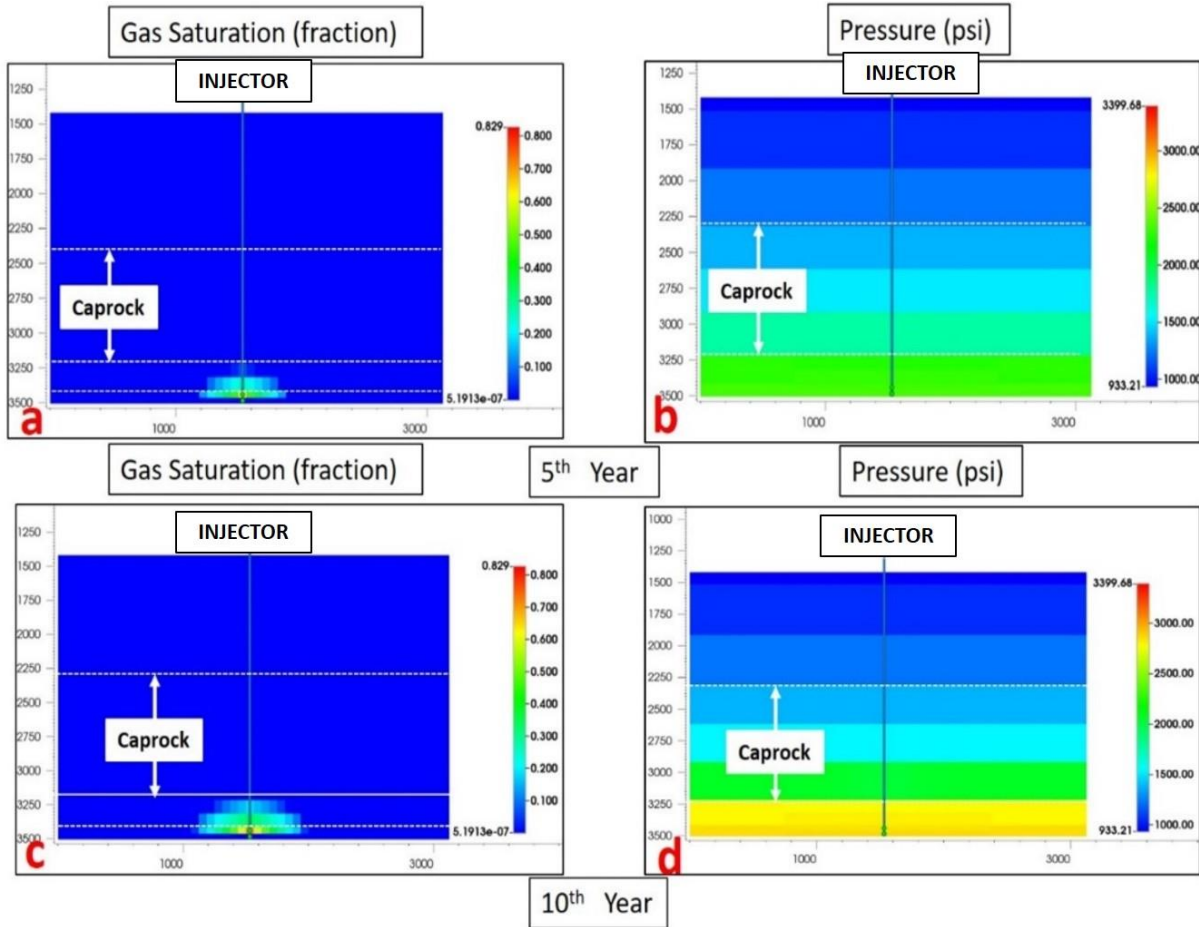


Figure A.1.2 The schematic description for properties at cross-sectional slice J=13 for Case A indicating distribution of Gas Saturation and Pressure(psi) at the end of 5th year a) and b) and 10th year c) and d) respectively.

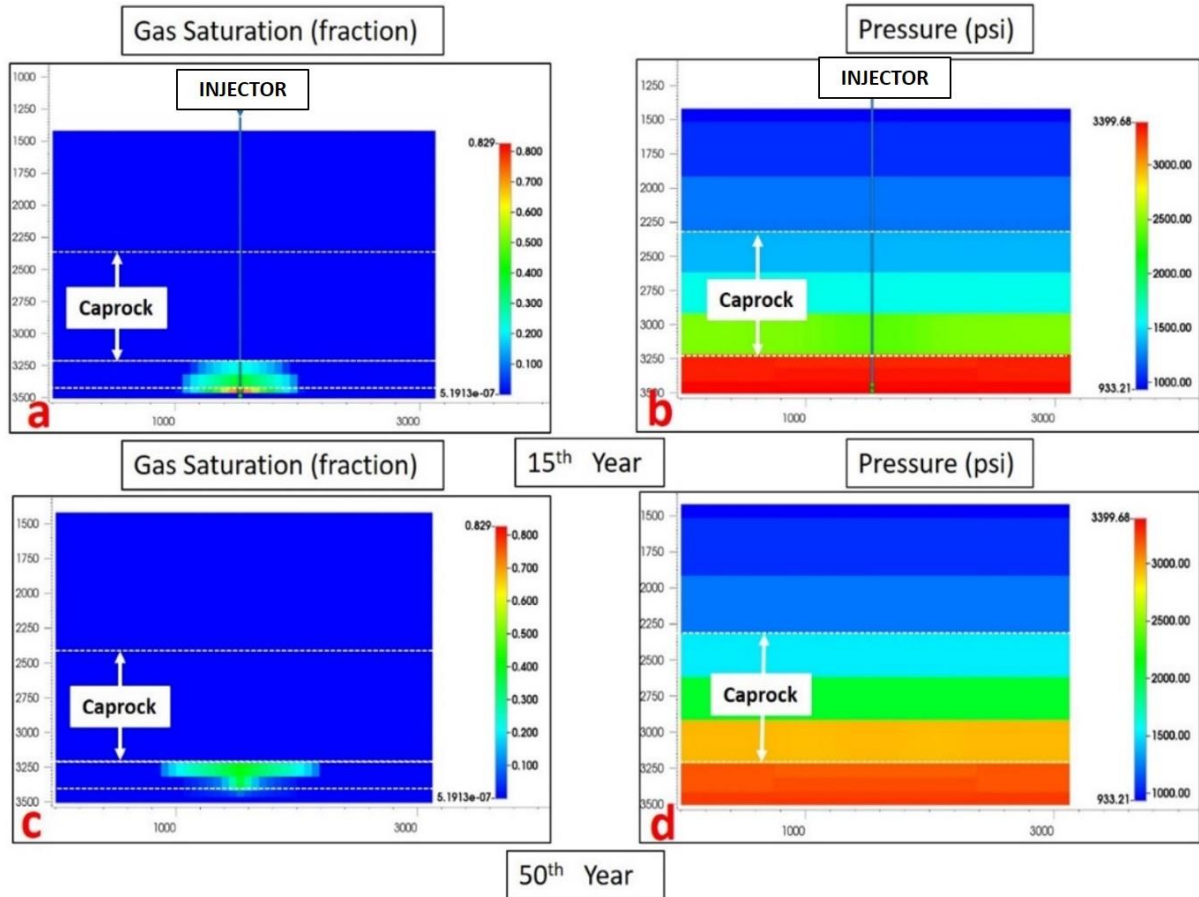


Figure A.1.3 The schematic description for properties at cross-sectional slice J=13 for Case A indicating distribution of Gas Saturation and Pressure(psi) at the end of 15th year a) and b) and 50th year c) and d) respectively.

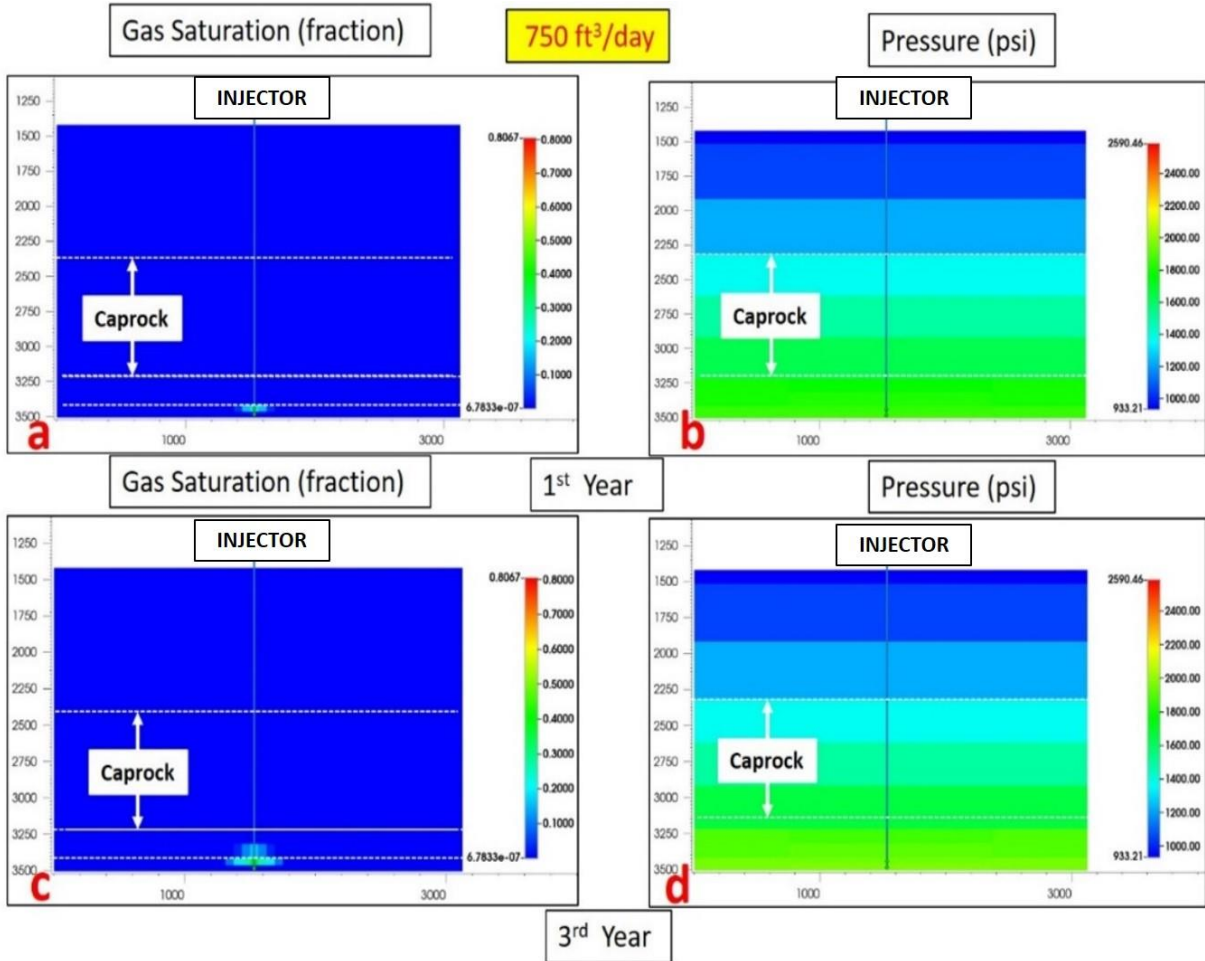


Figure A.1.4 The schematic description for properties at cross-sectional slice J=13 for Case A indicating distribution of Gas Saturation and Pressure(psi) at the end of 1st year a) and b) and 3rd year c) and d) respectively.

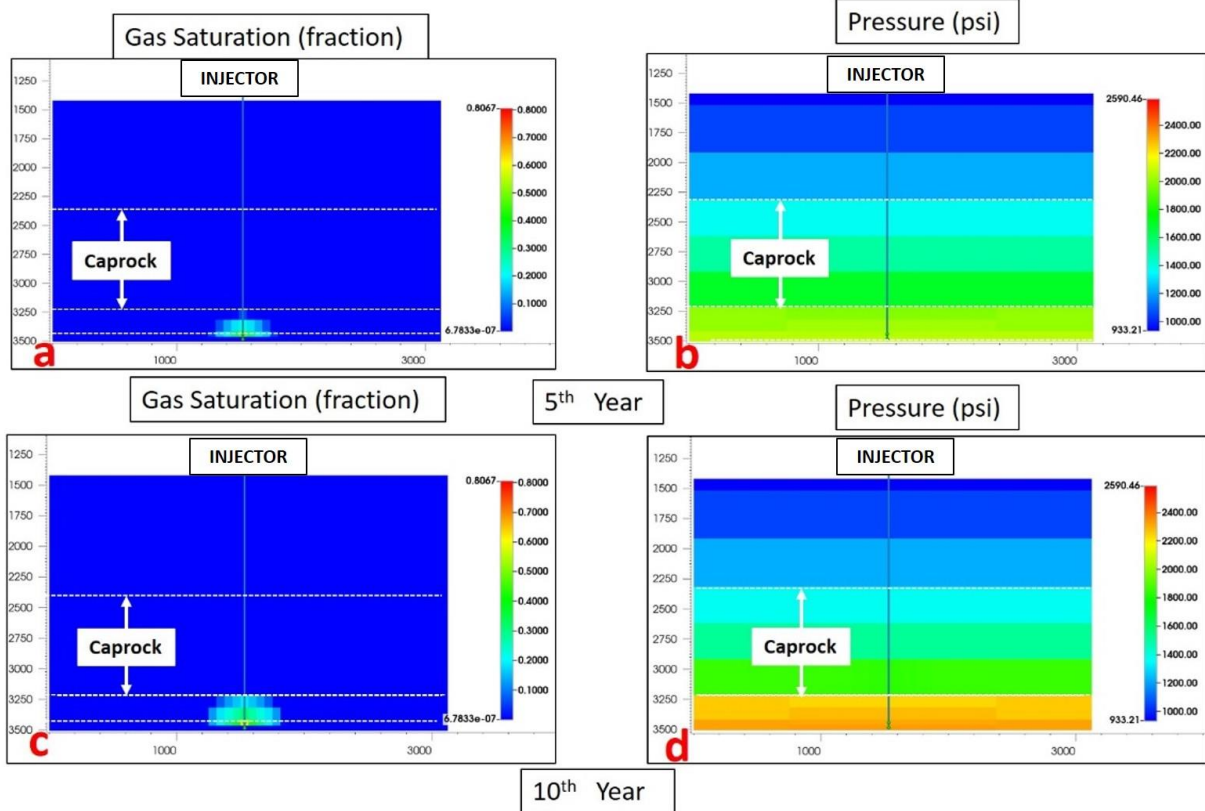


Figure A.1.5 The schematic description for properties at cross-sectional slice J=13 for Case A indicating distribution of Gas Saturation and Pressure(psi) at the end of 5th year a) and b) and 10th year c) and d) respectively.

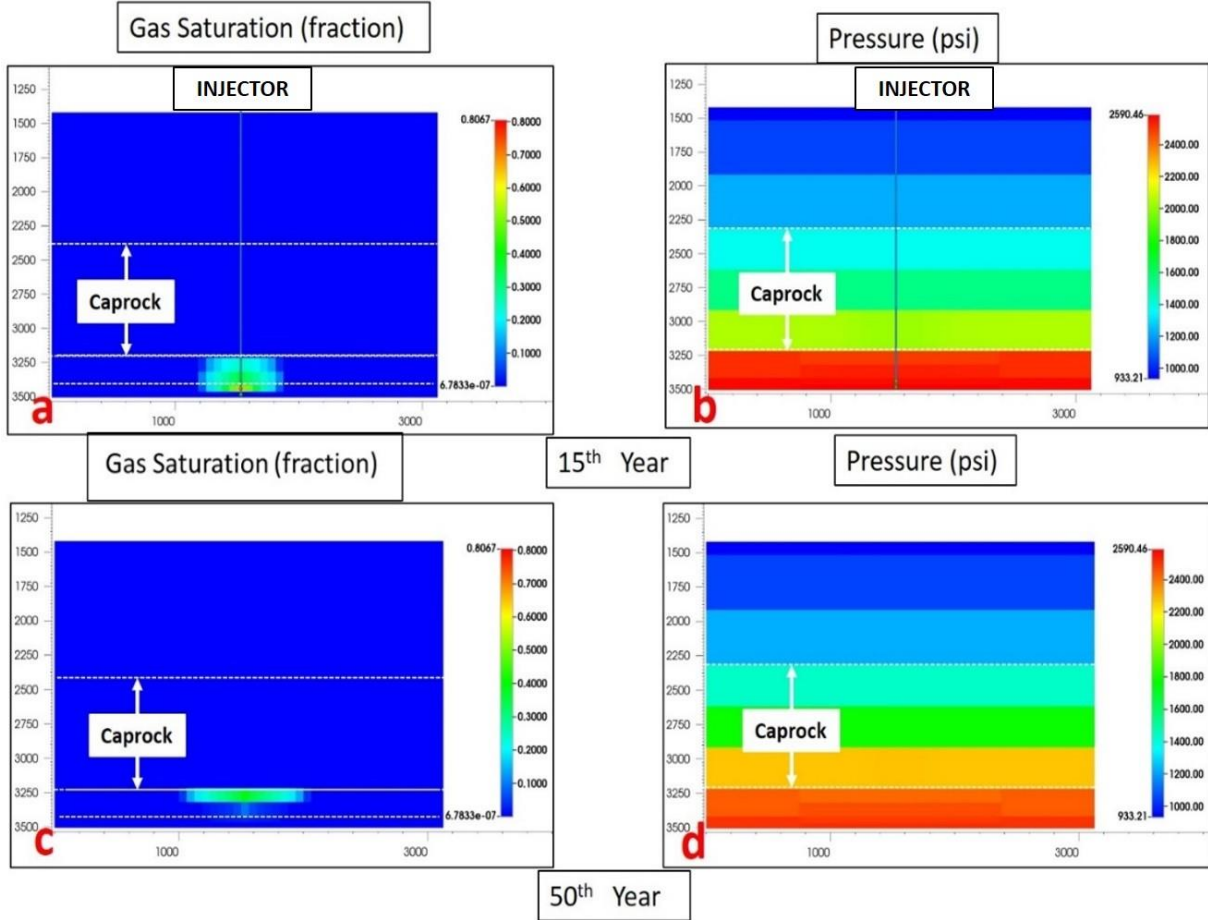


Figure A.1.6 The schematic description for properties at cross-sectional slice J=13 for Case A indicating distribution of Gas Saturation and Pressure(psi) at the end of 15th year a) and b) and 50th year c) and d) respectively.

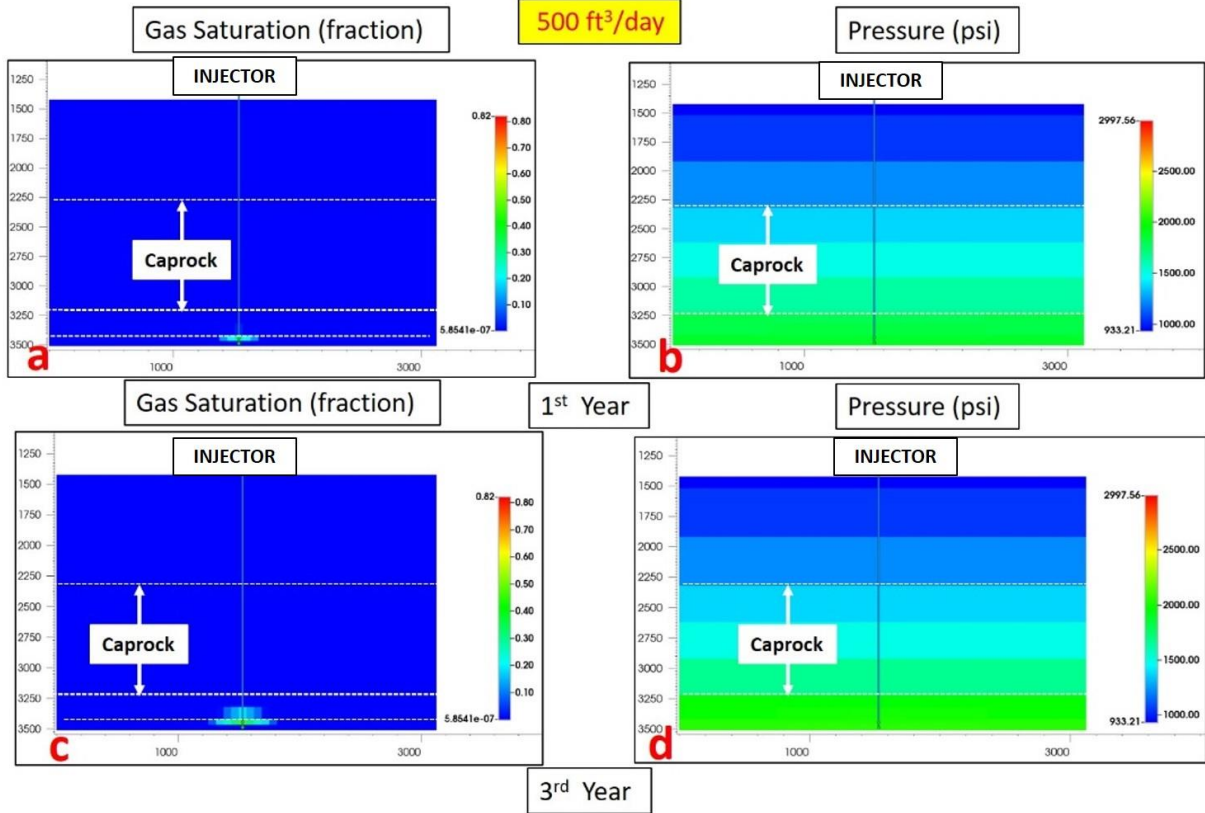


Figure A.1.7 The schematic description for properties at cross-sectional slice J=13 for Case A indicating distribution of Gas Saturation and Pressure(psi) at the end of 1st year a) and b) and 3rd year c) and d) respectively.

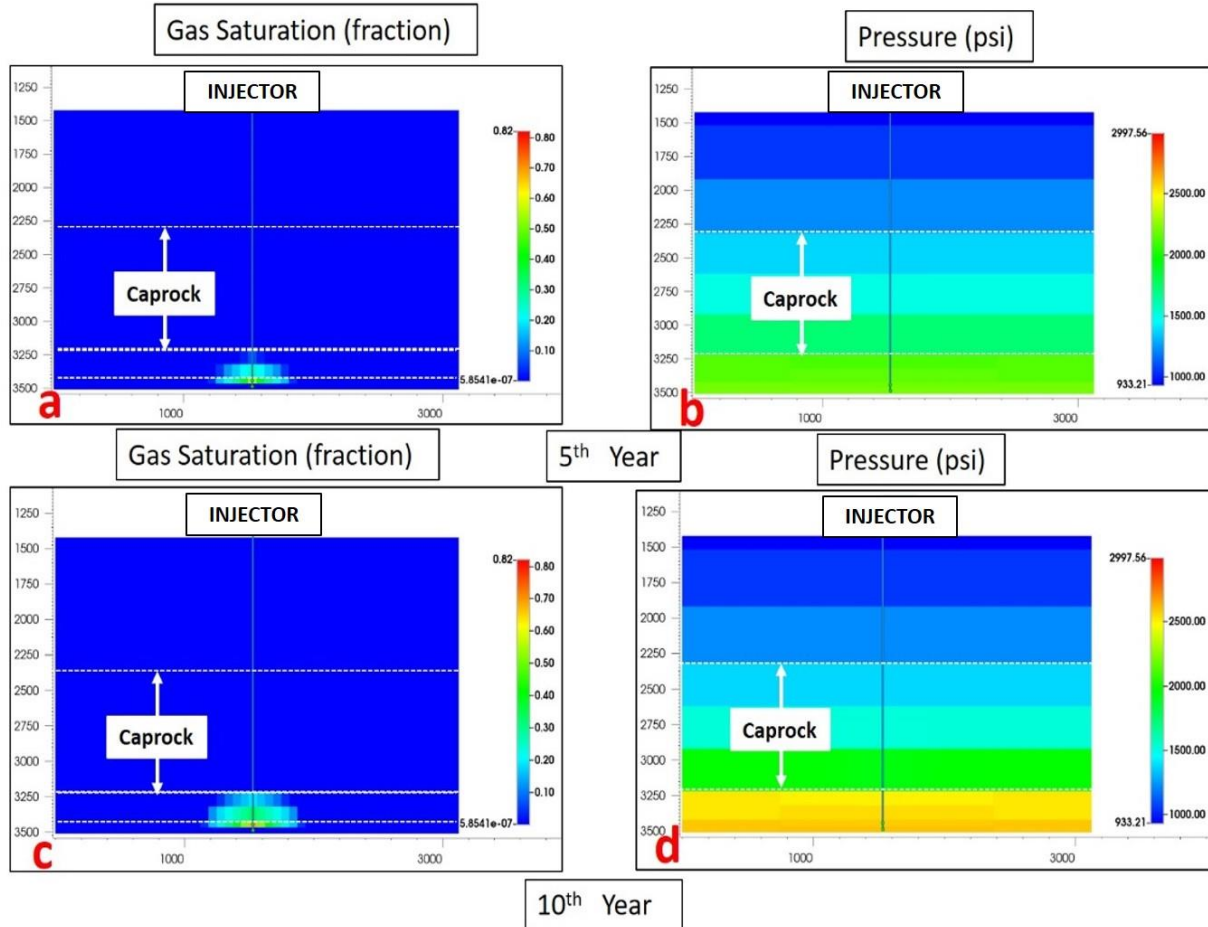


Figure A.1.8 The schematic description for properties at cross-sectional slice J=13 for Case A indicating distribution of Gas Saturation and Pressure(psi) at the end of 5th year a) and b) and 10th year c) and d) respectively.

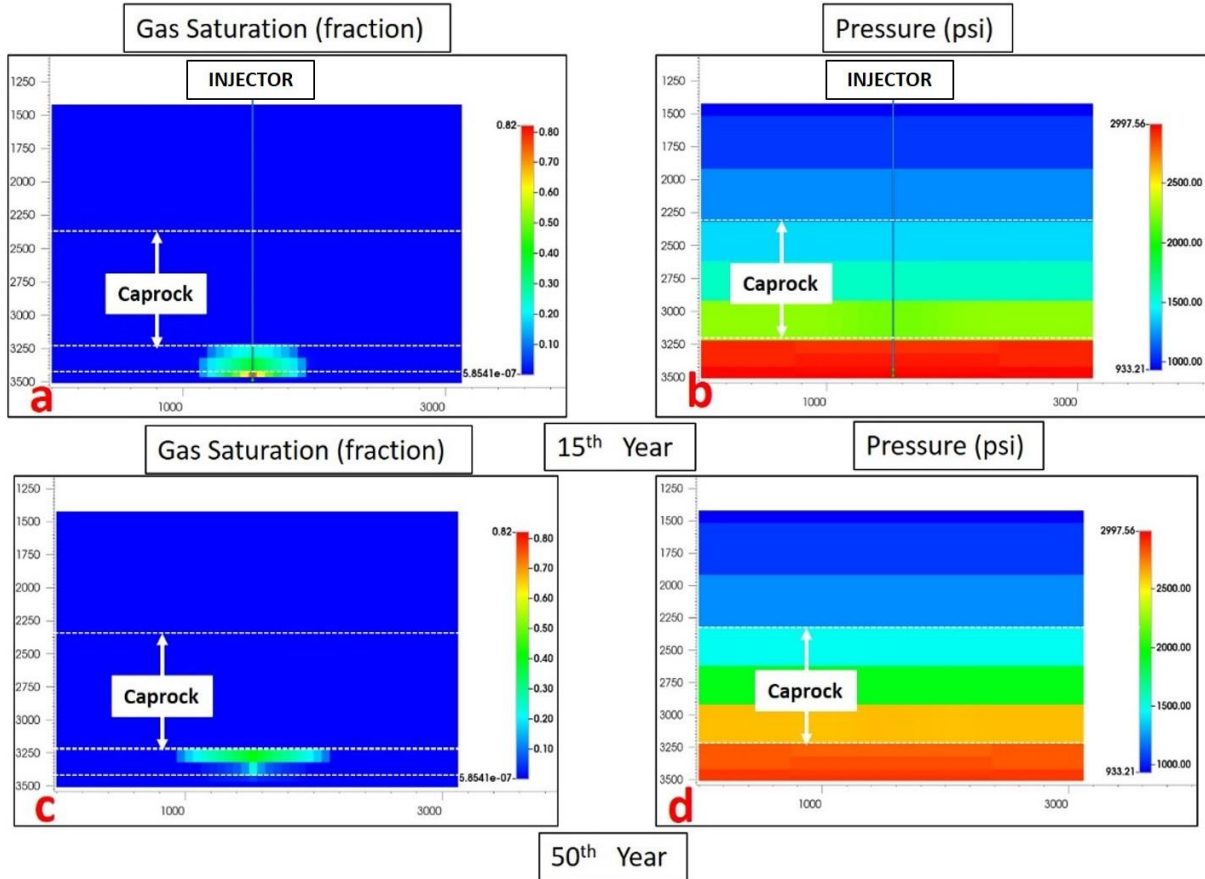


Figure A.1.9 The schematic description for properties at cross-sectional slice J=13 for Case A indicating distribution of Gas Saturation and Pressure(psi) at the end of 15th year a) and b) and 50th year c) and d) respectively.

A.2 Case B

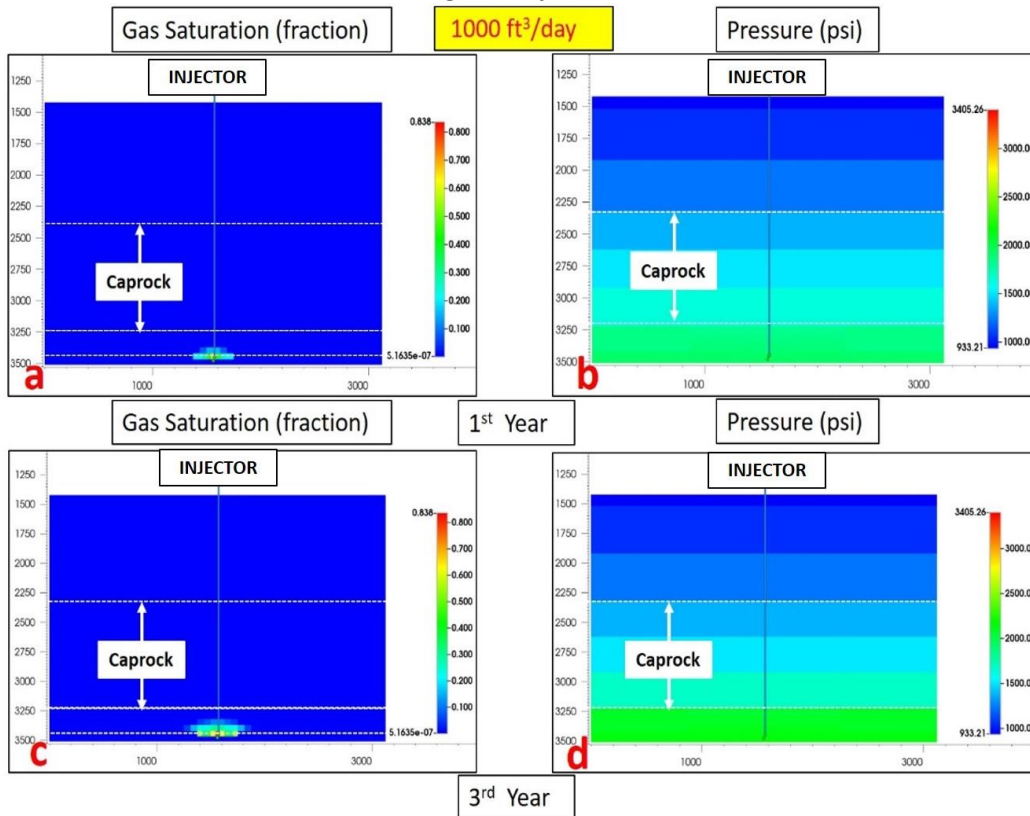


Figure A.2.1 The schematic description for properties at cross-sectional slice J=13 for Case B indicating distribution of Gas Saturation and Pressure(psi) at the end of 1st year a) and b) and 3rd year c) and d) respectively.

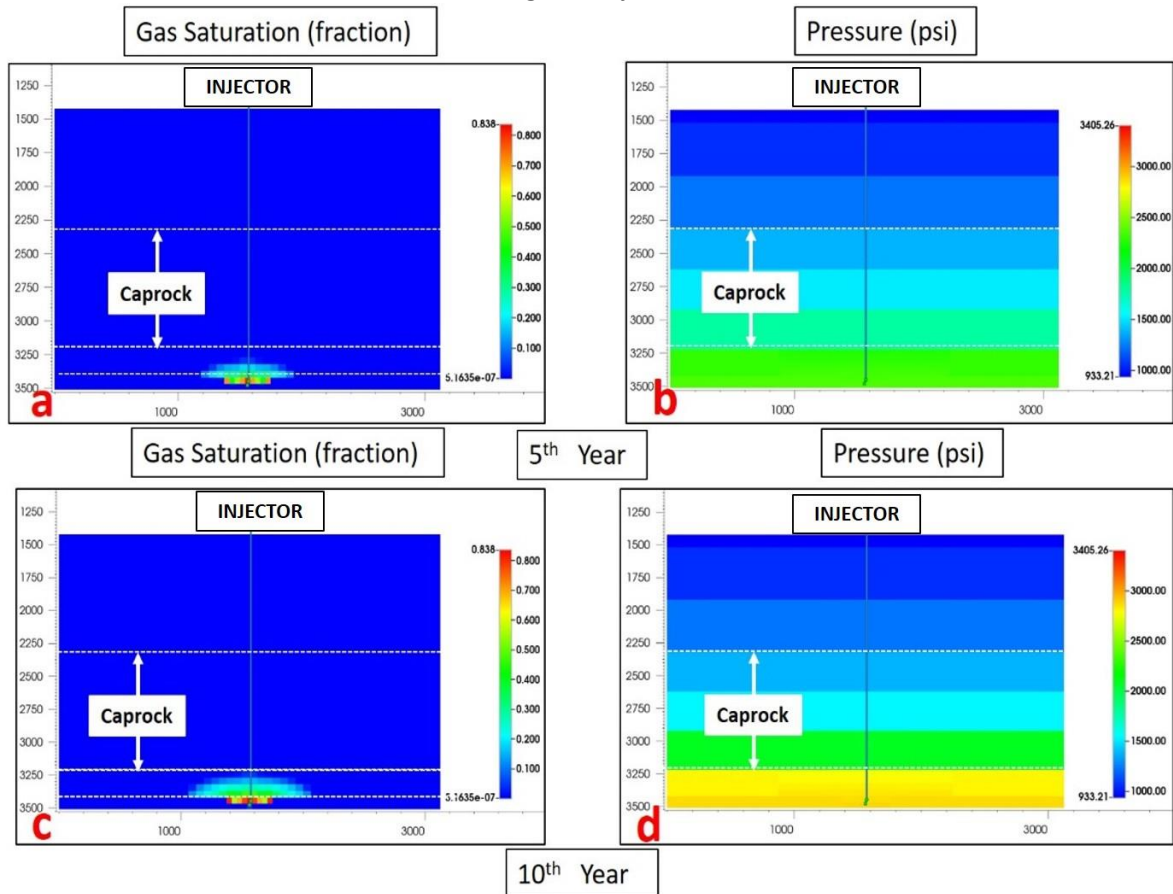


Figure A.2.2 The schematic description for properties at cross-sectional slice J=13 for Case B indicating the distribution of Gas Saturation and Pressure(psi) at the end of 5th year a) and b) and 10th year c) and d) respectively.

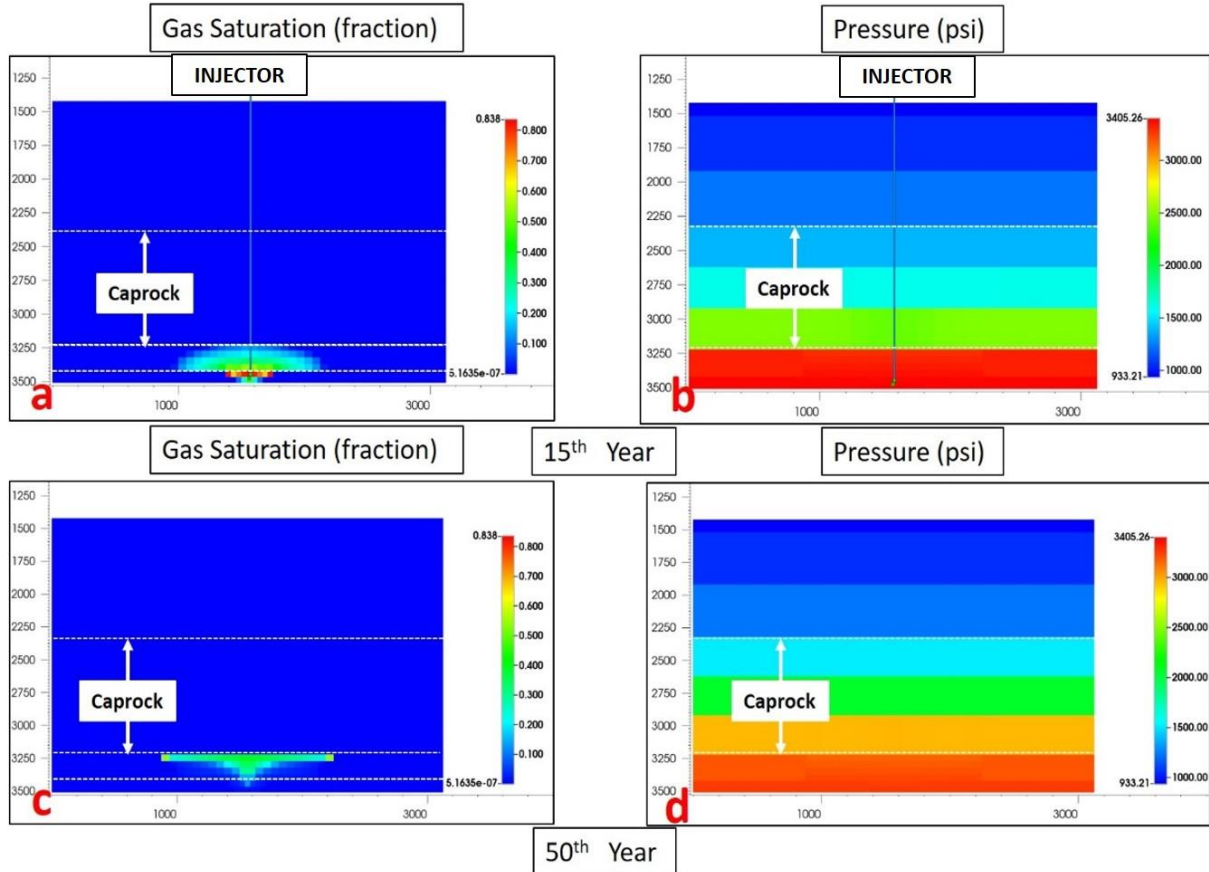


Figure A.2.3 The schematic description for properties at cross-sectional slice J=13 for Case B indicating the distribution of Gas Saturation and Pressure(psi) at the end of 15th year a) and b) and 50th year c) and d) respectively.

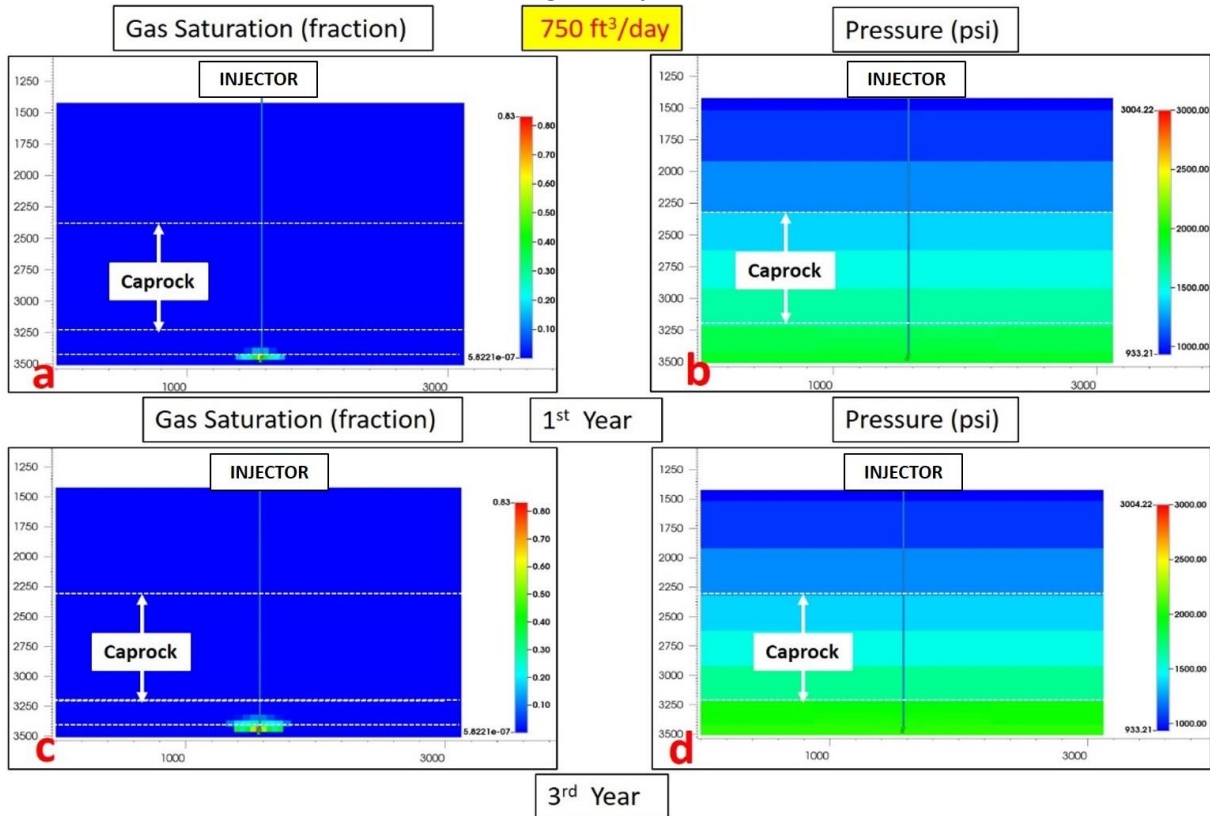


Figure A.2.4 The schematic description for properties at cross-sectional slice J=13 for Case B indicating the distribution of Gas Saturation and Pressure(psi) at the end of 1st year a) and b) and 3rd year c) and d) respectively.

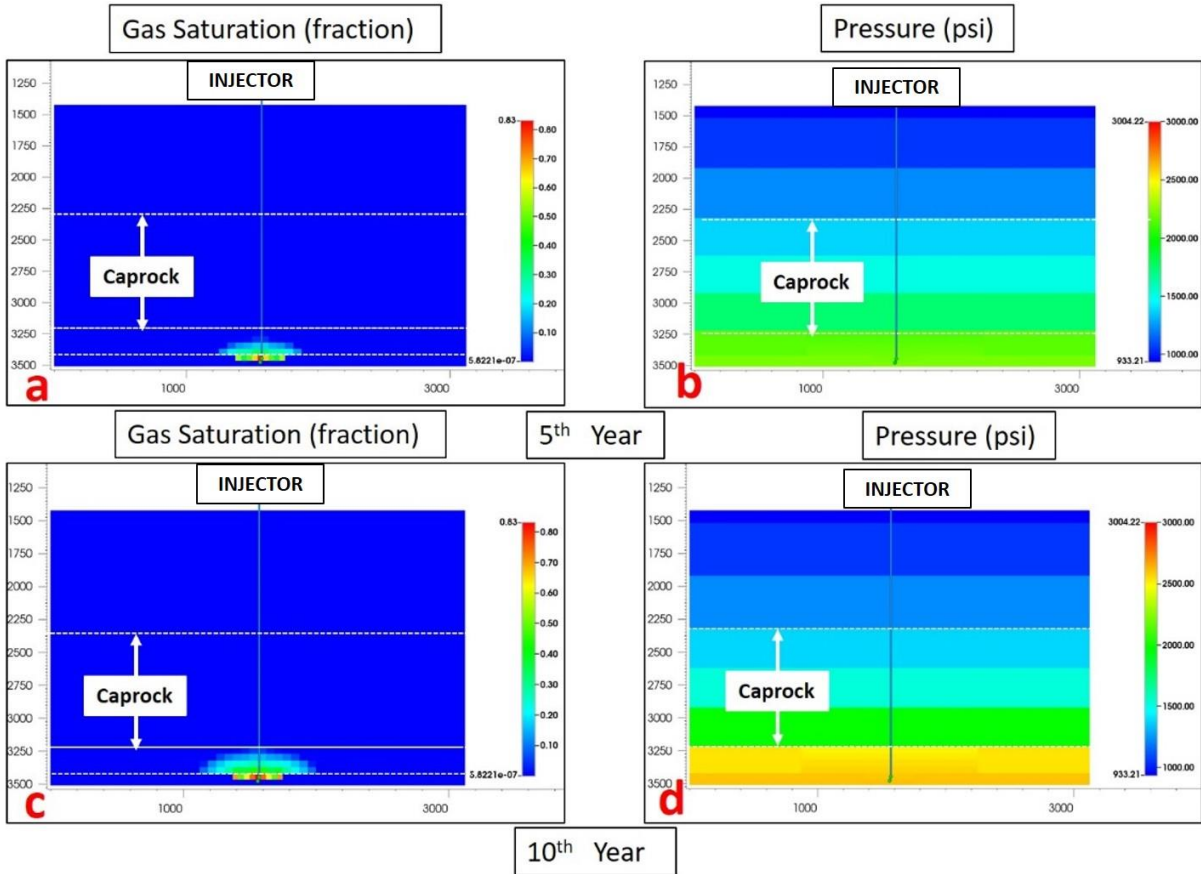


Figure A.2.5 The schematic description for properties at cross-sectional slice J=13 for Case B indicating the distribution of Gas Saturation and Pressure(psi) at the end of 5th year a) and b) and 10th year c) and d) respectively.

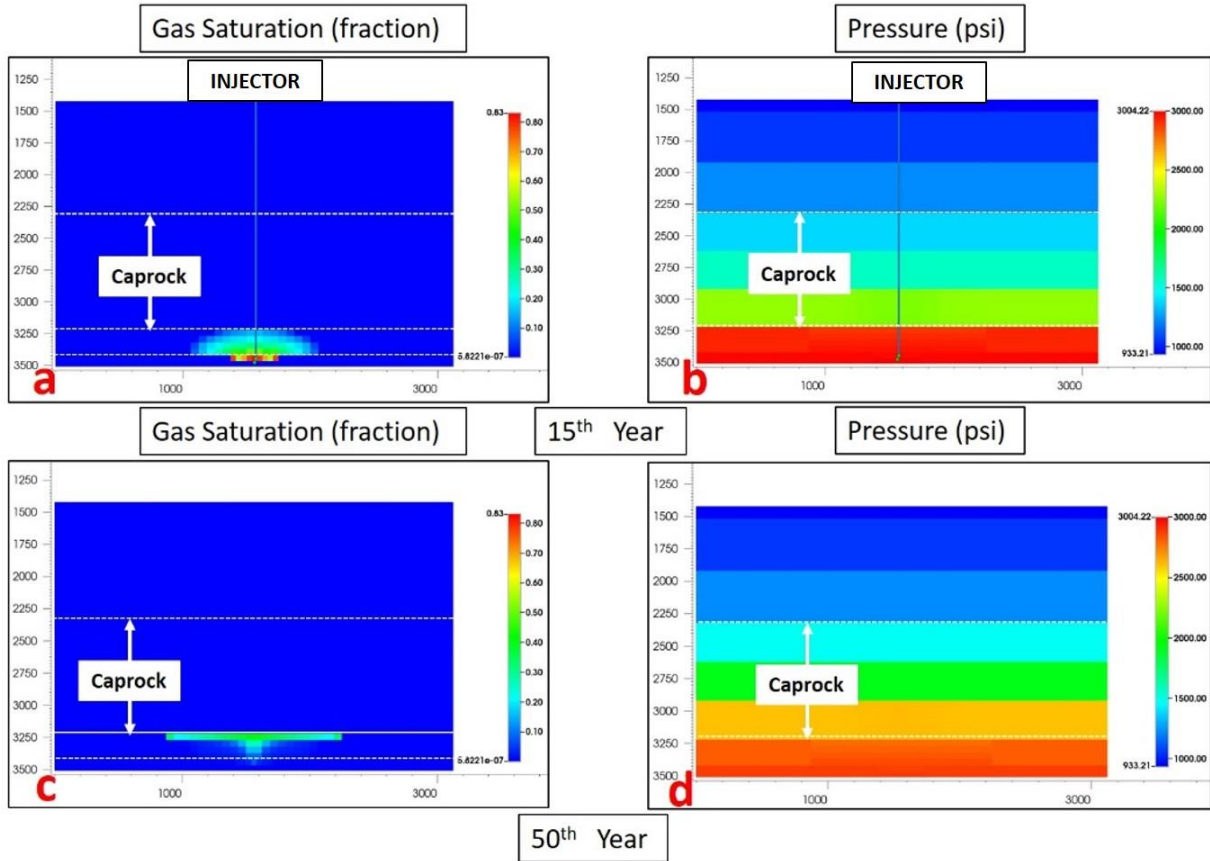


Figure A.2.6 The schematic description for properties at cross-sectional slice J=13 for Case B indicating the distribution of Gas Saturation and Pressure(psi) at the end of 15th year a) and b) and 50th year c) and d) respectively.

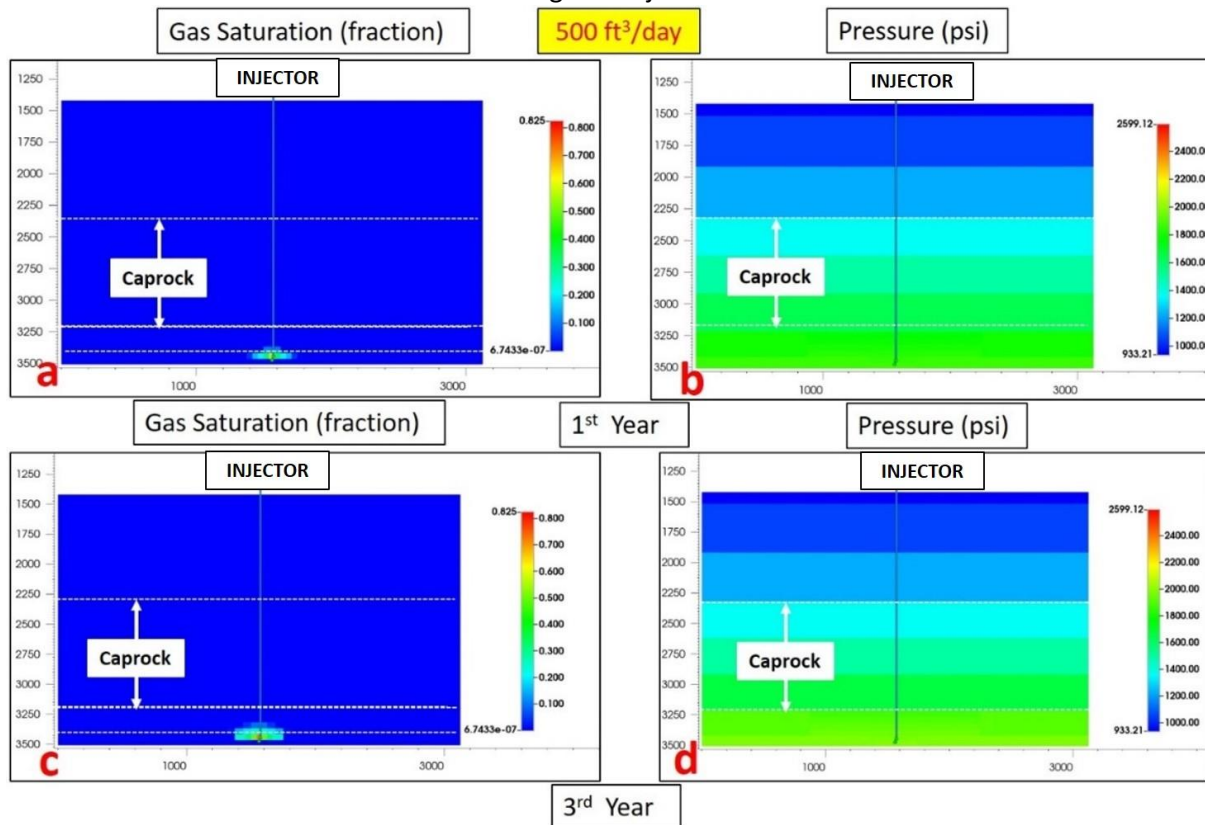


Figure A.2.7 The schematic description for properties at cross-sectional slice J=13 for Case B indicating the distribution of Gas Saturation and Pressure(psi) at the end of 1st year a) and b) and 3rd year c) and d) respectively.

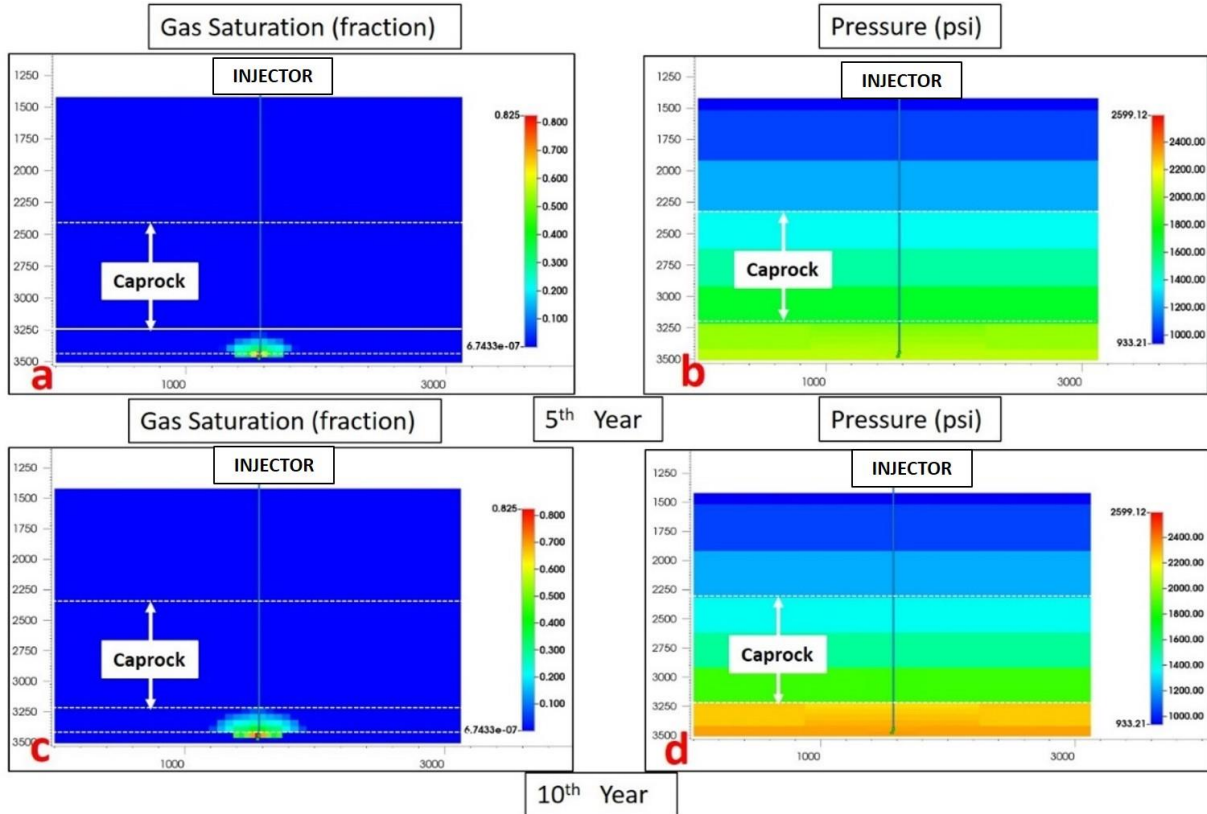


Figure A.2.8 The schematic description for properties at cross-sectional slice J=13 for Case B indicating the distribution of Gas Saturation and Pressure(psi) at the end of 5th year a) and b) and 10th year c) and d) respectively.

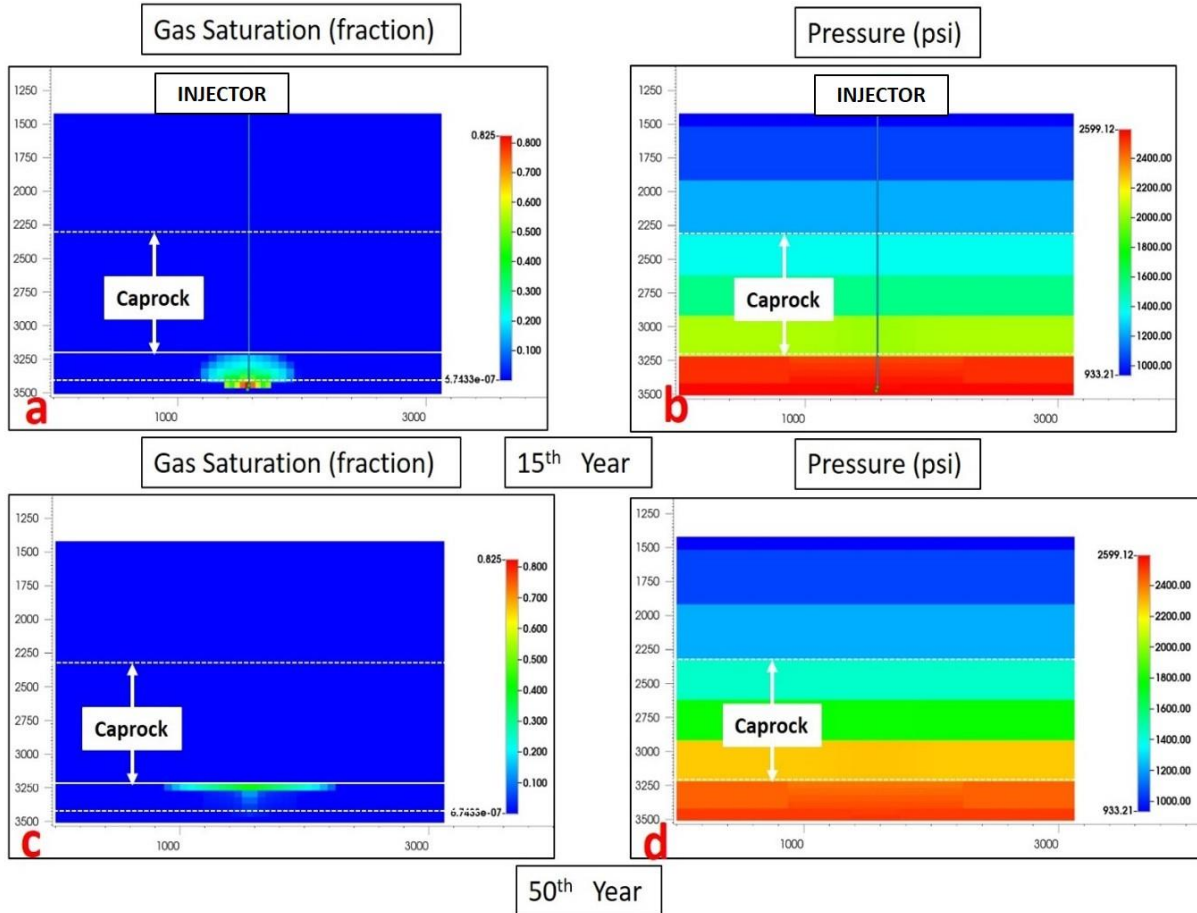


Figure A.2.9 The schematic description for properties at cross-sectional slice J=13 for Case B indicating the distribution of Gas Saturation and Pressure(psi) at the end of 15th year a) and b) and 50th year c) and d) respectively.

A.3 Case C

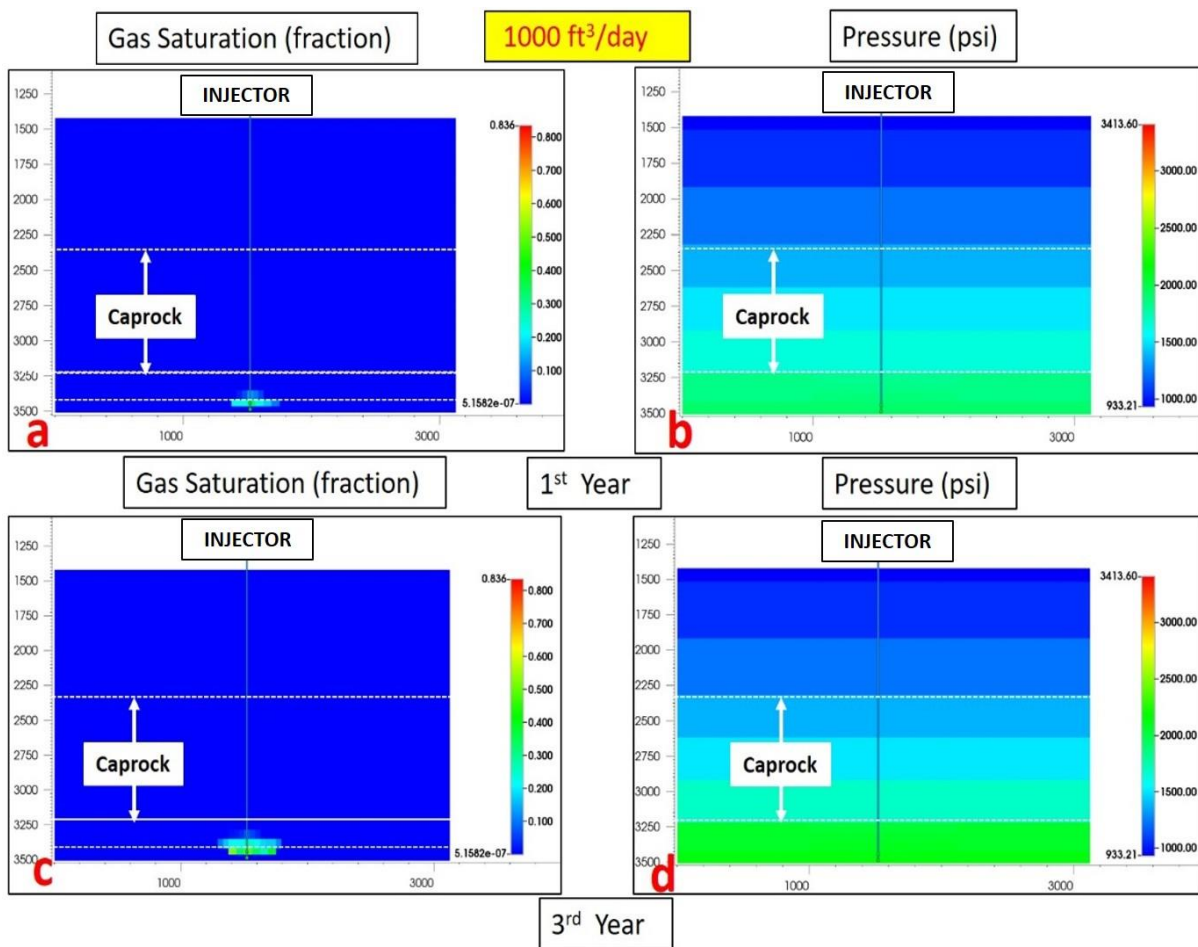


Figure A.3.1 The schematic description for properties at cross-sectional slice J=13 for Case C indicating the distribution of Gas Saturation and Pressure(psi) at the end of 1st year a) and b) and 3rd year c) and d) respectively.

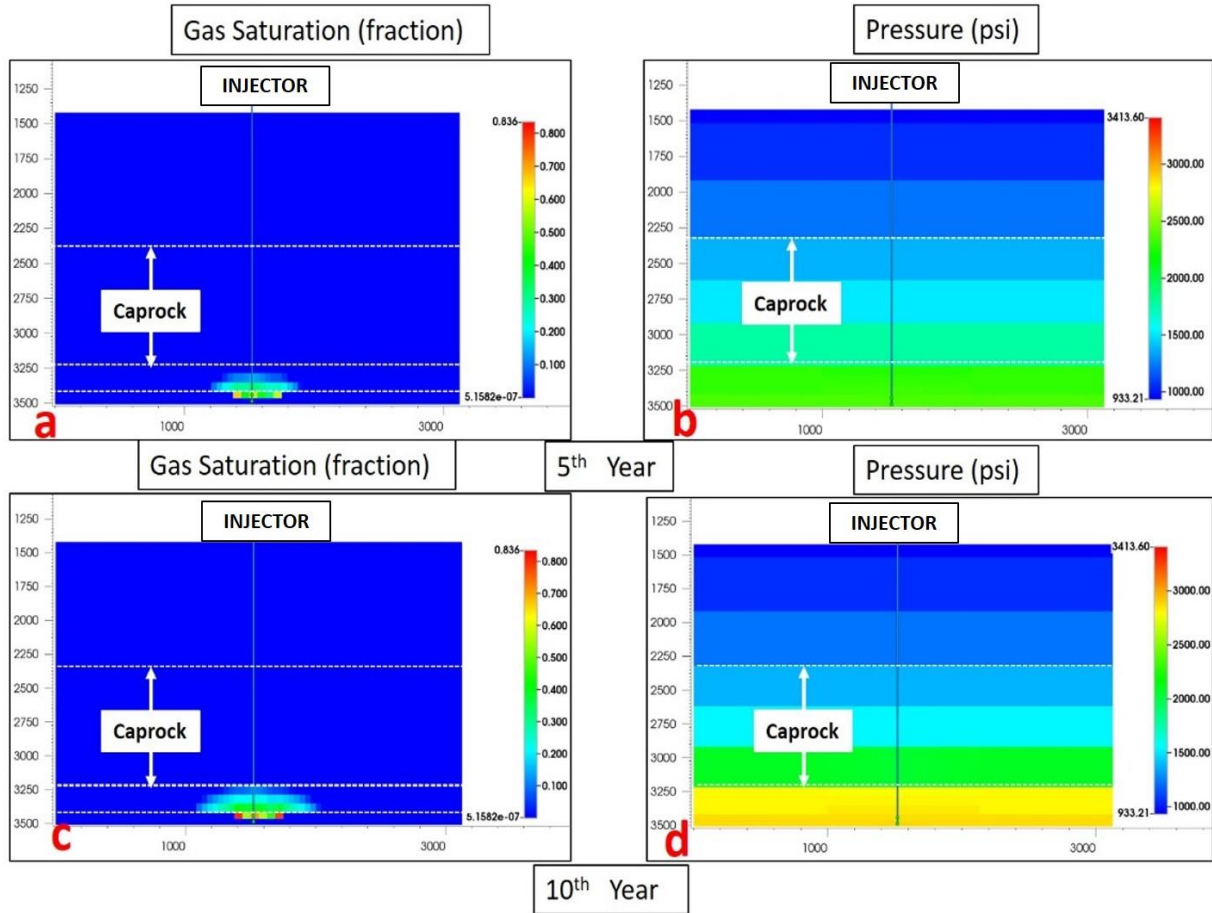


Figure A.3.2 The schematic description for properties at cross-sectional slice J=13 for Case C indicating the distribution of Gas Saturation and Pressure(psi) at the end of 5th year a) and b) and 10th year c) and d) respectively.

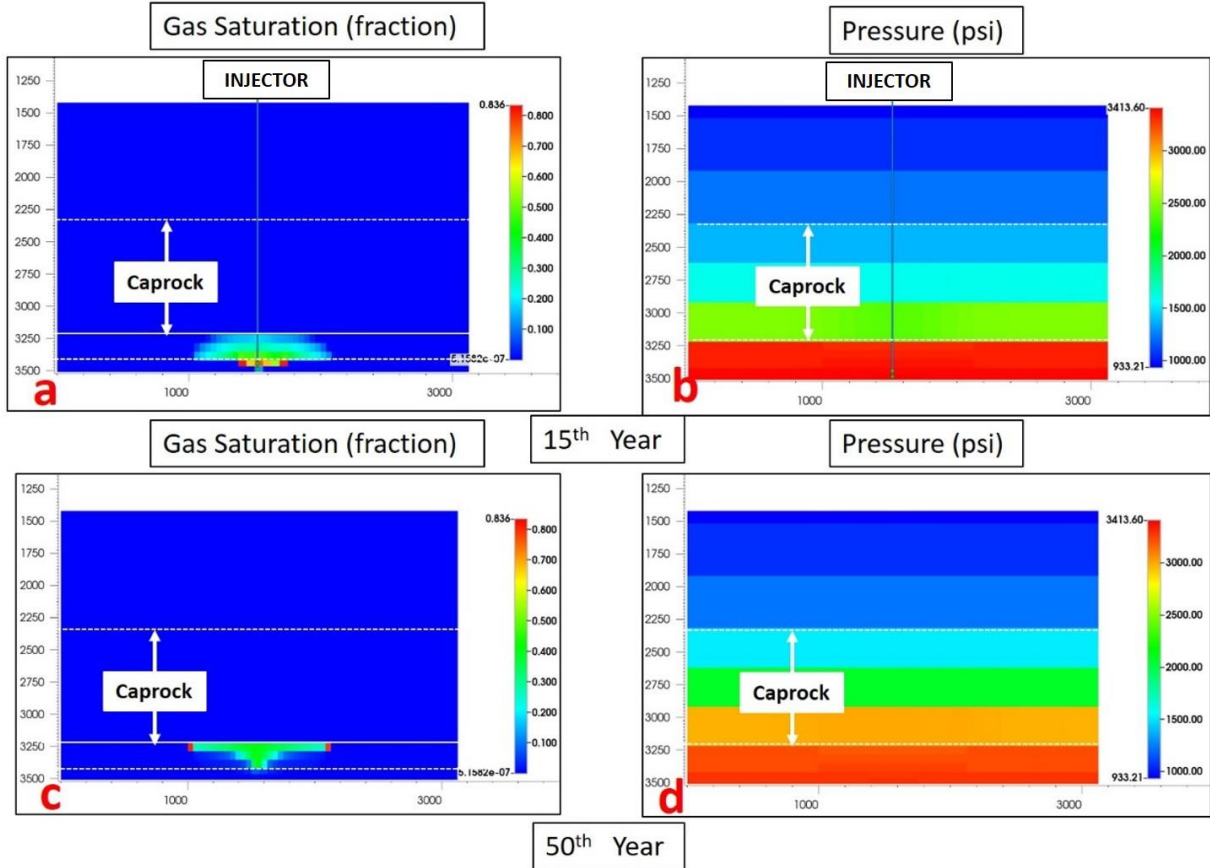


Figure A.3.3 The schematic description for properties at cross-sectional slice J=13 for Case C indicating the distribution of Gas Saturation and Pressure(psi) at the end of 15th year a) and b) and 50th year c) and d) respectively.

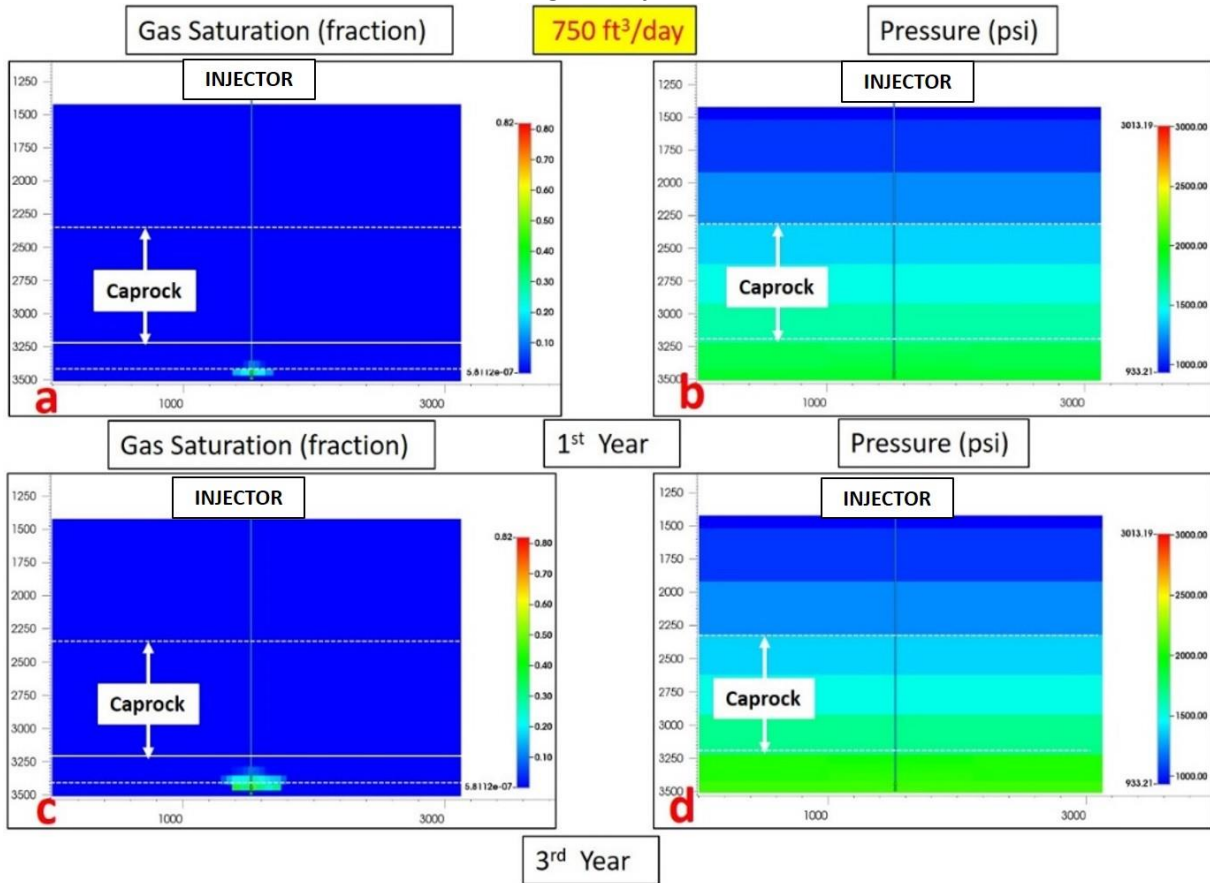


Figure A.3.4 The schematic description for properties at cross-sectional slice J=13 for Case C indicating the distribution of Gas Saturation and Pressure(psi) at the end of 1st year a) and b) and 3rd year c) and d) respectively.

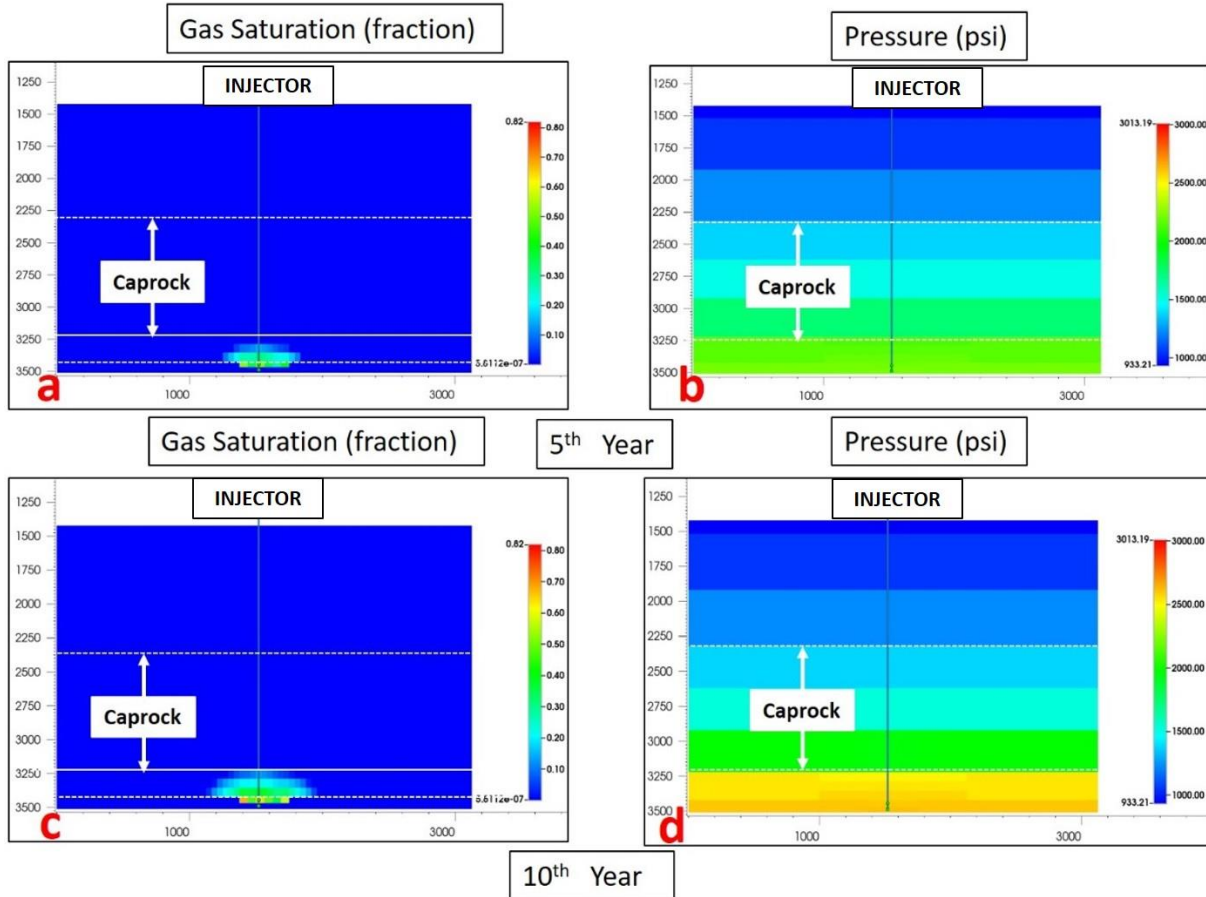


Figure A.3.5 The schematic description for properties at cross-sectional slice J=13 for Case C indicating the distribution of Gas Saturation and Pressure(psi) at the end of 5th year a) and b) and 10th year c) and d) respectively.

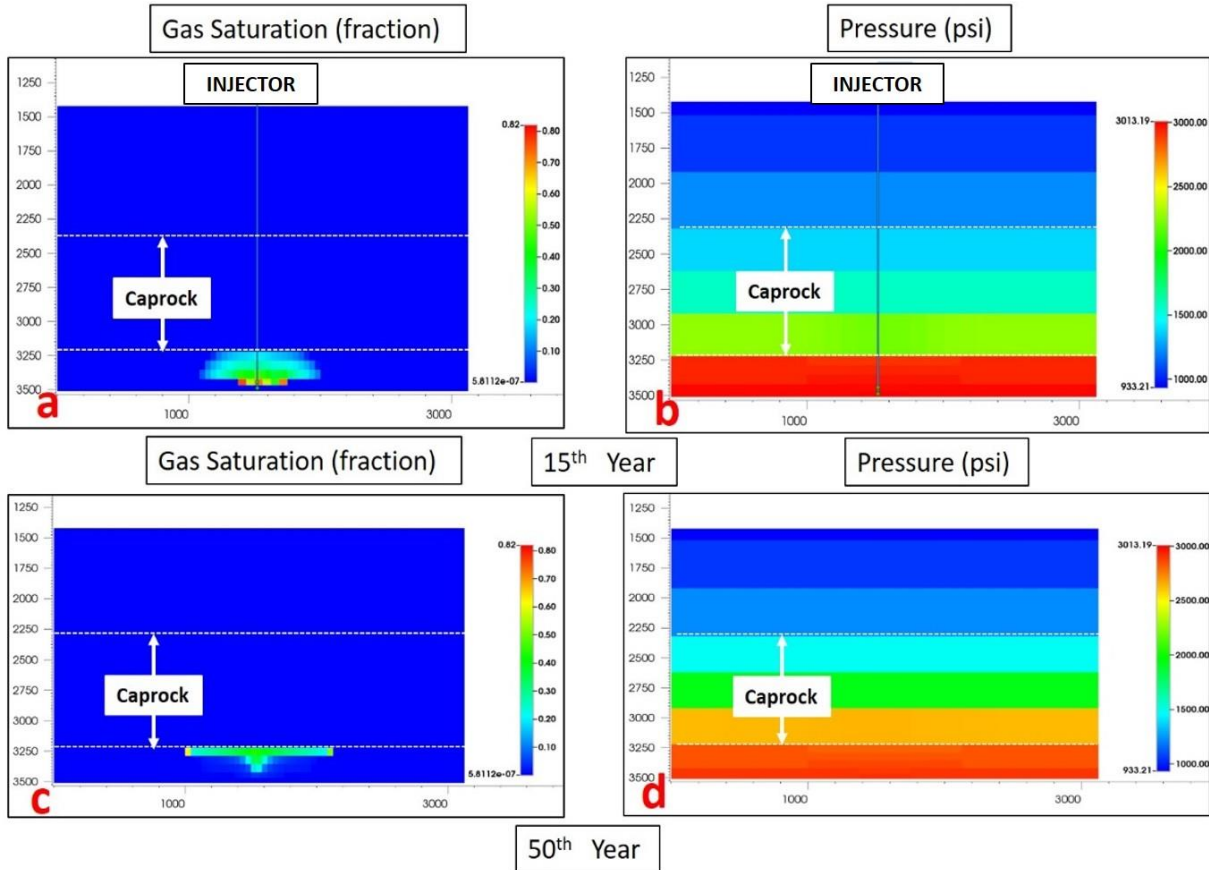


Figure A.3.6 The schematic description for properties at cross-sectional slice J=13 for Case C indicating the distribution of Gas Saturation and Pressure(psi) at the end of 15th year a) and b) and 50th year c) and d) respectively.

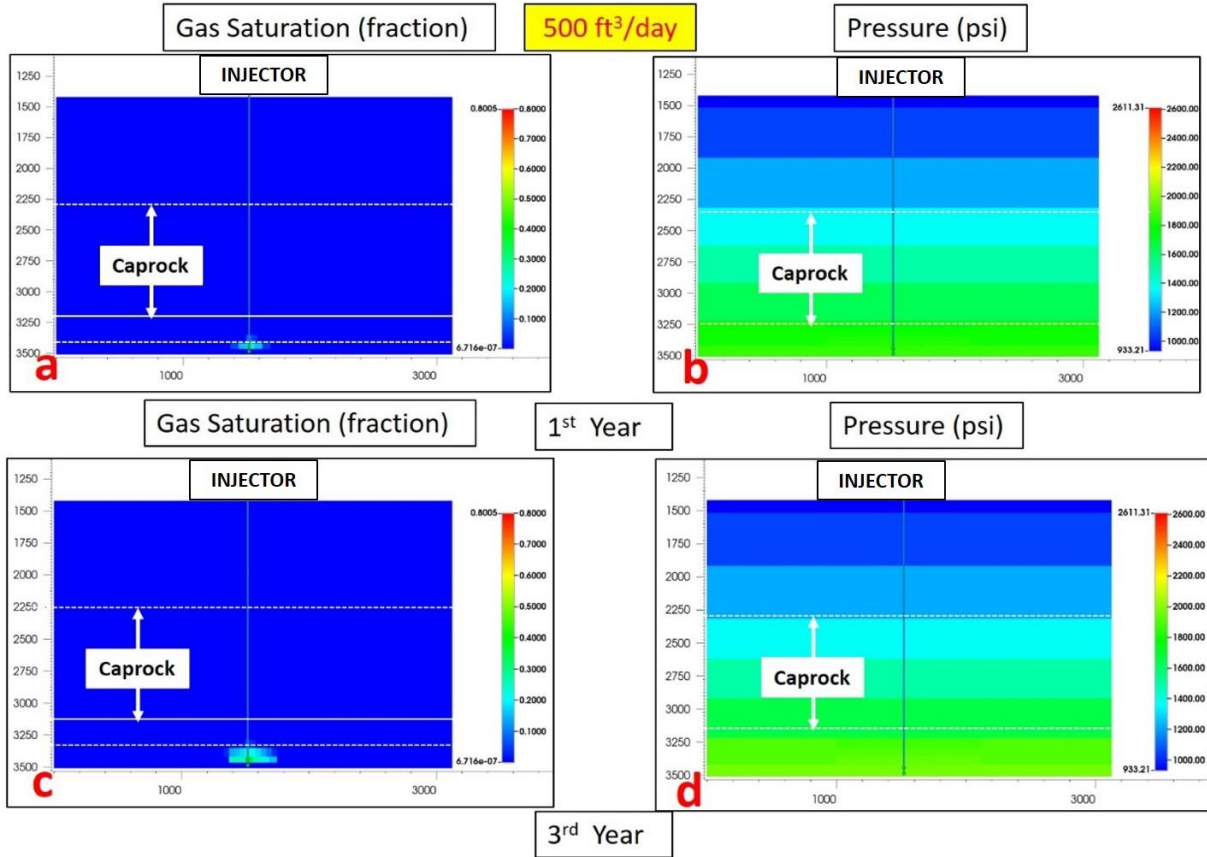


Figure A.3.7 The schematic description for properties at cross-sectional slice J=13 for Case C indicating the distribution of Gas Saturation and Pressure(psi) at the end of 1st year a) and b) and 3rd year c) and d) respectively.

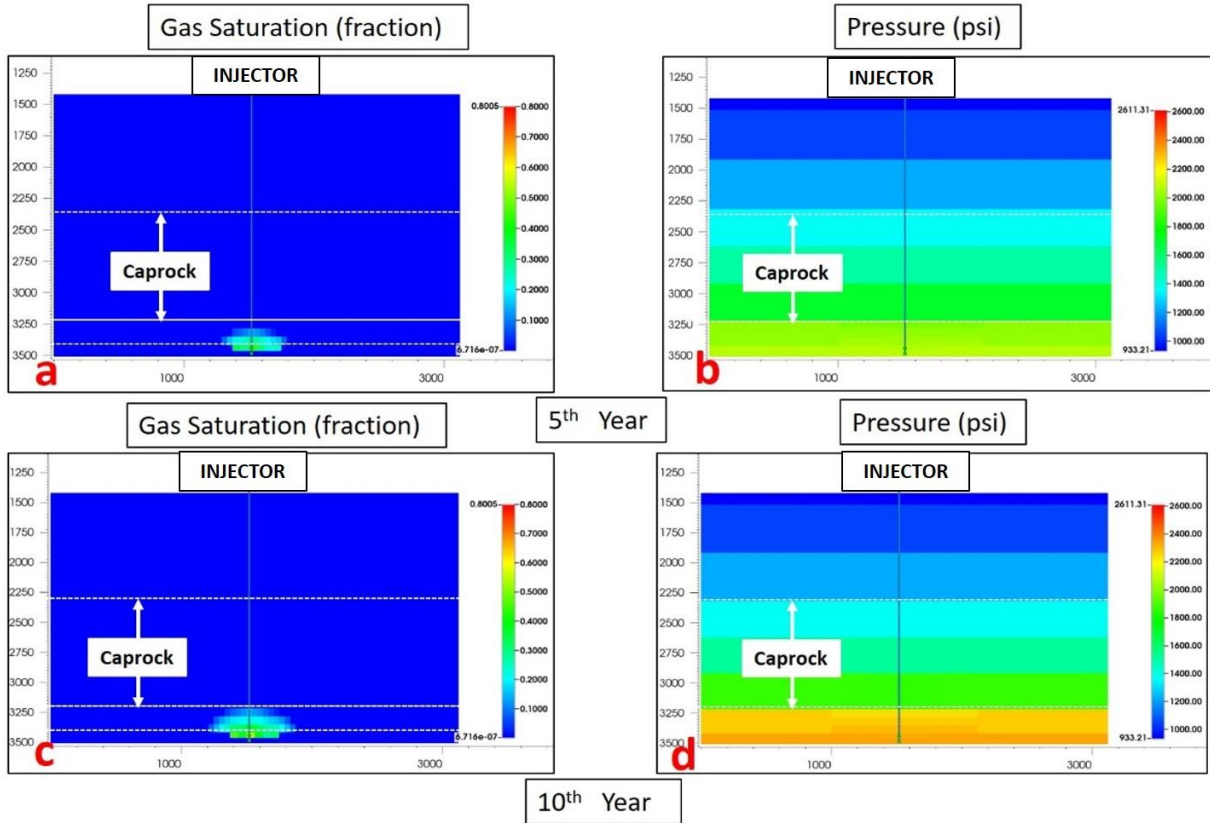


Figure A.3.8 The schematic description for properties at cross-sectional slice J=13 for Case C indicating the distribution of Gas Saturation and Pressure(psi) at the end of 5th year a) and b) and 10th year c) and d) respectively.

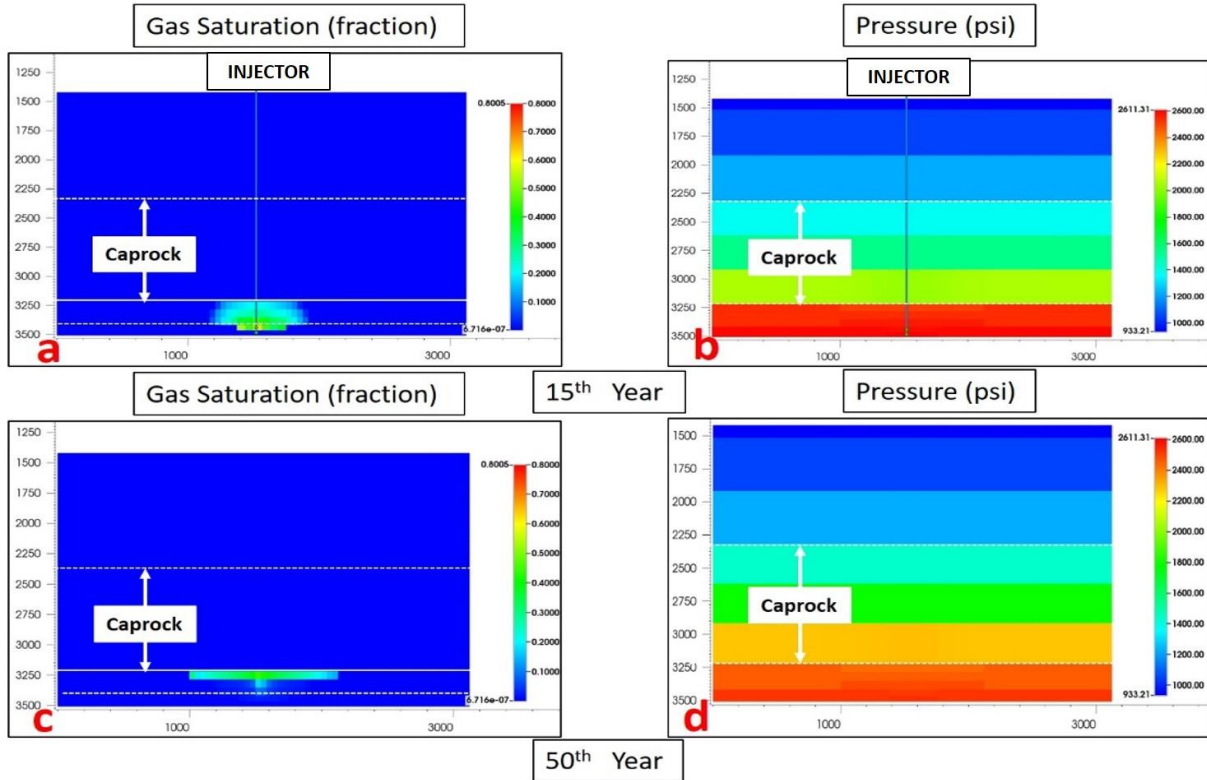


Figure A.3.9 The schematic description for properties at cross-sectional slice J=13 for Case B indicating the distribution of Gas Saturation and Pressure(psi) at the end of 15th year a) and b) and 50th year c) and d) respectively.

B. Field Case Study

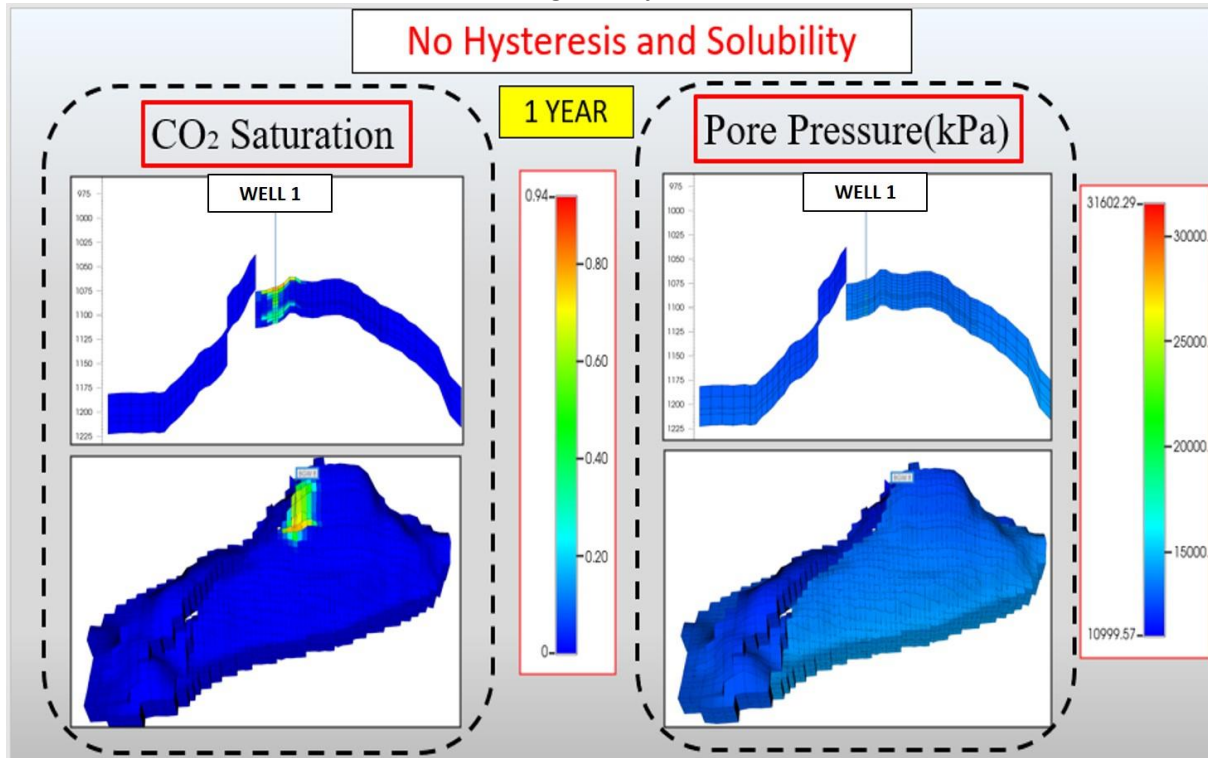


Figure B.1 The schematic description for properties at cross-sectional slice J=13(well location) above and 3D below for CO₂ Saturation left and Pressure(kPa) right at the end of 1st year for field scale model with no hysteresis and solubility assumption.

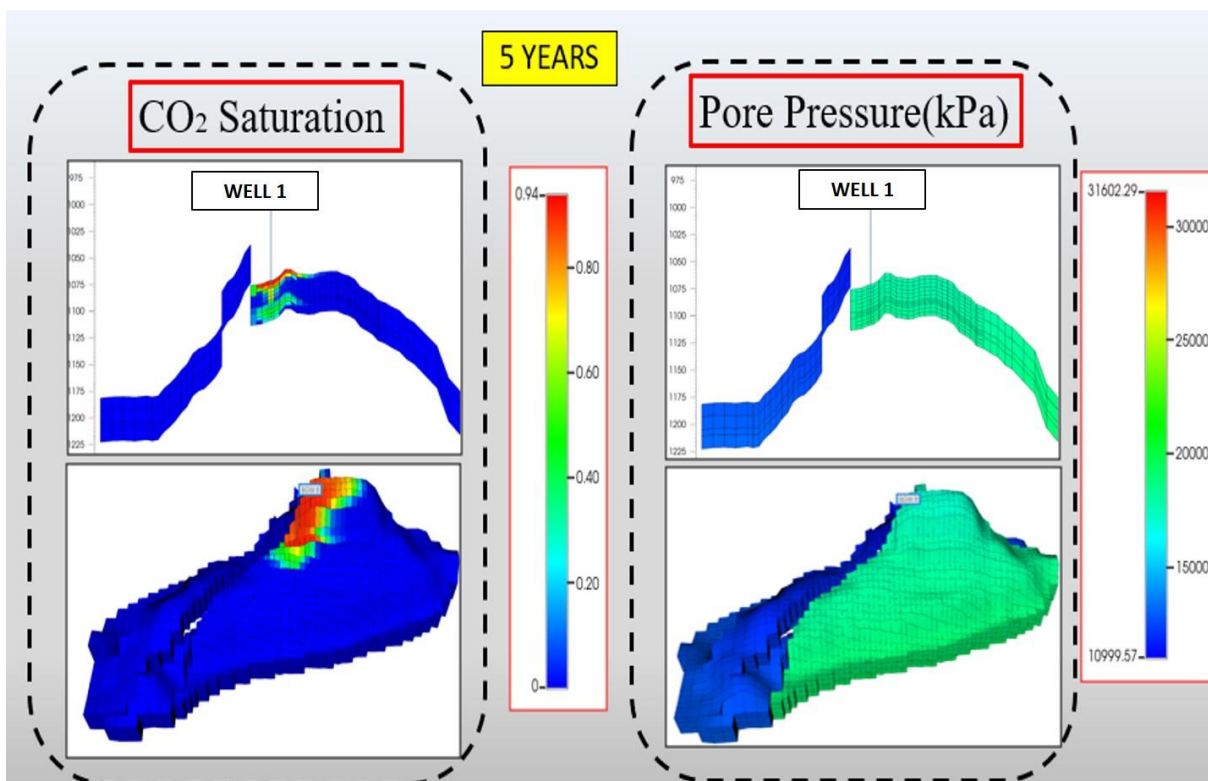


Figure B.2 The schematic description for properties at cross-sectional slice J=13(well location) above and 3D below for CO₂ Saturation left and Pressure(kPa) right at the end of 5th year for field scale model with no hysteresis and solubility assumption.

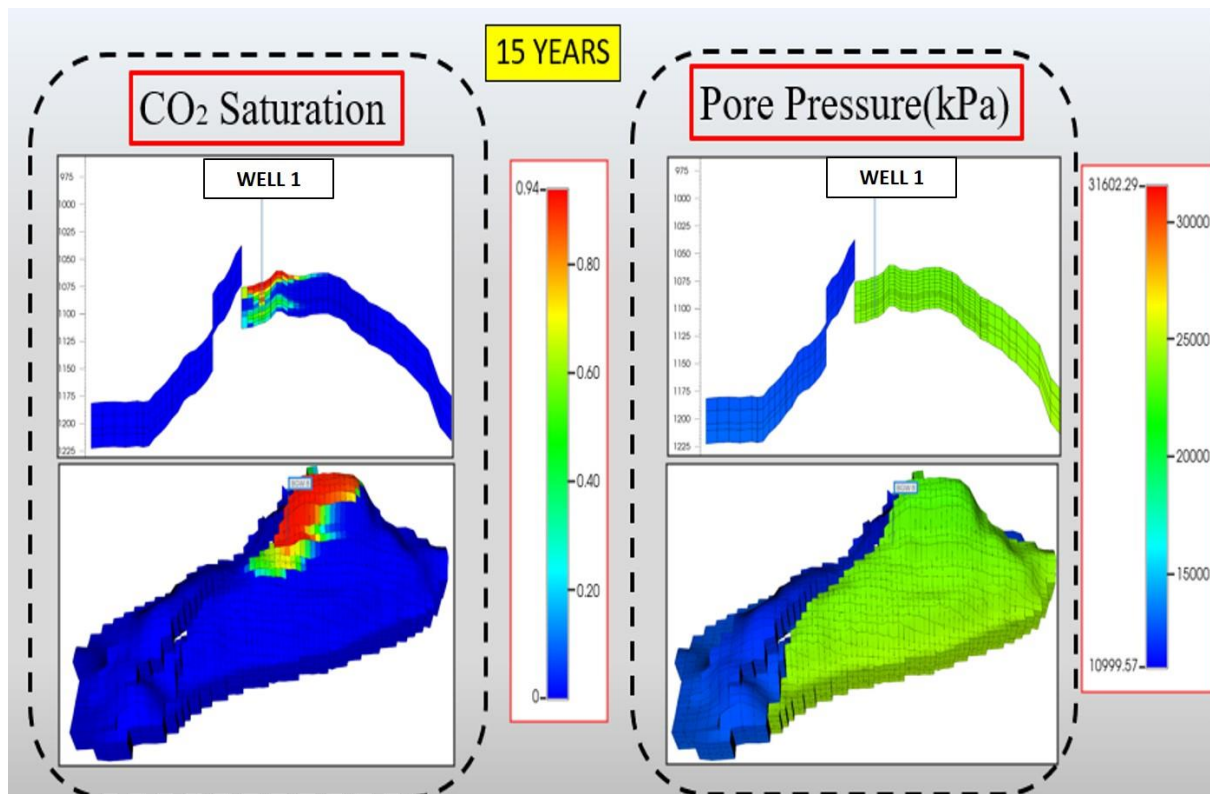


Figure B.3 The schematic description for properties at cross-sectional slice J=13(well location) above and 3D below for CO₂ Saturation left and Pressure(kPa) right at the end of 15th year for field scale model with no hysteresis and solubility assumption.

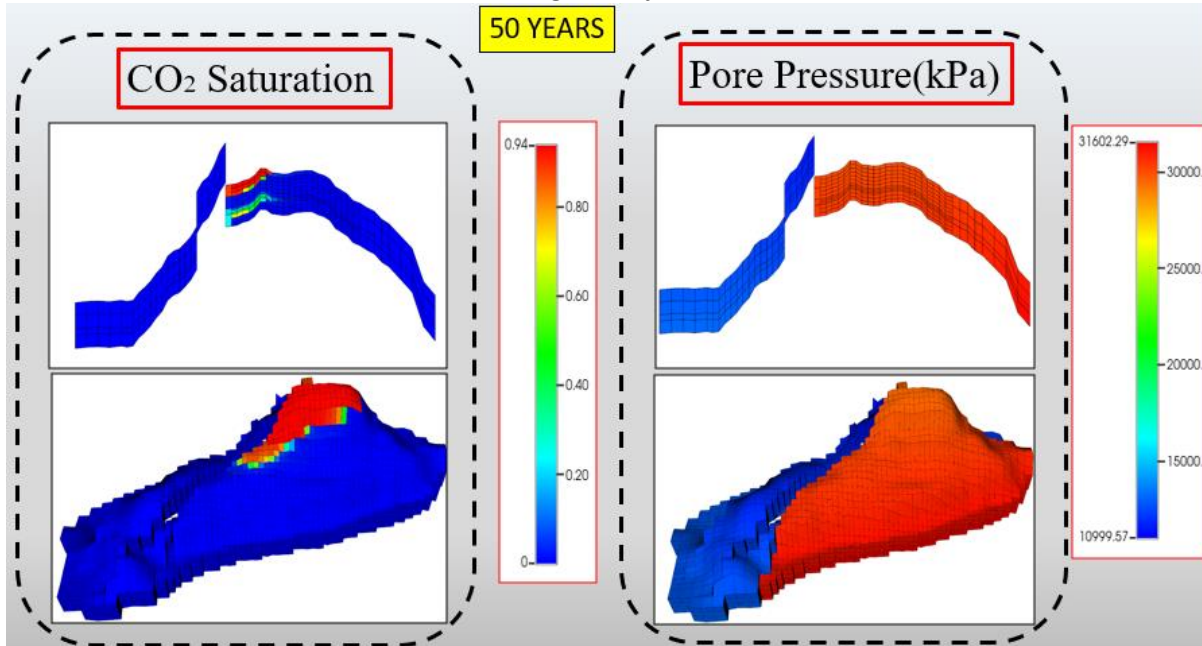


Figure B.4 The schematic description for properties at cross-sectional slice J=13 (well location) above and 3D below for CO₂ Saturation left and Pressure (kPa) right at the end of 50th year for field scale model with no hysteresis and solubility assumption.

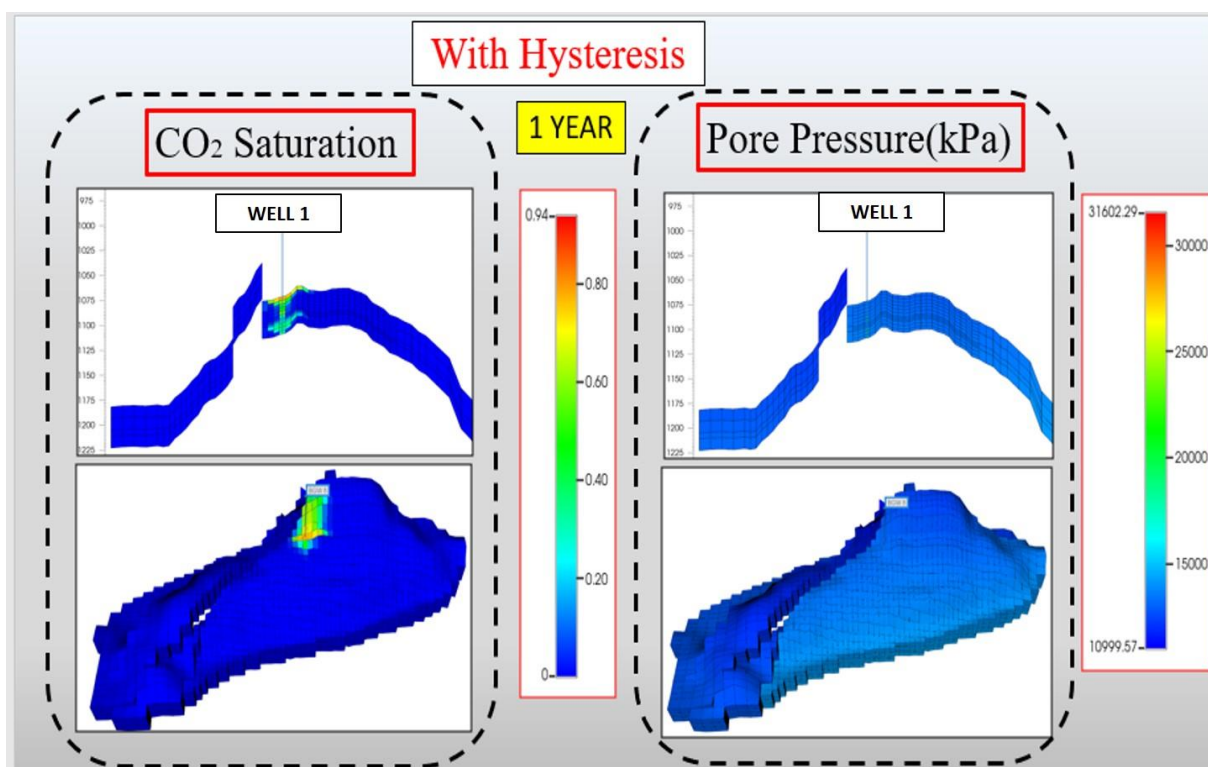


Figure B.5 The schematic description for properties at cross-sectional slice J=13 (well location) above and 3D below for CO₂ Saturation left and Pressure (kPa) right at the end of 1st year for field scale model with only hysteresis assumption.

Figure B.6 The schematic description for properties at cross-sectional slice J=13(well location) above and 3D below for CO₂ Saturation left and Pressure(kPa) right at the end of 5th year for field scale model with hysteresis assumption.

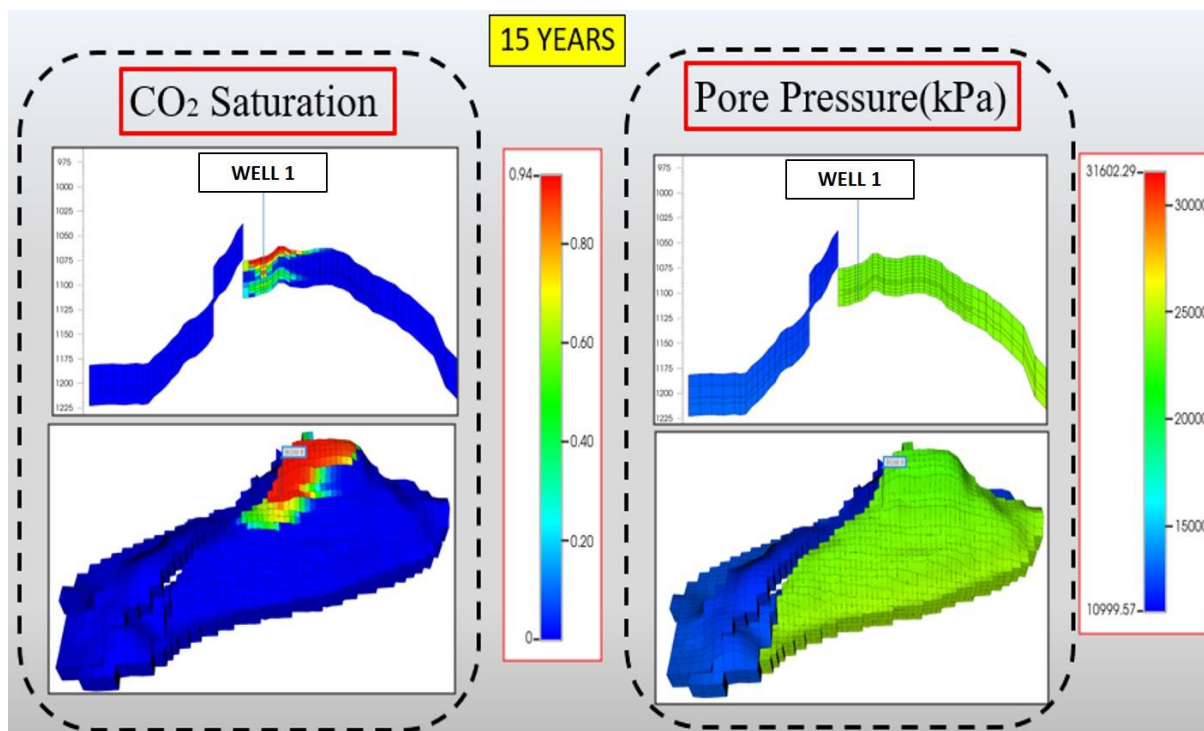


Figure B.7 The schematic description for properties at cross-sectional slice J=13(well location) above and 3D below for CO₂ Saturation left and Pressure(kPa) right at the end of 15th year for field scale model with hysteresis assumption.

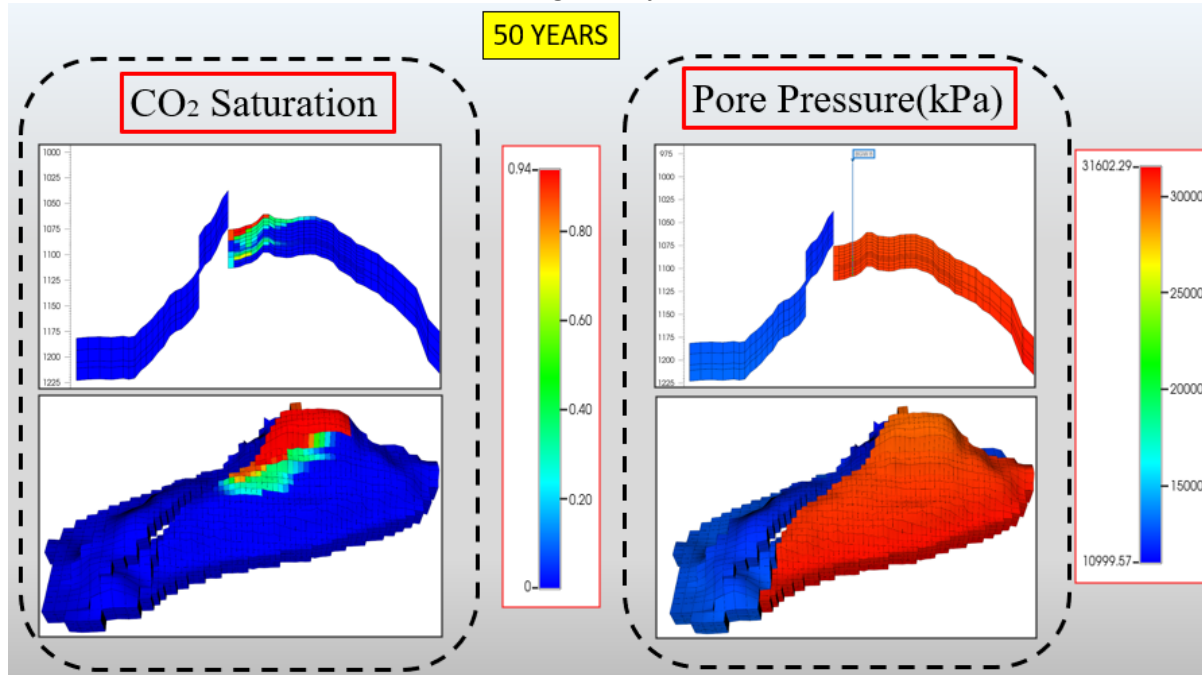


Figure B.8 The schematic description for properties at cross-sectional slice J=13(well location) above and 3D below for CO₂ Saturation left and Pressure(kPa) right at the end of 50th year for field scale model with hysteresis assumption.

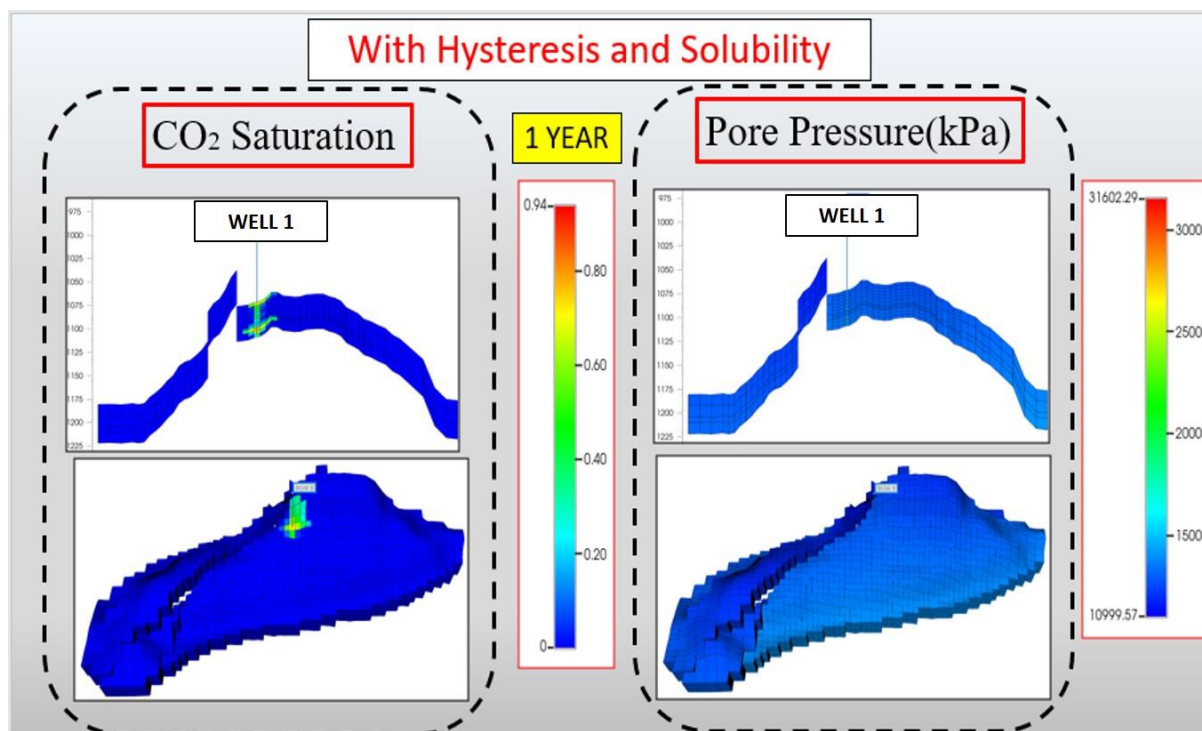


Figure B.9 The schematic description for properties at cross-sectional slice J=13(well location) above and 3D below for CO₂ Saturation left and Pressure(kPa) right at the end of 1st year for field scale model with hysteresis and solubility assumption.

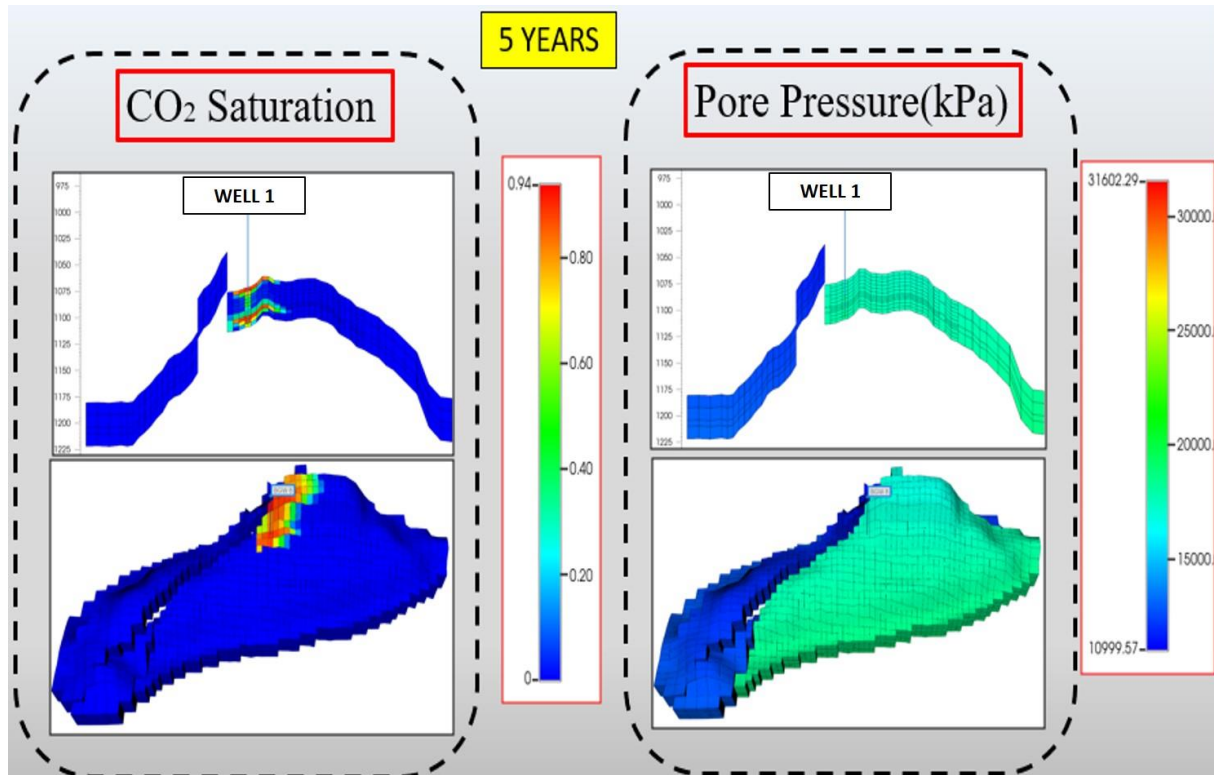


Figure B.10 The schematic description for properties at cross-sectional slice J=13(well location) above and 3D below for CO₂ Saturation left and Pressure(kPa) right at the end of 5th year for field scale model with hysteresis and solubility assumption.

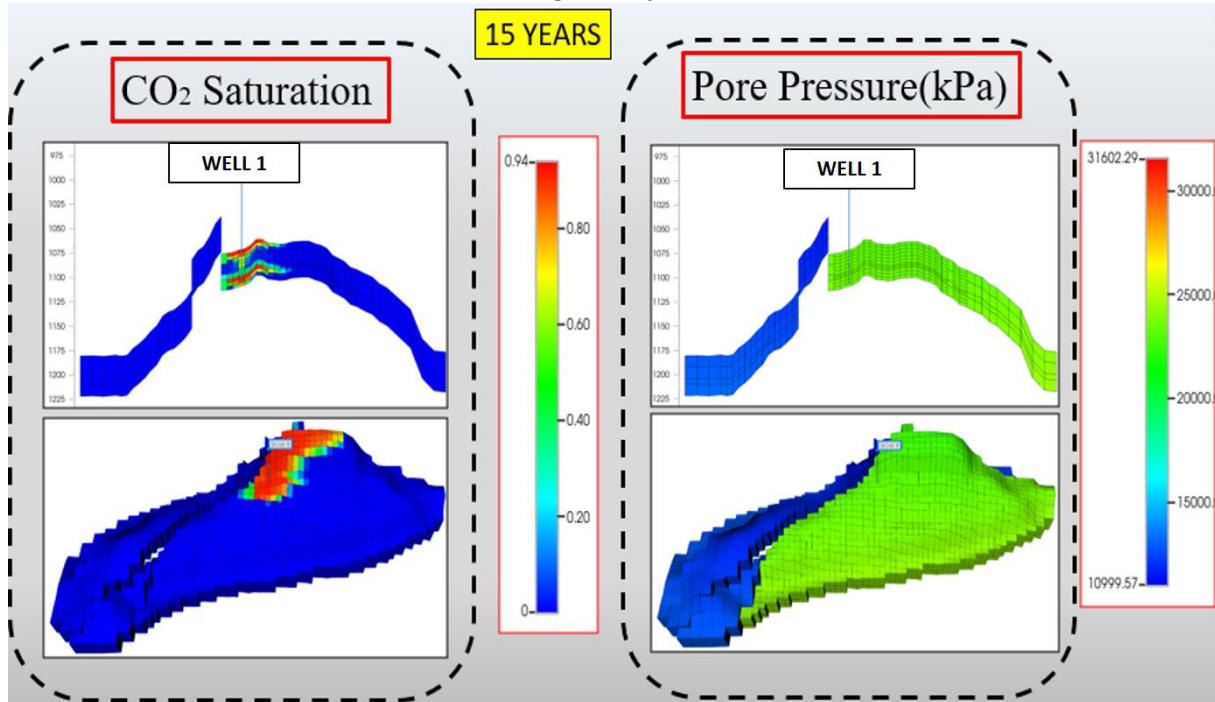


Figure B.11 The schematic description for properties at cross-sectional slice J=13(well location) above and 3D below for CO₂ Saturation left and Pressure(kPa) right at the end of 15th year for field scale model with hysteresis and solubility assumption.

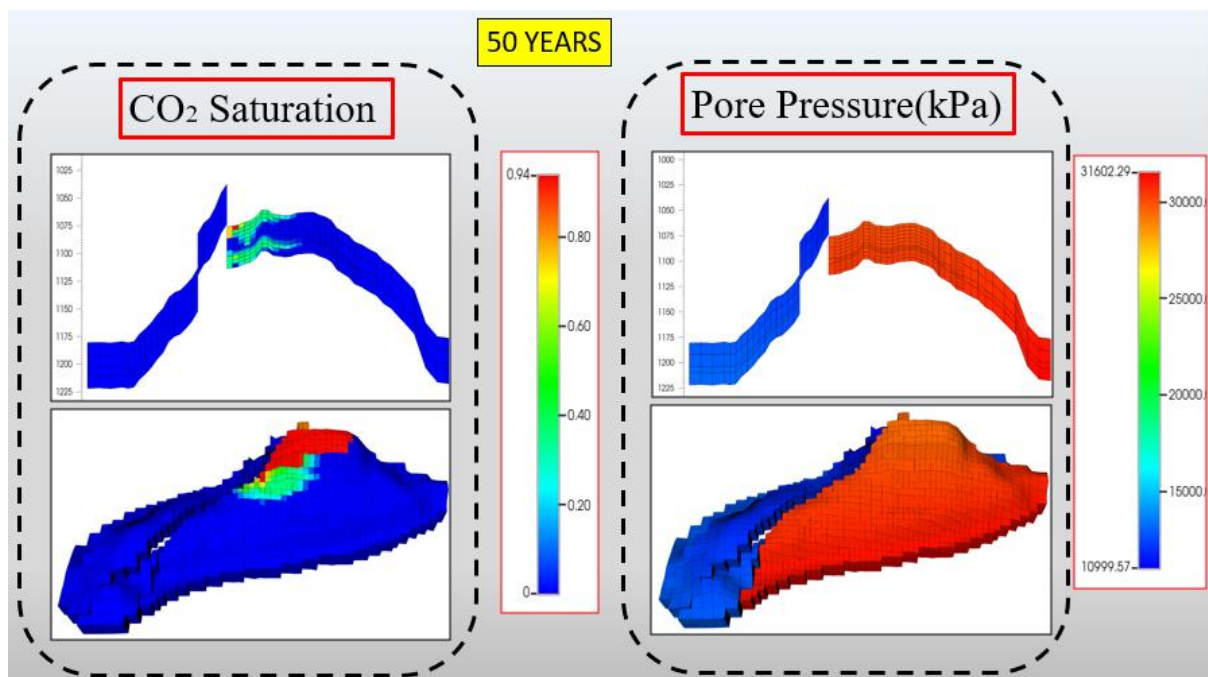


Figure B.12 The schematic description for properties at cross-sectional slice J=13(well location) above and 3D below for CO₂ Saturation left and Pressure(kPa) right at the end of 50th year for field scale model with hysteresis and solubility assumption.